Ph.D. Dissertation

MODELING AND SIMULATION OF NOVEL CATALYTIC REACTORS FOR CO_2 HYDROGENATION TO HYDROCARBON AT DIFFERENT MODES AND OPERATING CONDITIONS

Samrand Saeidi

Supervisors:

Dr. András Sápi

Associate Professor

Prof. Zoltán Kónya

Full Professor

DOCTORAL SCHOOL OF ENVIRONMENTAL SCIENCES

University of Szeged

Faculty of Science and Informatics

Department of Applied and Environmental Chemistry

Szeged

2023

List of symbols

A_C	cross sectional area of CR	[m^2]
A_z	surface area of AFSR	[m^2]
A_r	surface area of RFSR	[m^2]
b_{j,CO_2}	inhibition coefficient for CO_2 in the j-th reaction	[-]
a_{j,H_2O}	inhibition coefficient for H_2O in the j-th reaction	[-]
C_i	concentration of the i-th component	[mol m^{-3}]
C_{pg}	specific heat of the gas mixture in the reactor	[J mol^{-1} K^{-1}]
D_p	particle diameter	[m]
C_t	total concentration of the reactor mixture	[mol m^{-3}]
D_c	diameter of CR	[m]
h_r	heat transfer coefficient of the reactor	[Wm^{-2} K^{-1}]
E_j	apparent activation energy of the j-th reaction	[kJ mol^{-1}]
m_{cat}	catalyst weight	[g]
k_j	pre-exponential factor in Arrhenius law for the j-th reaction	[$mols^{-1}g^{-1}MPa^{-1}$]
K_{eq}	equilibrium constant of the shift reaction	[-]
K_j	reaction rate coefficient for the j-th reaction	[$mols^{-1}g^{-1}MPa^{-1}$]
R	universal gas constant	[J $mol^{-1}K^{-1}$]
Mw	molecular weight	[g/mol]
r_j	rate for the j-th reaction	[mol g_{cat}^{-1} s^{-1}]
L	reactor length	[m]
R_z	radius of AFSR	[m]
V_s	volumetric flow rate at reactor condition	[m^3 s^{-1}]
P	reactor pressure	[Pa]
r	radius of RFSR	[m]
Re	Reynolds number	[-]
U_c	overall heat transfer coefficient between jacket and CR	[Wm^{-2} K^{-1}]
u_r	velocity of gas mixture in RFSR	[m s^{-1}]
r_z	radius of AFSR at each z	[m]
u_z	velocity of gas mixture in AFSR	[m s^{-1}]
T	temperature of gas mixture in the reactor	[K]
T^j	temperature of jacket	[K]
z	axial dimension	[m]
U_z	overall heat transfer coefficient between jacket and AFSR	[Wm^{-2} K^{-1}]
U_r	overall heat transfer coefficient between jacket and RFSR	[Wm^{-2} K^{-1}]
u_c	velocity of gas mixture in CR	[m s^{-1}]

Greek letters

ρ_g	density of gas mixture in the reactor	[kg m^{-3}]
ε_b	bed porosity	[-]
ρ_p	density of catalyst particles	[g m^{-3}]
μ_g	viscosity of gas mixture in the reactor	[kg m^{-1} s^{-1}]
ρ_B	density of catalytic bed	[g m^{-3}]
ΔH_{fj}	enthalpy of formation for the j-th reaction	[J mol^{-1}]

Abbreviations

ABC	artificial bee colony
AFSR	axial flow spherical reactor
BET	brunauer–emmett–teller
O.F	objective function
DA	dragonfly algorithm
LHHW	langmuir-hinshelwood-hougen-watson
ER	experimental reactor
DE	differential evolution
DH	direct hydrogenation
CR	cylindrical reactor
GHSV	gas hourly space velocity
FT	fischer-tropsch
GA	genetic algorithm
RWGS	reverse water gas shift
GTL	gas to liquid
HC	hydrocarbons
WGS	water gas shift
RFSR	radial flow spherical reactor

List of Figures

List of Tables

1. Introduction

Since the industrial revolution, there has been a significant increase in the concentration of greenhouse gases, such as carbon dioxide, in the Earth's atmosphere. This has led to severe and irreversible changes in the global climate. With the growth of the population and improvements in living standards, particularly in developing nations, greenhouse gas emissions are expected to continue rising in the future [1]. To combat the effects of global warming, various efforts are underway to decrease CO_2 emissions. One promising approach involves using fossil natural gas that is enriched with CO_2 to create value-added products like chemicals and fuels, as CO_2 is the main component of fossil natural gas. It's important to note that several processes have been developed that use CO_2 as a reactant gas, making use of its inert and stable properties to overcome thermodynamic limitations [2].

There are some possible direct and indirect approaches to mitigating the emissions of carbon dioxide into the atmosphere. For example, CO_2 conversion to hydrocarbons is a direct process, while CO_2 conversion into a kind of intermediate such as methanol and then its conversion into hydrocarbons would be an indirect process. The direct approach, that is, hydrogenation of only carbon dioxide to hydrocarbon (C_2-C_4), known as modified Fischer-Tropsch synthesis (MFTS), is investigated in this study [3, 4]. As it is proven $Fe-K/\gamma-Al_2O_3$ catalyst can expedite this process. It means that MFTS is firmly dependent on the kind of promoter and active-site used in the catalyst based on the presented sequence and mechanism of the reaction, as shown in **Figure 1.** CO_2 is converted to CO via the reverse water gas shift (RWGS) reaction and then CO can be converted to hydrocarbons (C_2-C_4) through the Fischer-Tropsch (FT) reaction. It should be noted that the direct hydrogenation (DH) of CO_2 to hydrocarbons is insignificant [5-9]:

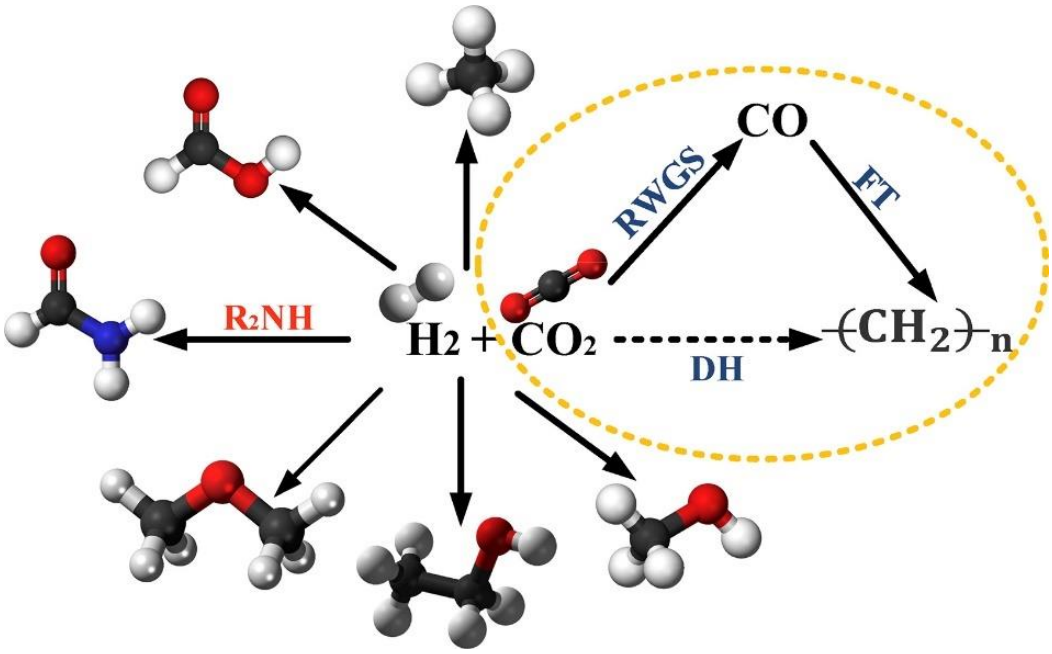

Figure 1. Schematic of value-added products from hydrogenation of CO_2 with special emphasis on the scope of this study [10].

1.1 Statement of the problem

The depletion of fossil fuels, the issue of global warming, climate change, and the sharp increase in fuel costs are motivating scientists to explore alternatives in the form of commercially viable and eco-friendly fuels. The process of converting CO_2 into hydrocarbons is being examined as a potential solution to meet these demands, but has the issues listed below:

1. Integration of reaction heat: due to the existence of both endothermic (RWGS) and exothermic (FTS) reactions in the single reactor.
2. Low CO_2 conversion: the formation of huge amounts of water along the single reactor causes catalyst deactivation due to the inhibition effect of water on the active sites of the catalyst, thereby shortening the catalyst's lifetime.
3. Low production capacity: due to the loss of hydrogen in the sweep part of the membrane reactor as H_2O, which means that hydrogen dosage might be required to adjust the H_2/CO_2 in the reactor.

4. Pressure drop across the reactor: due to the existence of an intrinsic limitation on the diffusion along the fixed-bed reactor.

The main goal of this research is to compare fixed-bed, annular, and spherical reactors with and without a membrane based on modeling and optimization. The comparison between the simulated data and the experimental ones will be made in order to validate the models for the production rate of the entire investigated reactors. Consequently, this case will demonstrate the viability of a new reactor alternative using theoretical investigations. The advantages of the new alternative over the conventional ones will be discussed based on the trajectory of temperature and component profiles (including reactants and products) along the reactors.

1.1.1 Annular reactor

The annular reactor design is particularly advantageous for CO_2 hydrogenation to hydrocarbons because it allows for precise temperature control and a reduction of radial dispersion. The reaction mixture is circulated through the reactor and is in continuous contact with the reactor walls, which act as a heat transfer surface. The temperature of the reactor can be controlled by adjusting the flow rate and temperature of the coolant circulating in the annular space between the reactor and the jacket.

1.1.2 In situ H_2O removal using H-SOD membrane

The use of the H-SOD (hydroxyl sodalite) membrane for in situ H_2O removal during CO_2 hydrogenation to hydrocarbons is a promising approach to improving the selectivity and conversion rates of the reaction. During the CO_2 hydrogenation process, water is produced as a by-product, which can accumulate in the reactor and limit the reaction's efficiency. By using an H-SOD membrane, water molecules can be selectively removed from the reaction mixture without affecting the reactants or the products by selectively permeating through the membrane. H-SOD membranes have unique hydrophobic properties that allow the selective removal of water molecules

while retaining the reactant and product molecules (of course based on the pore size). The membrane is highly permeable to water molecules due to its hydrophobic nature and selective pore size, which can range from 0.4 to 0.8 nm, depending on the membrane's pore size distribution. The use of an H-SOD membrane has several advantages for CO_2 hydrogenation to hydrocarbons. First, it can prevent the accumulation of water in the reactor, which can cause catalyst deactivation and reduce the reaction efficiency. Second, the selective removal of water can shift the thermodynamic equilibrium of the RWGS reaction toward product formation, leading to higher CO formation and thus higher hydrocarbon selectivity via FTS. Finally, the in-situ removal of water can simplify the downstream processing steps, as the product mixture will be less contaminated with water.

1.1.3 Hydrogen perm-selective using pd/Ag membrane

One of the main issues regarding H_2O removal via membrane reactors is the removal of H_2 in the form of H_2O and, in turn, the resulting H_2 shortage. The use of a Pd/Ag membrane as a hydrogen perm-selective membrane in CO_2 hydrogenation to hydrocarbons is a promising approach to adjusting the H_2/CO_2 ratio during the H_2O removal. Because the Boudouard reaction would distort the reaction (**R1**), the reactor's performance would decrease at high temperatures. As a result, a hydrogen perm-selective membrane has been proposed as a method of controlling hydrogen dosage.

$$CO + CO \rightarrow C_{(s)} + CO_2 \qquad \Delta H_{300℃} = -173.5\ kJ/mol \qquad \textbf{(R1)}$$

Therefore, during CO_2 hydrogenation, hydrogen is an essential reactant that reacts with CO_2 to produce hydrocarbons. However, the presence of excess hydrogen in the reaction mixture can lead to the formation of undesirable by-products and decrease the selectivity of the desired hydrocarbon product. Therefore, it is crucial to maintain the appropriate feed ratio in the reaction mixture. By using a Pd/Ag membrane, hydrogen molecules can selectively permeate through the membrane. Pd/Ag membranes have excellent hydrogen perm-selective properties due to the high solubility and diffusivity of hydrogen in Pd and the catalytic activity of Ag. The Pd layer provides high hydrogen flux and selectivity, while the Ag layer enhances the stability and durability of the

membrane. Finally, the Pd/Ag membrane is highly durable and stable, which can reduce the downtime and maintenance costs of the reactor.

1.1.4 Spherical packed-bed reactor

One of the new possibilities for improving the efficiency of a single (fixed-bed) reactor is the application of spherical packed-bed reactor technology. A spherical reactor is particularly attractive for highly exothermic reactions because of its superior heat transfer ability, excellent temperature control, proper mixing, elimination of diffusion limitations and small pressure drop. Despite such obvious advantages, spherical membrane reactors have not been widely used by the petrochemical industry [11-13]. All specifications of the water-permselective reactor in the spherical packed-bed membrane reactor are the same as those of the cylindrical packed-bed and annular modified FT reactors, except for the reactor length.

1.2 Objectives of the study

The overall objective of this research is to propose a one-dimensional transient mathematical model for studying and comparing different reactor modes, such as fixed-bed, annular, and spherical reactors. The specific goals of the research are as follows:

1. Modeling and optimization of a fixed-bed reactor: Estimation of kinetic parameters using Artificial Bee Colony (ABC) and Differential Evolution (DE) algorithms.
2. Modeling and optimization, including the estimation of kinetic parameters using the dragonfly algorithm (DA) and comparison of the performance of cylindrical and spherical reactors for CO_2 hydrogenation to hydrocarbons.
3. Modeling and statistical analysis of a three-side membrane reactor.

1.3 Research contributions

This study proposes a new reactor configuration for CO_2 hydrogenation to improve the selectivity of hydrocarbon products. The significant contributions can be summarized as follows:

1. Modeling and simulation of a packed-bed reactor with different modes (H_2O and H_2 perm-selective) to determine the trajectory of components (reactants and products) along the length of the reactor while considering the kinetics rate of the Fe-based catalyst.
2. Modeling and simulation of spherical packed-bed and annular reactors with different modes to determine the trajectory of components (reactants and products) along the reactor length based on the kinetics rate of the catalyst.
3. Modeling and statistical analysis of a three-side membrane reactor for the optimization of hydrocarbon production.

2. Literature background

In 1980, Hashimoto and his colleagues were the first to suggest a combination of CO_2 methanation and seawater electrolysis to reduce CO_2 emissions [14]. CO_2 is a stable molecule, both chemically and thermodynamically, and researchers are exploring different methods to transform it into valuable products such as hydrocarbons (methane into long-chain hydrocarbons) and chemicals (methanol and DME, etc.), as shown in **Figure 2**. These methods include photo, electro, plasma, and catalytic thermal, but only catalytic thermal is currently nearing implementation in industry. The other technologies are still in their early stages of development, but may be commercialized in the coming decades.

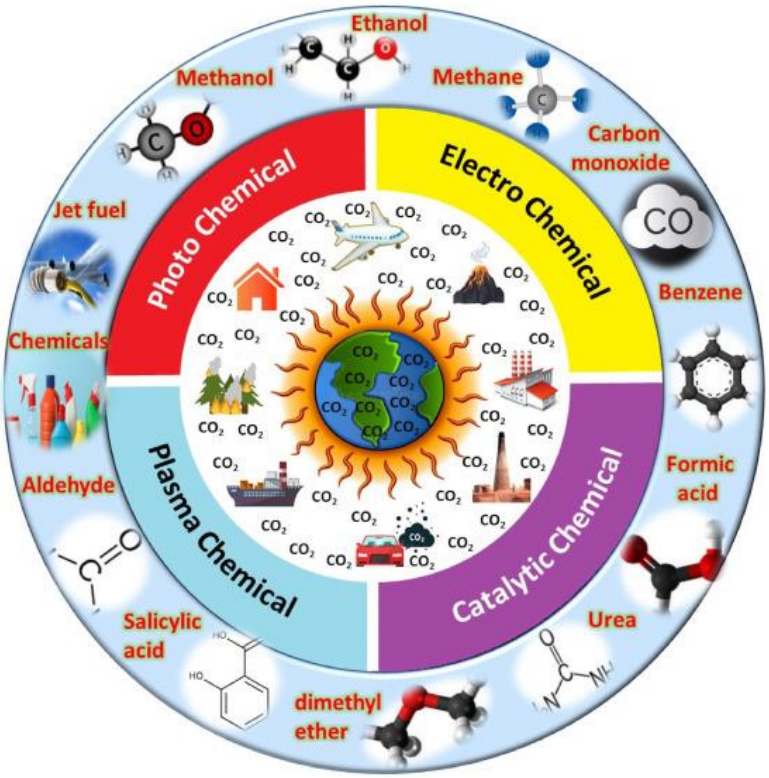

Figure 2. Schematic of all available technologies for CO_2 hydrogenation into value-added products.

Saeidi et al. [15] have comprehensively scrutinized two different processes, hydrogenation of CO_2 to hydrocarbons and methanol, including effects of catalyst, operating conditions and reactor type on the efficiency enhancement of each process. The results can be found as follows:

2.1 Influence of catalyst type

The findings show that four catalyst aspects, such as the effect of the active site, promoter, support, and binder, were thoroughly investigated to fully understand the effect of catalyst type on H_2/CO_2 to hydrocarbon conversion. Therefore, a complete review of these four aspects is presented in the following.

Saeidi et al. [16] found that the yields of light hydrocarbons (C_2-C_4) were generally below 30%, with some exceptions such as catalysts containing Fe and K which yielded between 20 and 30%. The highest yields for hydrocarbon synthesis belong to the catalysts comprising Fe and K. Besides, it is noteworthy that using 5K-10Co/Fe [17] in a two-stage fixed-bed reactor with ex-situ water removal could result in improved CO_2 conversion and thus HCs yield with respect to a two-stage reactor without water removal. Catalysts with yields lower than 1% all had Fe in their composition, like K-Mn-Fe [18], Mn-Fe [18], Fe/TiO_2, and Fe/SiO_2 [19], which shows that addition of Mn and support with TiO_2 and SiO_2 could not enhance the performance of the resultant Fe-containing catalysts. According to Liu et al. [20], dispersion of Fe-oxides in MOF matrix could improve the catalyst's performance in terms of both stability and selectivity towards hydrocarbons. In conclusion, much research is still required to improve the performance of these catalysts in terms of both CO_2 conversion and HCs selectivity since this process is still in its infancy.

However, while previous results highlighted that both catalyst properties and reactor design play important roles in the hydrogenation of CO_2 to methane, methanol, and especially HCs, this review identified the crucial role of reactor configuration. Therefore, a new reactor configuration consisting of perm-selective walls to water (RWGS fixed-bed reactor) and hydrogen (fluidized-bed FT reaction) is proposed to take advantage of the controlled removal and dosing potentials of the membrane with the excellent gas-solid contact and heat transfer capabilities of a fluidized-bed in one configuration. Moreover, the proposed reactor type usually has high selectivity and activity, as well as long catalyst activity for the CO_2 hydrogenation. The aim of this new reactor configuration is to achieve higher CO_2 conversion to C_2-C_4 hydrocarbons.

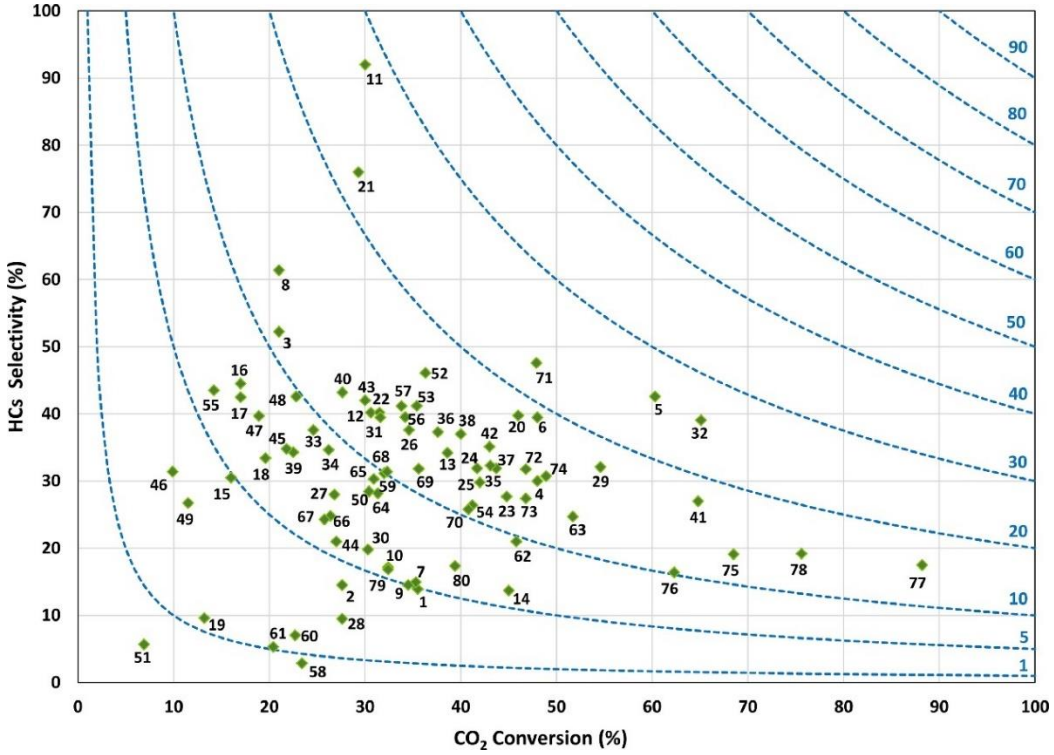

Figure 3. Analysis of the selectivity of HCs and CO_2 conversion during catalytic CO2 hydrogenation to hydrocarbons [16].

Iron-based catalysts have become popular due to their low cost and potential applications [21]. CO_2 is reduced by iron (II), followed by H radical scission via adsorbed species on the catalyst surface (**Figure 4**). The reaction between residual H and carbonyl C results in the formation of OH, formic acid, and CO. The Fe-CH_2 radical forms in a similar manner as a carbon-carbon propagation product. The primary reaction route is chain propagation, as higher hydrocarbons are identified as major products. The selectivity of α-olefins is higher than that of paraffins due to less H_2 uptake and the absence of extra H_2 in the reaction, which highlights the significance of hydrogen dosing during the reaction [22].

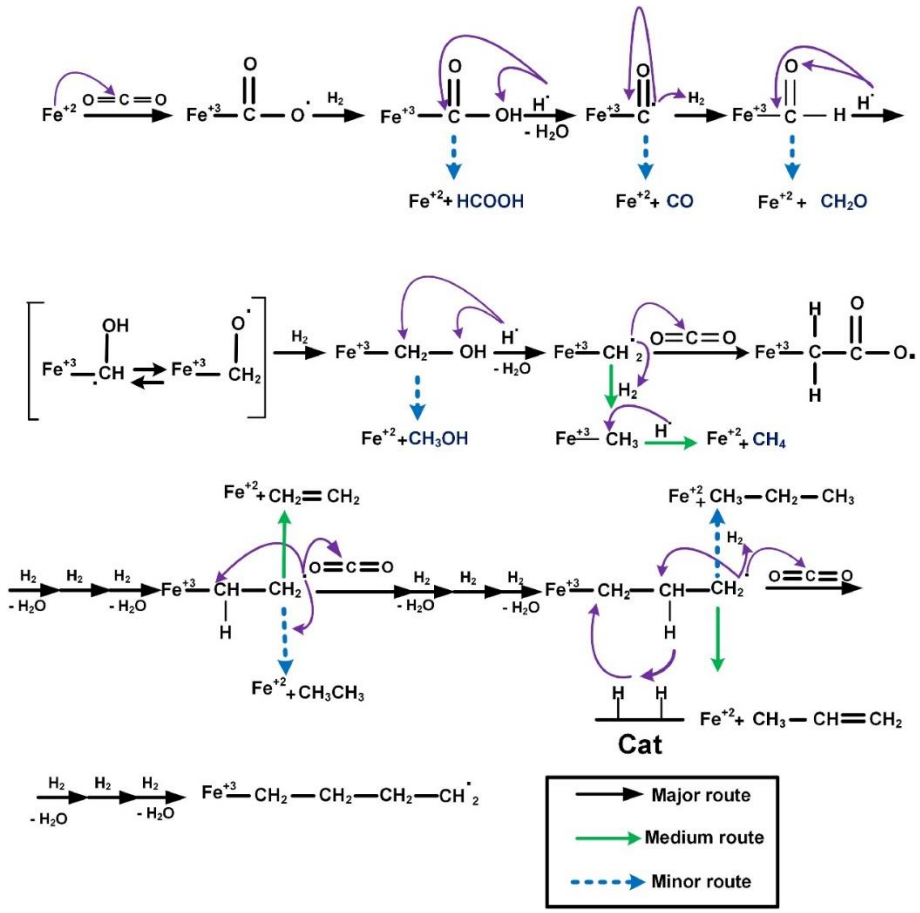

Figure 4. Possible routes for CO_2 hydrogenation to value-added products over Fe catalyst [22].

The activation of CO_2 and -(CH_2)-$_n$ growth using a Fe-based catalyst typically involves a multi-step mechanism. In the first step, the Fe catalyst activates CO_2 by reducing it to CO, which is a key intermediate in the subsequent steps of the reaction. This reduction of CO_2 is often facilitated by the presence of Fe(II) and Fe(III) species in the catalyst, which both exist in Fe_3O_4 that can be formed via hydrogenation of Fe_2O_3 during reduction and/or reaction.

Once CO is generated over the Fe-oxide, it can undergo a series of reactions with hydrogen to form hydrocarbons on the formed Fe-carbide (mainly Fe_5C_2), the active phase for FT and chain-propagation. Nevertheless, the specific reaction pathway and the resulting product distribution depend on the conditions of the reaction, including temperature, pressure, and the type of catalyst and promoter used. Fe-based catalysts have two main routes, based on the second active metal or promoter for hydrocarbon formation: the FT route and the methanol-mediated route. In the FT route,

CO reacts with hydrogen to form a range of hydrocarbons, including olefins and paraffins, through a series of polymerization and hydrogenation reactions. In the methanol-mediated route, CO is first converted to methanol, which can then undergo further reactions to produce hydrocarbons. It is worth mentioning that, the Fe itself promotes the FT route while the addition of other metals such as Cu and Zn can facilitate the methanol-mediated route.

It should be noted that some researchers have suggested that the presence of carbonate is not favorable for CO_2 activation and hydrocarbon formation using Fe-based catalysts [23]. This is because carbonate can compete with CO_2 for adsorption sites on the catalyst surface, thereby reducing the amount of CO_2 available for reaction. Carbonate can also form a stable layer on the catalyst surface, inhibiting the reaction altogether.

2.2. Influence of operating conditions

The hydrogenation of CO_2 into hydrocarbons is a highly exothermic and sensitive reaction. Therefore, the operating conditions, such as space velocity, temperature, and pressure, have a significant impact on the performance of the hydrogenation process. Low space velocity (SV) and high residence time lead to increased CO_2 conversion, enhanced HC yield, and the formation of a significant amount of H_2O. Conversely, high space velocity and short residence time result in a low contact time between CO_2 and the catalyst, leading to a low conversion of CO_2 and a decrease in HC yield. Additionally, elevated pressure reduces space velocity and leads to a considerable shift in the product distribution towards long-chain HCs. The RWGS reaction being reversible means that an increase in pressure does not affect CO_2 conversion unless the CO produced via the RWGS reaction is consumed through the FT reaction, thus shifting the equilibrium. However, the resulting H_2O obstructs the RWGS reaction, which can lead to catalyst deactivation. Therefore, removing H_2O is crucial to avoiding the shift in equilibrium towards the WGS reaction and hindering catalyst deactivation. Furthermore, CO_2 conversion and CO yield increase slowly with temperature through the reversible endothermic RWGS reaction, whereas the exothermic FT reaction proceeds faster at high temperatures. Therefore, finding a system to avoid this thermal conflict between these reactions is critical. Moreover, the dependence of HC yield on

temperature is not unequivocal due to the larger tendency of catalyst deactivation as a result of inert carbon deposition, making temperature an essential factor in shifting equilibrium and reaction rates. The pressure of the reaction influences the thermodynamics of the hydrogenation process. A higher pressure favors product formation because it shifts the equilibrium towards them. However, high pressure increases the cost of operation, and the equipment used must be able to withstand high pressure. Therefore, choosing an optimum operating condition that balances the cost of operation with the process's performance is crucial. The details of these three operating conditions can be found in our recent publication [16].

2.3. Influence of reactor configuration

As previously noted, it is possible to combine endothermic RWGS and exothermic FT reactions in one reactor to increase energy efficiency. While fixed-bed reactors have been widely used to produce hydrocarbons through CO_2 hydrogenation, they may have drawbacks such as difficulty controlling temperature and creating hot spots. Therefore, slurry and fluidized-bed reactors have been utilized to improve the performance of CO_2 hydrogenation to hydrocarbons. Studies have shown that these reactors have advantageous results in removing the heat generated from this highly exothermic process, as seen in **Figure 5** [16].

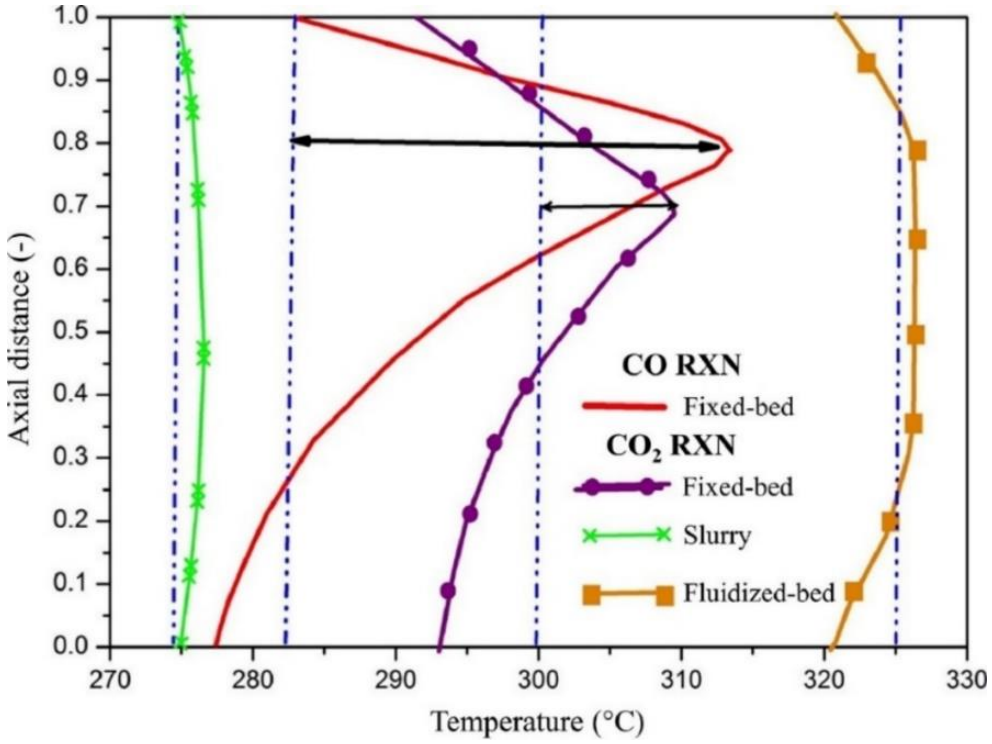

Figure 5. Schematic of hot-spot occurrence in various reactor types for CO_2 hydrogenation to HCs [16].

To enhance catalytic performance, slurry and fluidized-bed reactors utilizing Fe-Cu-K-Al catalysts have been found to outperform fixed-bed reactors in CO_2 hydrogenation to hydrocarbons. Space-time yields of fluidized-bed, slurry, and fixed-bed reactors were reported as 41.8, 35.2, and 31.8, respectively [16]. **Figure 6** shows that slurry and fluidized-bed reactors can produce heavy hydrocarbons and light olefins [24, 25]. Slurry reactors are better suited for products with high boiling points and saturated hydrocarbons, whereas fluidized-bed reactors are ideal for unsaturated hydrocarbons, with an olefin selectivity of approximately 86.7% at 300°C. Reactor coupling in series has been proposed to increase both CO_2 conversion and selectivity towards heavy hydrocarbons, but high pressure drops make this approach impractical [26]. Recycle reactors with a residence time for hydrogenation have been proposed as an alternative and have shown to improve CO_2 conversion and selectivity towards C5+ hydrocarbons, with a maximum conversion rate of 88.2%. However, when the recycle reactor's GHSV was 2000 ml/gcat.hr and R = 5, selectivity towards CH_4 and light paraffins increased while C_{5+} selectivity decreased to 68.3%.

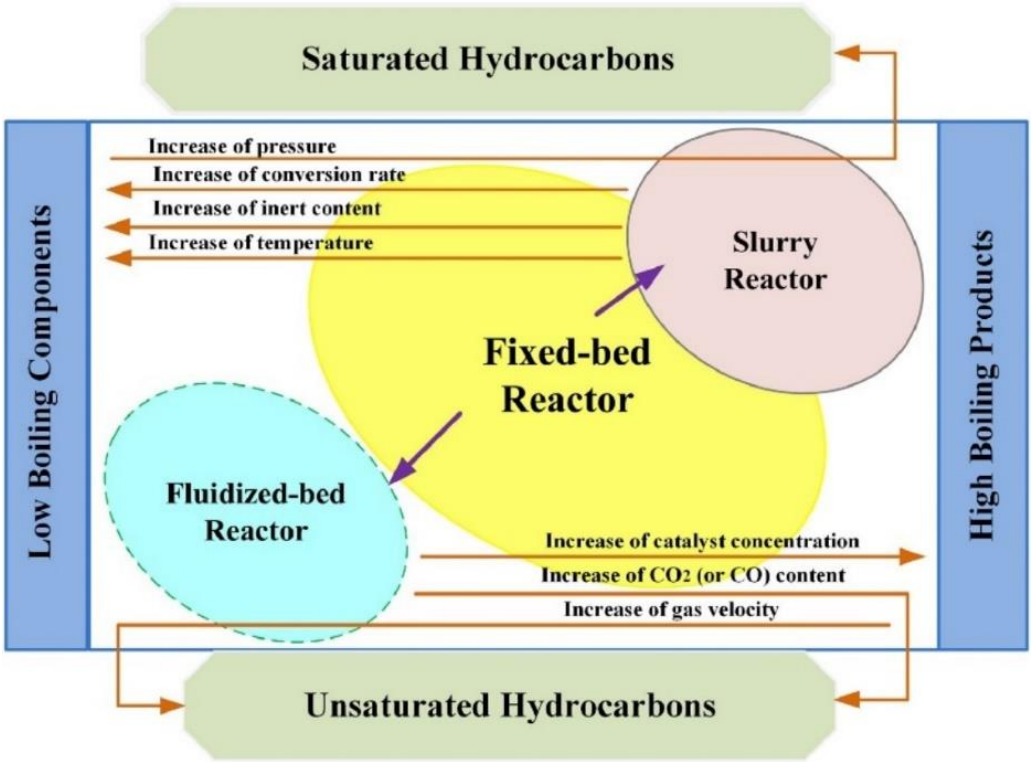

Figure 6. Influence of process parameters on product distribution in various reactors [24, 25].

According to the literature, which concentrated on the role of catalyst type, the role of catalyst type on hydrocarbon production efficiency through hydrogenation of carbon dioxide is not significant. Since it has been proven that the best catalyst with the best catalyst aspects in the best operating conditions would not lead to high levels of hydrocarbon production efficiency due to the deactivation of these catalysts by produced water and the occurrence of hot spots along the single reactor. Furthermore, in these catalyst-type studies, the negative effect of H_2 waste on hydrocarbon production efficiency is examined, and all of these practical studies have utilized the single-bed reactor. Previous studies that focused on the role of reactor type on hydrocarbon production efficiency expended much effort to identify the most efficient reactor for this case by comparing different types of reactors in practice, and the results identified the most efficient reactors while revealing the rank of other reactor configurations in terms of hydrocarbon production efficiency at the same time.

Based on the results obtained, the fixed-bed reactor has been identified as the least efficient type, followed by slurry and fluidized-bed reactors. This is justifiable since catalyst deactivation in these three reactor types is attributed to water formation and thermal conflicts, which are complementary to the influence of process parameters in different reactor types on product distribution. Conversely, the efficiency of hydrocarbon production in a series reactor type has been demonstrated to be better than the other three, as this reactor mitigates the negative effects of thermal conflicts and enhances HC yield by increasing resident time through low space velocity. The researchers have suggested the recycle reactor as the most efficient reactor type for this process due to its distinctive configuration that eliminates thermal conflicts and results in lower catalyst deactivation, leading to higher efficiency. Moreover, this reactor preheats the input feed for endothermic reactions. It should be noted that reactor type primarily affects CO_2 conversion, while catalyst type and operating conditions mainly affect product selectivity. This confirms the need for changes in reactor configurations.

Furthermore, the general consensus in the hydrogenation of CO_2 to hydrocarbons is that iron is the best active site, with γ-Al_2O_3 as the support and K as the promoter; however, the nature of the active sites and interactions among active components, support, and promoter, as well as reaction mechanisms, remain controversial. However, it should be highlighted that the novel reactor configuration for hydrogenation of CO_2 to hydrocarbon is based on surface science approaches in line with reaction mechanisms that bridge the gap between the macroscopic characteristics of practical catalysts and the potential drawbacks of a fixed-bed reactor in order to overcome hydrocarbon enhancement (C_2-C_4).

There has been no theoretical study on this issue, which means that none of the previous research works has investigated the effects of reactor configuration. Therefore, the author investigated this case theoretically, which led to the identification of a spherical packed-bed membrane reactor and an annular membrane reactor. The proposed reactor is able to eradicate catalyst deactivation associated with the other types of reactors while simultaneously adjusting the dosing of hydrogen because this annular membrane reactor is perm-selective towards water and also perm-selective towards H_2 to adjust the H_2 concentration, which prevents reaction distortion

caused by the temperature effect. Furthermore, annular and spherical membrane reactors have already been demonstrated to be the most efficient configuration for the hydrocarbon synthesis process in terms of theoretically increasing product efficiency, so it can be verified that this configuration can be applied to this process.

It should also be noted that the proposed reactor type usually possesses higher activity, selectivity, and a longer life in the hydrogenation of CO_2. However, this novel reactor configuration can suffer from high manufacturing costs; therefore, in order to make CO_2 hydrogenation economically feasible, significant improvements in reactor design according to the novel reactor configuration would be necessary.

3. Modeling and optimization of process

Modeling and simulation are useful methods to investigate the performance of reactors under different operating conditions, as well as to estimate kinetic parameters for reactor design [27-35]. Understanding the CO_2 hydrogenation mechanism and rate expressions is essential for this process. In addition, the estimation of kinetic parameters is of significant importance in reactor modelling and design [36-41]. To this end, the mechanism of CO_2 hydrogenation and rate expressions are prerequisites [22]. Since the initial work by Riedel et al. [3], have been conducted to examine the kinetics of CO_2 hydrogenation for producing added-value chemicals. The kinetics of the corresponding rate expressions for RWGS, FT, and DH were estimated by fitting the calculated and experimental data via regression using DATA FIT and ASPEN HYSYS, where propylene was the main product over K/Fe-Al_2O_3. Willauer et al. [42] extended this approach by including methane as another product over Al_2O_3-supported K/Mn/Fe, using the kinetic data obtained to calculate the corresponding kinetic parameters with the COMSOL package.

Moreover, Riedel et al. [3] investigated the effects of temperature and residence time on CO_2 hydrogenation using a plug flow model. It was reported that light olefins and paraffins were the main products in the 300–400 °C temperature range and 1 MPa pressure. Besides, CO_2 conversion and CO yield increased at lower residence times of about 12 g s cm^{-3}. In addition, Rohde et al. [43] modeled a fixed-bed plug flow reactor to study the influence of temperature and hydrogen amount on CO_2 hydrogenation to hydrocarbons. Results showed that a 50 °C increment in temperature led to higher conversions and consequently more hydrocarbon production. Moreover, the main impact of temperature elevation was an increase in the formation of short-chain hydrocarbons. Indeed, the key role of reaction temperature was ascribed to shift RWGS equilibrium instead of increasing the reaction rates at the studied temperature range. Willauer et al. [42] studied CO_2 hydrogenation in a fixed-bed reactor both experimentally and theoretically. It was revealed that FT was the rate-limiting step for olefin production through the two-step process consisting of RWGS and FT reactions. It was indicated that the maximum hydrocarbon yield in a fixed-bed reactor was 38.4% at 0.000093 L $g^{-1}s^{-1}$, which was 49% higher with respect to that achieved in a CSTR reactor, while it decreased to 13.6% when SV increased to 0.0015

L $g^{-1}s^{-1}$. Moreover, it was proven that increasing the reaction temperature, pressure, and feed ratio all gave higher CO_2 conversion with enhanced hydrocarbon yield. Higher yields of hydrocarbons were usually accompanied by a shift in distribution toward long-chain products, except in the case of increasing temperatures. Simultaneous increases in the yield of hydrocarbons and the olefin/paraffin ratio were obtained only when the reaction temperature was increased [10]. Consequently, a full factorial design was used to conduct statistical analysis, which examines all the possible variable combinations to evaluate the impact of input parameters (such as reactor, tube, shell temperatures, pressure ratio, and sweep ratio) and their interactions on product yields. This analysis helped to determine the optimal input variables for maximizing olefin yields.

3.1 Different reactor configurations

In the process of hydrogenation of CO_2 into hydrocarbons, water is produced as a main byproduct of the reaction. This water can negatively affect the catalytic performance of the catalyst used in the process. One approach to mitigate this issue is to use a water adsorbent to remove the water from the reaction mixture. The use of a water adsorbent offers several advantages over a membrane, including:

(i) Low capital and operating costs: Adsorbents are typically cheaper than membranes due to the fact that they do not require the energy-intensive process of compressing gases for separation.
(ii) Higher selectivity: Adsorbents can be designed to specifically target water molecules, resulting in high selectivity.
(iii) Simpler process design: Adsorbents can be easily loaded in the reactor, making the process design simpler and more straightforward.

Some examples of water adsorbents that can be used in the process of hydrogenation of CO_2 into hydrocarbons include zeolites, silica gels, alumina, silica-alumina composites, and activated carbon. These adsorbents can be regenerated by heating or by purging with an inert gas, allowing them to be reused multiple times. The disadvantages of adsorption include the need for a fixed-bed reactor that is often large in size, leading to issues with pressure drop and design. Additionally, if the adsorbent

cannot be regenerated, it creates more waste and makes it difficult to separate selectively when the reaction is catalyzed heterogeneously. Besides, since adsorption is favored at low temperatures and high pressures, using adsorbents in a high-temperature reactor (300 to 340 °C) cannot result in high water sorption efficiency. The other approach is the MR where zeolitic membranes can be used at high temperatures to remove water in-situ. The in-situ water removal shifts the equilibrium RWGS reaction towards the production of more CO and in turn, provides more feed for the FT reaction.

This study is theoretically conducted in a fixed-bed, annular, and spherical packed-bed configuration in two different modes: without a membrane and using a water-permeable, perm-selective membrane, as shown in **Figure 7**. In brief, both the annular and spherical packed-bed reactors operate under similar operating conditions to those of the fixed-bed case but with changes applied to the reactor's configuration. Indeed, the cross-sectional areas of these reactors are considered equal to those of fixed-bed reactors, and catalysts are loaded on both sides of the reactors' shells. Besides, the wall of the tube is coated by a water-perm-selective membrane layer in the membrane reactor. Water permeates through the membrane layer due to a partial pressure gradient. An inert gas, such as N_2, is introduced into the tube side and sweeps the penetrated water away. The mass and heat transfers occur simultaneously between both sides of the membrane. **Figure 7** illustrates the elemental volumes of all type of reactors.

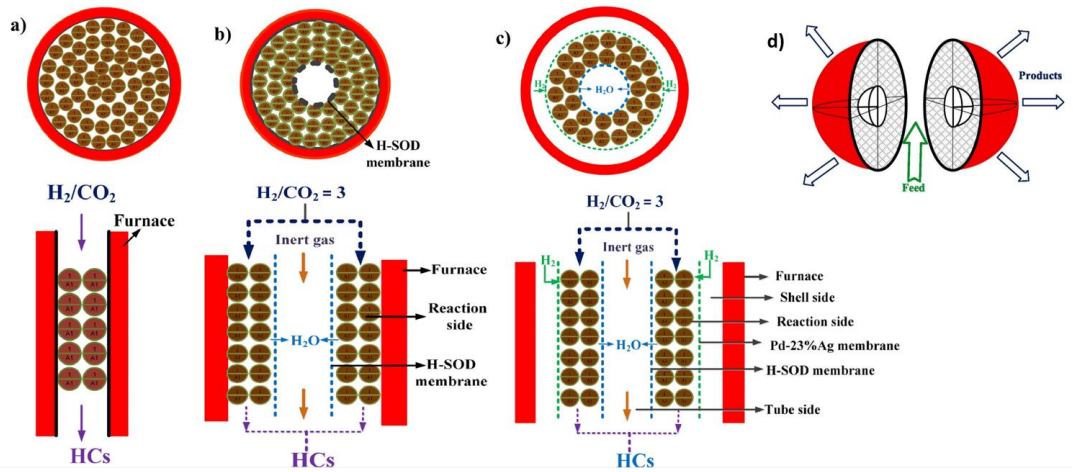

Figure 7. a) Schematic diagram of Fixed-bed b) Annular H_2O perm-selective c) Annular H_2 and H_2O perm-selective d) Spherical packed-bed.

3.2 Mathematical modeling

This study presents a mathematical model for a vertical reactor with three distinct parts based on the kinetic data from a previous study [46]. The first section, or shell, introduces H_2, which permeates through a Pd-based membrane to the reaction compartment. The goal of using this type of reactor is to counteract the loss of H_2 during H_2O removal, which would otherwise cause large temperature fluctuations in the reactor. The second section is where the RWGS and FT reactions take place simultaneously. The third section is a tube containing a sweep gas that removes water from the reaction side through a zeolitic membrane. **Figure 7** provides a schematic illustration of all types of reactors.

The mathematical model of the proposed reactor configuration is based on the following assumptions:

All gases are assumed to be ideal.

Condition of constant state.

In comparison to convective heat transfer, conductive heat transmission is negligible.

Constant furnace temperature

One-dimensional plug flow reactor

The H-SOD membrane has excellent water selectivity.

The furnace heats up the reactor at a consistent temperature that matches the initial temperature of the feed, providing the necessary heat to initiate the endothermic RWGS reaction. Both the endothermic RWGS and exothermic FT reactions occur simultaneously within the reactor. The mass and energy balances for each side are outlined below.

3.2.1 Annular reactor

3.2.1.1 Shell side

Mass balance:

$$\frac{1}{A_{csh}}\frac{dy_{H_2}^{sh}}{dz} = -\Delta t\frac{N_{H_2}}{v_{sh}}A_{sh}\left(\left(P_{H_2}^{sh}\right)^{0.5} - \left(P_{H_2}^{r}\right)^{0.5}\right) \quad (1)$$

where $y_{H_2}^{sh}$ is the mole fraction of hydrogen in the shell side. $P_{H_2}^{sh}$ and $P_{H_2}^{r}$ are partial pressures of hydrogen in the shell and reactor, respectively. Hydrogen permeance (N_{H_2}) is considered temperature-dependent and is presented as follows [44]:

$$\frac{N_{H_2}}{\delta} = 8.686 \times 10^{-6} \exp\left(-\frac{10300}{8.31 T_{avg}} \right) \tag{2}$$

$$T_{avg} = \left(\frac{T^{sh} + T^{r}}{2} \right) \tag{3}$$

Energy balance:

$$\frac{1}{A_{csh}} \frac{dT^{sh}}{dz} = \frac{\Delta t}{f_{sh} C p_{sh}} \left[(UA)_{sh} (T^{f} - T^{sh}) + \frac{N_{H_2}}{v_r} A_{lsh} \left(\left(P_{H_2}^{sh} \right)^{0.5} - \left(P_{H_2}^{r} \right)^{0.5} \right) C_{PH_2} (T^{sh} - T^{r}) \right] \tag{4}$$

Eq. (4) includes heat transfer between shell, furnace, and reactor along with the heat of permeated H_2 from the shell.

3.2.1.2 Reaction side

Mass balance:

$$\frac{1}{A_{cr}} \frac{dy_{H_2}^{r}}{dz} = -\Delta t \left[(1 - \varepsilon_b) \rho_B (\eta_1 r_1 + 3\eta_2 r_2 + 4\eta_3 r_3 + 5\eta_4 r_4 + 6\eta_5 r_5 + 7\eta_6 r_6 + 8\eta_7 r_7 + 9\eta_8 r_8 + \eta_9 r_9) - \frac{N_{H_2}}{v_{sh}} A_{lsh} \left(\left(P_{H_2}^{sh} \right)^{0.5} - \left(P_{H_2}^{r} \right)^{0.5} \right) \right] \tag{5}$$

$$\frac{1}{A_{cr}} \frac{dy_{CO_2}^{r}}{dz} = -\Delta t (1 - \varepsilon_b) \rho_B (\eta_1 r_1 + \eta_9 r_9) \tag{6}$$

$$\frac{1}{A_{cr}} \frac{dy_{CO}^{r}}{dz} = \Delta t (1 - \varepsilon_b) \rho_B (\eta_1 r_1 - \eta_2 r_2 - 2\eta_3 r_3 - 2\eta_4 r_4 - 3\eta_5 r_5 - 3\eta_6 r_6 - 4\eta_7 r_7 - 4\eta_8 r_8) \tag{7}$$

$$\frac{1}{A_{cr}} \frac{dy_{CH_4}^{r}}{dz} = \Delta t (1 - \varepsilon_b) \rho_B (\eta_2 r_2) \tag{8}$$

$$\frac{1}{A_{cr}}\frac{dy^r_{C_2H_4}}{dz} = \Delta t(1-\varepsilon_b)\rho_B(\eta_3 r_3) \tag{9}$$

$$\frac{1}{A_{cr}}\frac{dy^r_{C_2H_6}}{dz} = \Delta t(1-\varepsilon_b)\rho_B(\eta_4 r_4) \tag{10}$$

$$\frac{1}{A_{cr}}\frac{dy^r_{C_3H_6}}{dz} = \Delta t(1-\varepsilon_b)\rho_B(\eta_5 r_5) \tag{11}$$

$$\frac{1}{A_{cr}}\frac{dy^r_{C_3H_8}}{dz} = \Delta t(1-\varepsilon_b)\rho_B(\eta_6 r_6) \tag{12}$$

$$\frac{1}{A_{cr}}\frac{dy^r_{C_4H_8}}{dz} = \Delta t(1-\varepsilon_b)\rho_B(\eta_7 r_7) \tag{13}$$

$$\frac{1}{A_{cr}}\frac{dy^r_{C_4H_{10}}}{dz} = \Delta t(1-\varepsilon_b)\rho_B(\eta_8 r_8) \tag{14}$$

$$\begin{aligned}\frac{1}{A_{cr}}\frac{dy^r_{H_2O}}{dz} = \Delta t\Big[&(1-\varepsilon_b)\rho_B(\eta_1 r_1 + \eta_2 r_2 + 2\eta_3 r_3 + 2\eta_4 r_4 + 3\eta_5 r_5 \\ &+ 3\eta_6 r_6 + 4\eta_7 r_7 + 4\eta_8 r_8 + \eta_9 r_9) \\ &- \frac{N_{H_2O}}{v_r}A_{lt}\left(P^r_{H_2O} - P^t_{H_2O}\right)\Big]\end{aligned} \tag{15}$$

The mole fractions of these components in the reactor are represented by y_i^r (i= CH_4, C_2H_4, C_2H_6, C_3H_6, C_3H_8, C_4H_8, C_4H_{10}). The reaction is affected by two factors: the reaction rate, represented by r_i, and the effectiveness factor, represented by η_i. The partial pressures of water in the tube and reactor are denoted as $P^t_{H_2O}$, and $P^r_{H_2O}$. Additionally, the water permeance, represented by N_{H_2O}, which measures the amount of water that passes through the H-SOD membrane. In zeolite-based membranes, this measurement is typically between 10^{-7} and 10^{-6} mol. s^{-1} m^{-2} Pa^{-1}. [45].

Energy balance:

$$Q^r = \sum_{i=1}^{9} \eta_i r_i \Delta H_{f_i} \tag{16}$$

$$\frac{1}{A_{cr}}\frac{dT^r}{dz} = \frac{\Delta t}{f_r Cp_r}\Bigg((1-\varepsilon_b)\rho_B Q^r + (UA)_r(T^{sh}-T^r) - (UA)_t(T^r-T^t) + \frac{N_{H_2}}{v_{sh}}A_{lsh}\left(\left(P_{H_2}^{sh}\right)^{0.5}-\left(P_{H_2}^{r}\right)^{0.5}\right)Cp_{H_2}(T^{sh}-T^r) - \frac{N_{H_2O}}{v_r}A_{lt}\left(P_{H_2O}^{r}-P_{H_2O}^{t}\right)Cp_{H_2O}(T^r-T^t)\Bigg) \quad (17)$$

Eq. (17) comprises heat transfer between reactor, tube and shell along with the heat of permeated hydrogen from the tube and removed water from the reactor to the shell.

3.2.1.3 Tube side

Mass balance:

$$\frac{1}{A_{ct}}\frac{dy_{H_2O}^t}{dz} = \Delta t\frac{N_{H_2O}}{v_r}A_{lt}\left(P_{H_2O}^{r}-P_{H_2O}^{t}\right) \quad (18)$$

Energy balance:

$$\frac{1}{A_{ct}}\frac{dT^t}{dz} = \frac{\Delta t}{f_t Cp_t}\left[(UA)_t - \frac{N_{H_2O}}{v_r}A_{lt}\left(P_{H_2O}^{r}-P_{H_2O}^{t}\right)C_{PH_2O}\right](T^r-T^t) \quad (19)$$

The heat of the penetrated water from the reactor and the heat transfer between the reactor and the tube are shown **in Eq (19).** The following definitions apply to pressure ratio (φ) and sweep ratio (θ):

$$\varphi = \frac{P}{P_t} \quad (20)$$

$$\theta = \frac{f_t}{f_{sh}} \quad (21)$$

The **supplementary section** of our recent study describes the necessary parameters, physical properties, and auxiliary equations to determine surface concentrations [46]. The governing equations are derived and solved employing the Rung-Kutta technique (ode15s) in MATLAB.

3.2.2 Axial spherical reactor

The feed is introduced into the reactor from the top in this mathematical model, like many industrial processes. However, the limited cross-sectional area of the entrance and outlet can lead to significant pressure drops. To prevent this issue, two grids are used to hold the catalysts near the inlet and outlet of the reactor (as shown in **Figure 8**.). These catalysts facilitate the chemical reaction and increase the process's efficiency. By regulating the feed flow through the reactor with the grids, the pressure drop remains within acceptable limits. Additionally, the grids help prevent the catalysts from being carried away by the flow of feed, which could cause blockages and other problems downstream, leading to costly downtime and repairs.

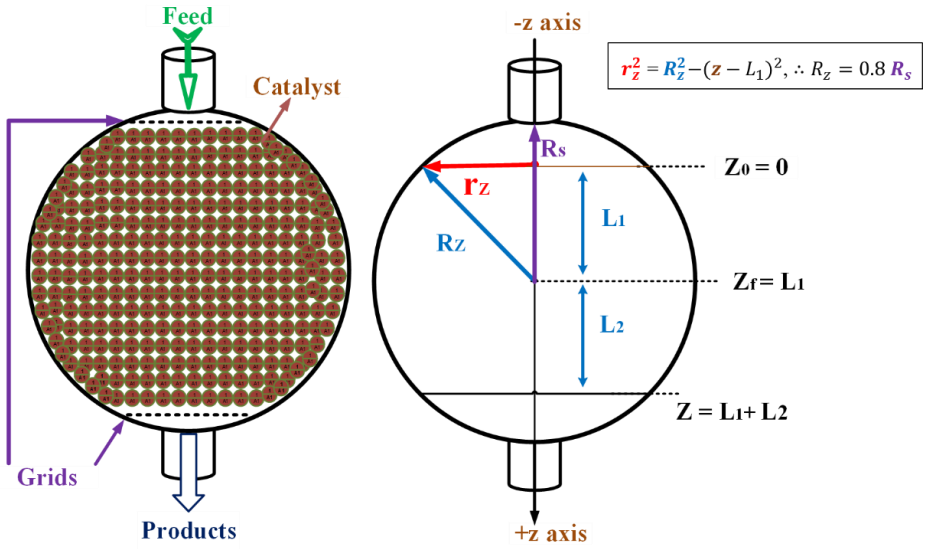

Figure 8. Schematic diagram of an axial flow spherical reactor (AFSR).

Eqs. (22), **(23)** and **(24)** depict the species balance, heat balance, and pressure drop over the AFSR. In this configuration, as shown in **Eq. (25)**, the cross-sectional area varies with length, or z.

$$\frac{dC_i}{dz} = \frac{1}{u_z}\left[\rho_p(1-\varepsilon_b)r_i - \frac{C_i}{A_z}\left(A_z\frac{du_z}{dz} + u_z\frac{dA_z}{dz}\right)\right] \tag{22}$$

$$\frac{dT}{dz} = \frac{1}{C_t\, C_{pg}\, u_z}\left(\sum_{j=1}^{9} \rho_p(1-\varepsilon_b)\, r_j(-\Delta H_{f,j}) + \frac{2\pi r_z U_z}{A_z}\left(T_j - T\right) - \frac{C_{pg}}{A_z}\left(u_z A_z T\frac{dC_t}{dz} + C_t T\frac{d(A_z u_z)}{dz}\right)\right) \quad (23)$$

$$\frac{dP}{dz} = -\left[150\frac{(1-\varepsilon_b)^2 \mu_g\, V_s}{{\varepsilon_b}^3 {d_p}^2\, {A_z}^2} + 1.75\frac{(1-\varepsilon_b)\,\rho_g\, V_s^2}{{\varepsilon_b}^3 d_p\, {A_z}^2}\right] \quad (24)$$

$$A_z = \pi\left[{R_z}^2 - (z-L_1)^2\right] \;,\; L_1 = L_2 \quad (25)$$

$$u_z = \frac{V_s}{\varepsilon_b A_z} \quad (26)$$

The variables r_z and A_z represent the radius and cross-sectional area of the AFSR, respectively, while U_z denotes the heat transfer coefficient between the jacket and AFSR. V_s and u_z indicate volumetric flow rate, and the velocity in AFSR respectively. **Figure 8** displays the geometries of the AFSR, and therefore, the radius and surface area of the reactor can be calculated using the information provided in **Eq. (25).**

3.2.3 Radial spherical reactor

This mathematical model assumes that the feed enters the reactor from the center, and two potential locations for the jacket (either inside or outside) are taken into account, as shown in **Figure 9 (a)** and **(b).**

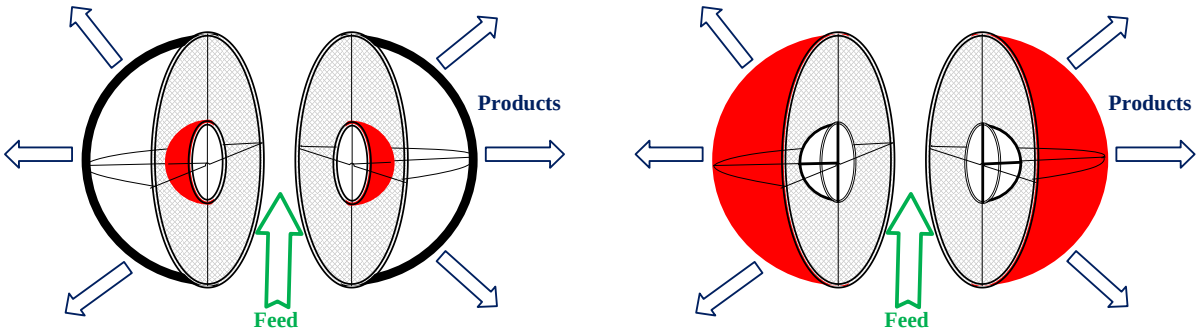

(a) **(b)**

Figure 9. Radial flow spherical reactor (RFSR) schematics showing **(a)** the inner jacket and **(b)** the outer jacket (The radii of the inner and outer spheres are Ri and Ro, respectively, and Ri = 0.2 Ro).

Eqs. (27), **(28)**, and **(29)** represent the species balance, heat balance, and pressure drop across the AFSR, respectively. Additionally, the cross-sectional area changes with the diameter, r, in this theoretical model, as indicated in **Eq. (30).**

$$\frac{dC_i}{dr} = \frac{1}{u_r}\left[\rho_p(1-\varepsilon_b)r_i - \frac{C_i}{A_r}\left(A_r\frac{du_r}{dr} + u_r\frac{dA_r}{dr}\right)\right] \tag{27}$$

$$\frac{dT}{dr} = \frac{1}{C_t\, C_{pg}\, u_r}\left(\sum_{j=1}^{9}\rho_p(1-\varepsilon_b)\, r_j(-\Delta H_{f,j}) + \frac{8\pi r U_r}{A_r}(T_j - T)\right. \tag{28}$$

$$\left. - \frac{C_{pg}}{A_r}\left(u_r A_r T\frac{dC_t}{dr} + C_t T\frac{d(A_r u_r)}{dr}\right)\right)$$

$$\frac{dP}{dr} = -\left[150\frac{(1-\varepsilon_b)^2\mu_g\, V_s}{{\varepsilon_b}^3 {d_p}^2\, {A_r}} + 1.75\frac{(1-\varepsilon_b)\,\rho_g\, {V_s}^2}{{\varepsilon_b}^3 d_p\, {A_r}^2}\right] \tag{29}$$

$$A_r = 4\pi r^2 \tag{30}$$

$$u_r = \frac{V_s}{\varepsilon_b A_r} \tag{31}$$

where the variables r and A_r denote the radius and cross-sectional area of the RFSR, respectively, while U_r represents the heat transfer coefficient between the jacket and RFSR, and u_r indicates the velocity in the RFSR. The necessary correlations and auxiliary equations are provided in Appendix A of our recent publication [47].

3.3 Exploited algorithms and analysis

3.3.1 Artificial Bee Colony (ABC) algorithm

This section introduces an optimization method that mimics chemical reactions found in nature. The algorithm uses exploiting and exploring mechanisms in combination with an elitist survival strategy to prevent the algorithm from getting stuck in local optima. The chemical reaction algorithm was evaluated on a set of complex benchmark functions and compared to other optimization algorithms. The results showed that the algorithm was able to reach near-optimal values for some functions and outperformed previously established models. However, further tests are needed to compare the algorithm against other established methods that are known to seek good solutions for larger dimensions [48].

The goal of this process is to minimize errors in simulations by creating an objective function (O.F.) that can be effectively optimized. Previous efforts used conventional optimization methods like multivariable regression, gradient-based optimization techniques, coordinate transformation, simplex, and others. However, these methods had a tendency to get stuck in local optima, which are areas of relatively low performance. This shows the need for additional methods that can find more robust solutions.

The ABC algorithm was proposed by Karaboga to optimize numerical problems by simulating the foraging behavior of honey bee swarms [49]. The ABC Algorithm is a search algorithm that uses three types of bees: employed bees, onlookers, and scouts. Employed bees are responsible for finding good solutions to the optimization problem at hand. Each employed bee is associated with a solution in the search space, and it evaluates the quality of its solution using an objective function. Employed bees exchange information with each other by exploiting their best solutions using a local search operator. Onlooker bees are responsible for choosing good solutions from the employed bees. Onlookers select an employed bee to follow based on the quality of its solution, which is determined by the objective function. The onlooker bees also use a stochastic selection operator to choose the employed bees. Scout bees are responsible for exploring new regions of the search space. Scouts

randomly generate new solutions, and if a new solution is better than the ones currently known to the colony, it becomes an employed bee. The scouts help prevent the colony from becoming stuck in local optima (**Figure 10**). The quality of a solution is determined by the nectar content of the corresponding food source. The number of employed bees is equal to the number of food sources being exploited at the moment. The algorithm iterates between these three phases until it meets a stopping criterion. The algorithm is explained in more detail in a recent publication (**Appendix B, B.1**), which includes a flowchart of the ABC algorithm.

Figure 10. Schematic of the ABC algorithm flowchart [49].

3.3.2 Differential Evolution (DE) algorithm

The DE algorithm is a type of population-based algorithm that bears some resemblance to the genetic algorithm. Both algorithms utilize three key operators:

mutation, crossover, and selection. However, the primary difference between the two lies in how they create more optimal solutions. Genetic algorithms rely on crossover, while DE relies on mutation operations. Specifically, DE generates mutations by calculating the differences between randomly selected pairs of solutions within the population. **Figure 11(a)** depicts how the DE algorithm works. It employs the mutation operation to look for potential solutions and the selection operator to guide the search towards likely regions in the search space. To generate child vector parameters, the DE algorithm utilizes non-uniform crossover, which typically involves using one parent more than others. By combining elements from the current population to create trial vectors, the recombination (crossover) operator is able to effectively rearrange data into promising combinations, making it easier to search for better solutions. [52].

In the DE algorithm, a set of solution vectors that are close to optimal is randomly generated to start with. These vectors are then improved by utilizing the mutation, crossover, and selection operators. **Figure 11(b)** illustrates the flowchart of the DE algorithm, which includes all these key stages. For a more comprehensive explanation of the DE algorithm, please refer to our recent publication (**Appendix B, B.2**) [48].

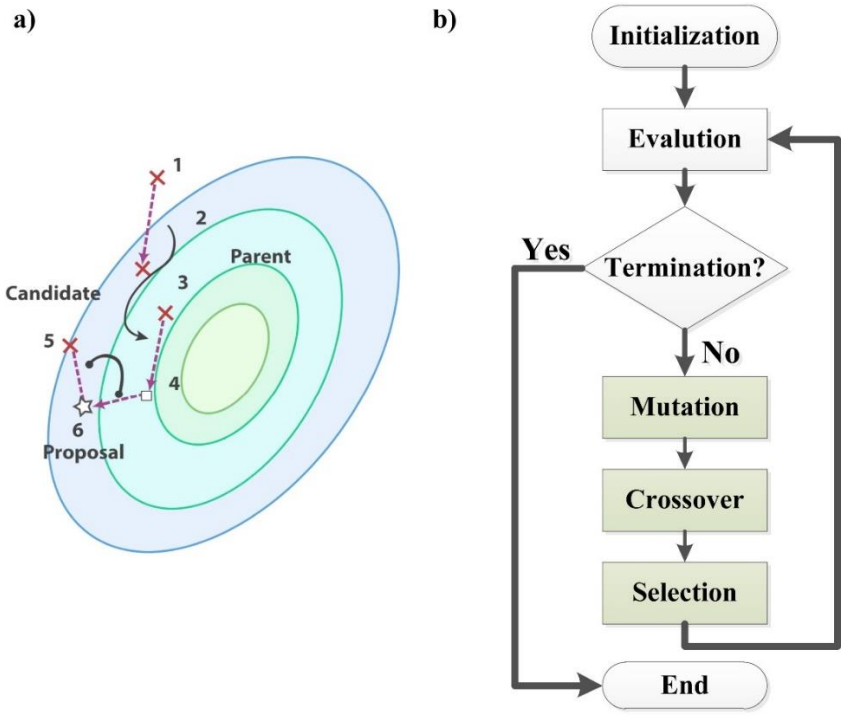

Figure 11. a) A pattern for discovering a new proposal in the DE algorithm and b) schematic diagram of flowchart [48].

3.3.3 Dragonfly algorithm

The dragonfly algorithm (DA), a type of swarm intelligence (SI) algorithm [50], is used to estimate the kinetic parameters [51]. The effectiveness of SI-based algorithms in scientific and industrial optimization problems indicates their practical benefits. Compared to evolutionary algorithms (EA), DA and other SI-based methods retain information about the search space during optimization, employ fewer controlling parameters and operators, and are flexible enough to be used in various fields. The DA algorithm draws inspiration from the static and dynamic behaviors of swarming, which correspond to the exploration and exploitation phases of optimization, respectively. In static swarms, small sub-swarms of dragonflies explore short distances, while in dynamic swarms, larger populations of dragonflies move in a coordinated direction for exploitation. The optimization process of DA starts with generating random sets of solutions and using random values to initialize the position and step vectors within the variable's bounds. During each iteration, equations are used to update the position and step for each dragonfly. The neighborhood of each dragonfly is determined by calculating the Euclidean distance between all dragonflies and selecting N of them to update the vectors of X and ΔX. The position updating is repeated iteratively until the criterion is met [51].

As a result, the root mean square error (RMSE), which measures the discrepancy between model predictions ($Y_{model,i}$) and experimental data ($Y_{exp,i}$), may be used to estimate the kinetic parameters. This objective function is described by **Eq (32)**.

$$\boldsymbol{O.F} = Min\left(\sqrt{\frac{\sum_{i=1}^{N}\left(Y_{exp,i} - Y_{model,i}\right)^2}{N}}\right) \tag{32}$$

3.3.4 Statistical analysis

Sensitivity analysis is a useful tool for obtaining information about the relationships between process variables. Statistical methods can be employed to achieve this goal and assess the significant interactions between parameters. This approach can help identify the optimum input variables needed to achieve the desired responses [52-54]. A full factorial design is a powerful statistical method that can be used to study the effects of all possible interacting parameters on process outputs [55].

In this study, a two-level factorial design is used with five variables, including reactor temperature (Tr:A), shell temperature (Ts:B), tube temperature (Tt:C), sweep ratio (θ:D), reactor to tube pressure ratio (φ1:E) and shell to reactor pressure ratio (φ2:F). The responses are the yields of different compounds, which are obtained based on the 25 factorial design. After the primary analysis of the 64 runs, the shell-to-reactor pressure ratio was found to be of negligible significance and was removed from further analysis. The analysis of variance (ANOVA) test was used to validate the statistical analysis, with p-values indicating the significance of the effects. Variables with p-values less than 0.05 were considered very significant, while those with p-values higher than 0.1 were of negligible importance. Additionally, the determination coefficient (R^2) was used to assess the appropriateness of the multivariable model, with higher R^2 values indicating a better fit. The range of input variables is presented in **Table 1** [46].

Table 1. Independent variables and their levels based on factorial design [46].

Independent variables	**Low level**	**High level**
Tube temperature (°C)	25	325
Shell temperature (°C)	25	325
Reactor temperature (°C)	300	325
Pressure ratio	1	8
Sweep ratio	1	8

4. Result and discussion

4.1 Comparison between the ABC and DE algorithms

To assess the accuracy of the ABC and DE algorithms, their predicted results for the conversion of H_2 and CO_2 and product distribution were compared with experimental test results. The low conversion rate of CO_2, denoted as XCO_2, can be attributed to its chemical and thermodynamic stability, making it a challenging feedstock. The CO_2 must first be converted to CO through the RWGS reaction before being converted to hydrocarbons through the FT reaction, while hydrogen is needed for both reactions.

It should be noted that the results presented in this study are based on the model that estimates kinetic parameters to minimize errors between predicted and experimental hydrocarbon yields. However, the model does not include certain non-idealities such as catalyst deactivation or other parameters that can affect the reduction of CO_2 conversion. The Boudouard reaction, which causes coke formation and can hamper the formation of hydrocarbons, was not considered in the model since the temperature was below 633 K. Additionally, the accuracy of the ABC algorithm is highly dependent on the initial guess and the defined upper and lower bounds of variables, which were set based on data reported in a previous study [3]. It should be noted that the kinetic parameters of the FT reactions were estimated for only one hydrocarbon product in the previous study [3], whereas this study considered seven hydrocarbon products. Therefore, deviations from the ideal model are expected, but the product distribution is in agreement with trends reported in the literature [48]. The high errors observed with the DE algorithm are due to its inefficiency compared to the ABC algorithm, which generally produces lower relative errors (**Figure 12)**.

The outcomes of the simulation using the kinetic parameters estimated by the ABC and DE techniques are contrasted with previously published experimental results from seven different studies, labeled A to H in our recent article [48]. These codes specify the catalyst and reaction conditions used in each experiment and are displayed in **Figure 13**.

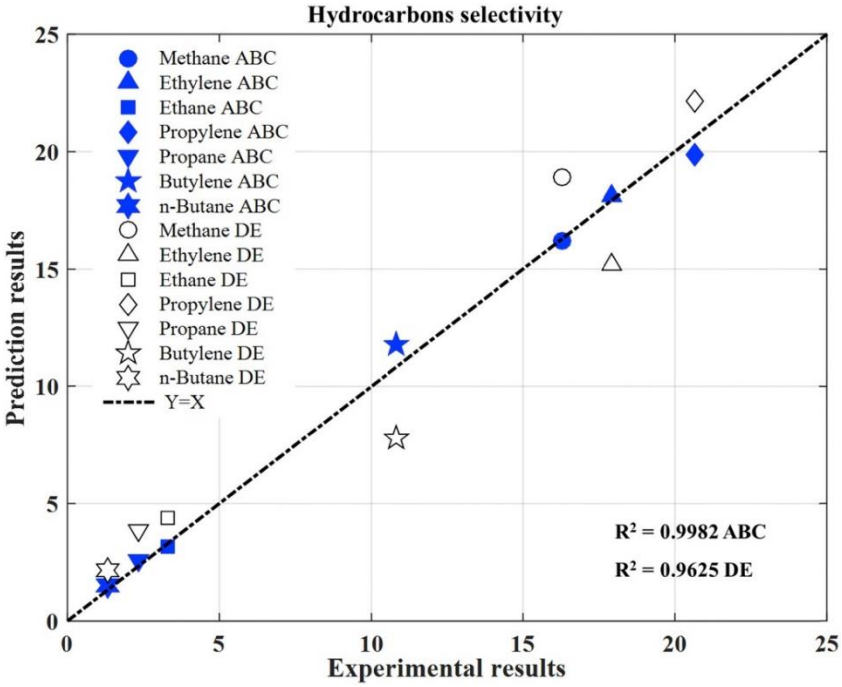

Figure 12. Comparison of two optimization algorithms (ABC and DE) in terms of hydrocarbon selectivity.

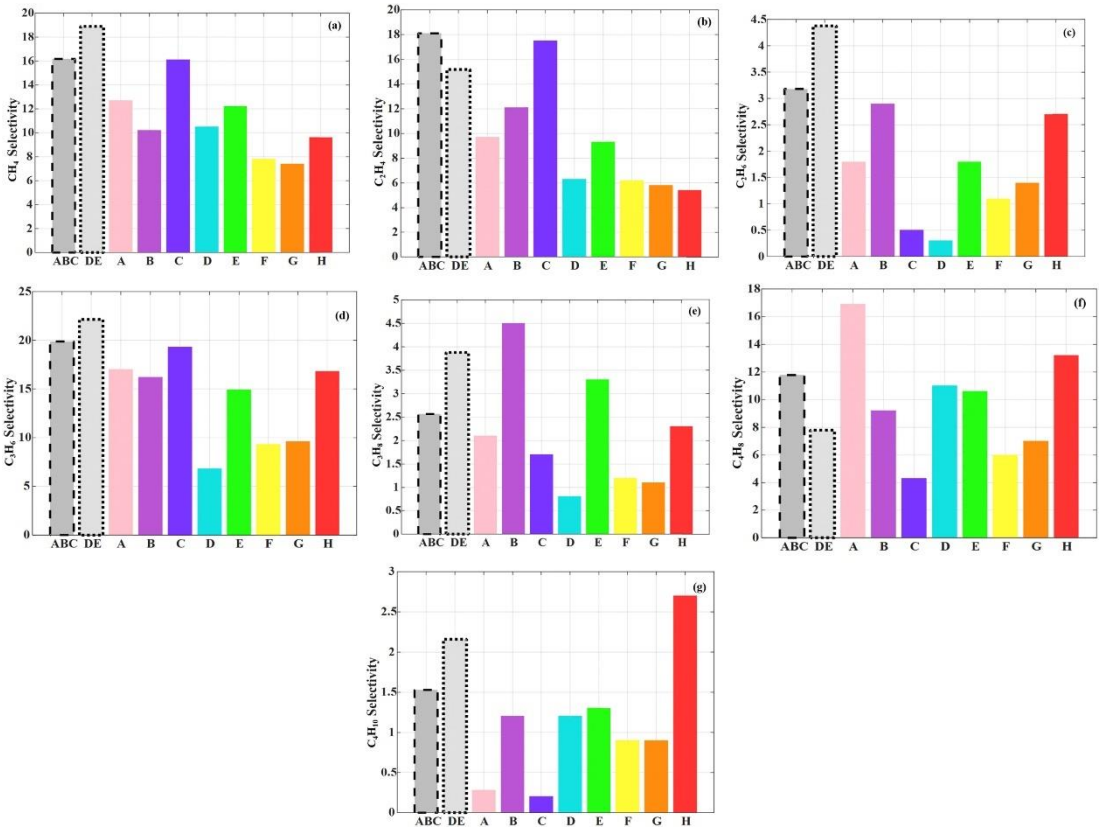

Figure 13. Comparison of literature data and modeling for various hydrocarbon selectivity of (a) methane, (b) ethylene, (c) ethane, (d) propylene, (e) propane, (f) butylene, and (g) butane.

4.2 Effects of operating conditions

The effects of three main operating conditions (temperature, pressure, and space velocity) have been investigated on the production of various kinds of hydrocarbons through hydrogenation of CO_2. This work may help to further understand how the reaction process works and help guide future efforts to improve hydrogenation-based processes and their applications in producing chemical and fuel products as follows:

4.2.1 Influence of temperature

It was indicated that the effect of operating conditions on hydrocarbon production efficiency is of great importance. According to the temperature dependencies of the reaction rates, product distributions change with temperature. The trajectories of hydrocarbons yield in terms of 100 × (mol/mol feed) along the reactor length are presented in **Figure 14 (a) to 14 (g)** as temperature changes from 300 to 350 °C. It can be observed that the trend of each component yield with temperature alterations differs from each other, which can be attributed to the nature of the reactions, which in turn are influenced by the determined kinetic parameters [46]. Generally, **Figure 14 (a) to 14 (g)** illustrate that hydrocarbon production increases sharply for all components at the reactor entrance, which is refereed to CO production via RWGS reaction, then slightly increases in the rest of the reactor, and finally remains constant due to gradually finishing CO and the equilibrium limitations of RWGS reaction. Although this trend is almost the same for all components at a distinct temperature, the influence of temperature is different for each one, which is shown with different arrows.

To offer a more comprehensive analysis of how temperature affects hydrocarbon distribution, **Figure. 15** show the final hydrocarbon yield at the reactor outlet (L = 0.6 m) and the extent to which they deviate from the values observed at 300 °C. According to **Figure 15**, yields of C_2H_4, C_2H_6 and C_3H_6 increase as the temperature rises, while those of CH_4, C_3H_8, C_4H_{10} and C_4H_8 decrease.

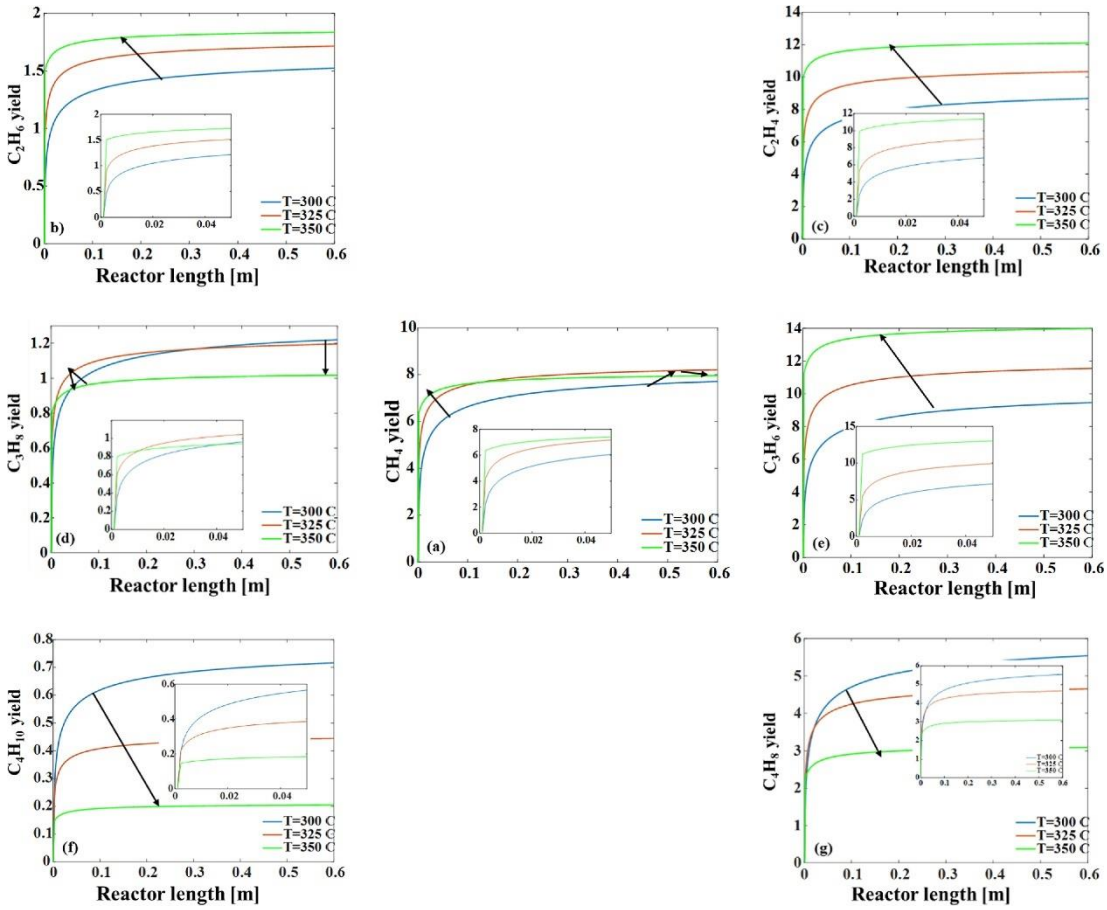

Figure 14. Hydrocarbons yield along the reactor length at various temperatures after 24 h at 1 MPa.

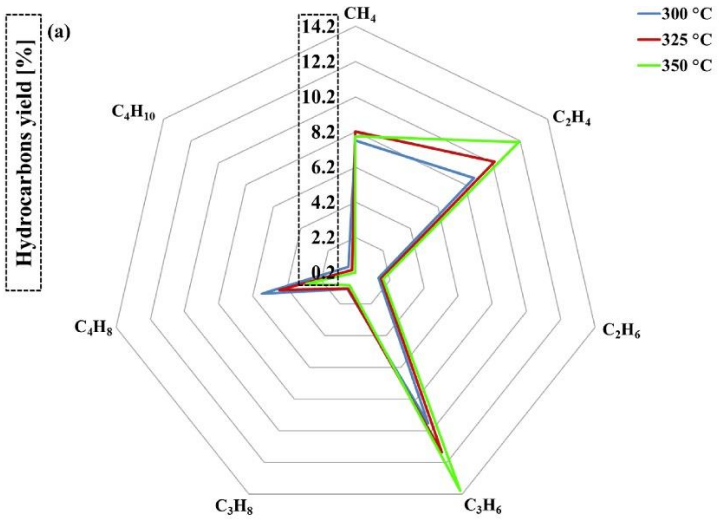

Figure 15

Effect of temperature on hydrocarbons yield at the reactor outlet at different temperatures with respect to T = 300 °C at 1 MPa.

It can be inferred that temperature rise has a positive effect on the production of light olefins (i.e., C_2H_4 and C_3H_6) while imposing an inverse effect on the yields of heavier components in the range of 300–350 °C, which can also be observed in **Figure 14**. The experimental investigations of Riedel et al. [3] also guided that products included 90% of primary olefins when temperature increased, and at higher temperatures (about 400 °C), the formation of long-chain and heavier hydrocarbons was not the dominant trend. Besides, CH_4 is the only light hydrocarbon that undergoes a reduction in yield with temperature increases. The same trend for CH4 formation was also addressed by Owen et al. [56] between 230 and 330 °C. They observed high CH_4 selectivity at low temperatures, while at high temperatures, product distribution shifted to C_{2+} hydrocarbons. This fact is more pronounced in **Figure 16**, which depicts the olefins and paraffins yield as a function of their carbon number. However, the economic issues and the catalyst deactivation related to the temperature increase should also be considered in order to find the optimum temperature.
It can be observed that, in contrast to light hydrocarbons with 2 carbons, the yield of hydrocarbons with 4 carbons experiences a considerable decrease as temperature elevates to 350 °C. However, saturated and unsaturated hydrocarbons with 3 carbons behave differently with temperature increase, and the olefin (C_3H_6) yield increases sharply contrary to that of its corresponding paraffin (C_3H_8).

Indeed, the breakage of the carbon-carbon chain (cracking effect) seems to be serious at high temperatures, leading to a higher CH_4 concentration in the product. It should be mentioned that the above explanations are valid for the proposed model, disregarding catalyst deactivation since our range of study is less than 360 °C. However, at elevated temperatures, the dependence of hydrocarbon yield on temperature is not so obvious in the compromise between a higher driving force in activity and a larger tendency of deactivation due to inert carbon deposition. In other words, the enhancement of temperature leads to higher CO_2 sorption while facilitating the elimination of hydrogen in the terminals of carbon–carbon compounds. This can highly increase the growth of carbon chains on the surface and consequently distort the reaction pathway to the Boudouard reaction. Therefore, hydrogen concentration should be adjusted appropriately to avoid this phenomenon.

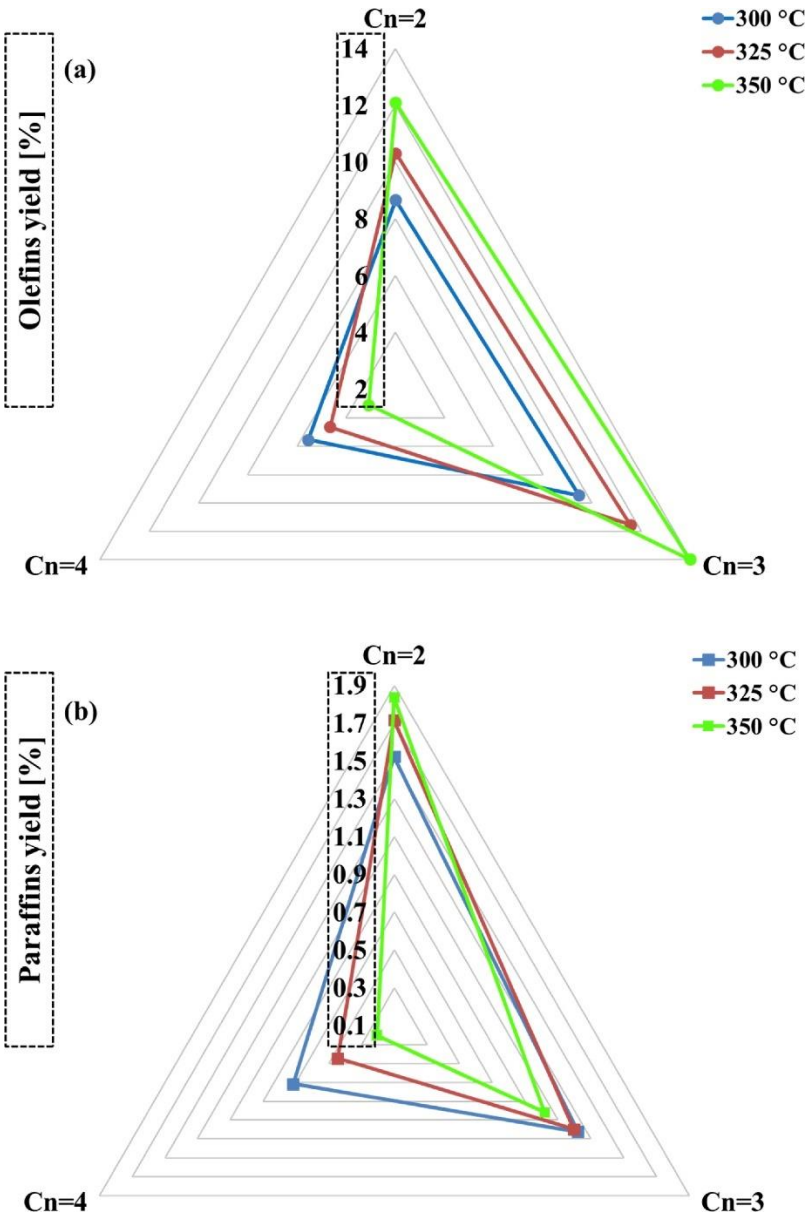

Figure 16. Effect of temperature on the yield of (a) olefins and (b) paraffins at 1 MPa.

4.2.2 Influence of pressure

Since the RWGS reaction is reversible, the pressure elevation should have no effect on CO_2 conversion unless the CO produced via the RWGS reaction is subsequently consumed by the FT reaction. Regarding the dependencies of the reaction rates on the partial pressures of components, product distribution has various trends. The yields of hydrocarbons at the reactor outlet (L = 0.6 m) are presented in **Figure 17** as pressure changes from 0.5 to 20 MPa. **Figure 17** demonstrates that hydrocarbons are produced according to the following order: C_3H_6> C_2H_4> CH_4> C_4H_8> C_2H_6> C_3H_8> and C_4H_{10} at all pressures, and pressure rise cannot alter this order. It can be observed that, at

higher pressures, especially 20 MPa, lighter olefins (C_3H_6 and C_2H_4) undergo a higher increase in their yields.

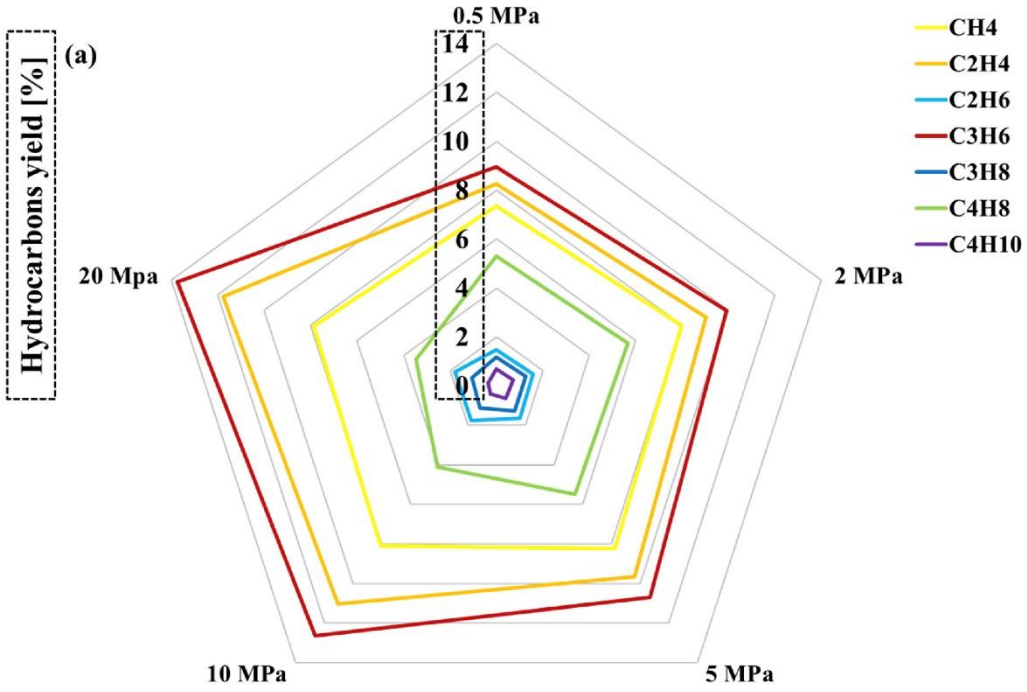

Figure 17. Effect of pressure on hydrocarbons yield at the reactor outlet.

Accordingly, pressure increases have a considerable positive effect on the yields of C_3H_6 and C_2H_4, which are light olefins. In contrast, pressure increases have an opposing impact on the yields of heavier hydrocarbons. Since hydrocarbons yield depends on both pressure and temperature, **Figure 18** is presented to demonstrate the interaction of these two important parameters on the total hydrocarbon yield.

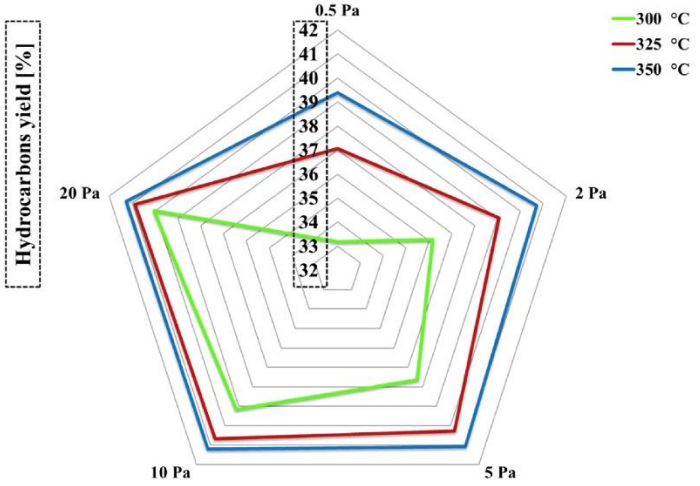

Figure 18. Effect of pressure at different temperatures on the total hydrocarbons yield at 1 MPa.

The impact of pressure on the overall hydrocarbon yield at various temperatures is illustrated in **Figure 18**. It is observed that lower temperatures are more sensitive to pressure changes, leading to a higher hydrocarbon yield. On the other hand, at higher temperatures, increasing pressure does not significantly improve the hydrocarbon yield.

4.2.3 Influence of space velocity

The effect of SV on CO and hydrocarbon yields at different temperatures is illustrated in **Figure 19**. It can be observed that at low temperatures, especially 300 °C, the decrease in hydrocarbon yield with an increase in SV is more remarkable compared to that at higher temperatures.

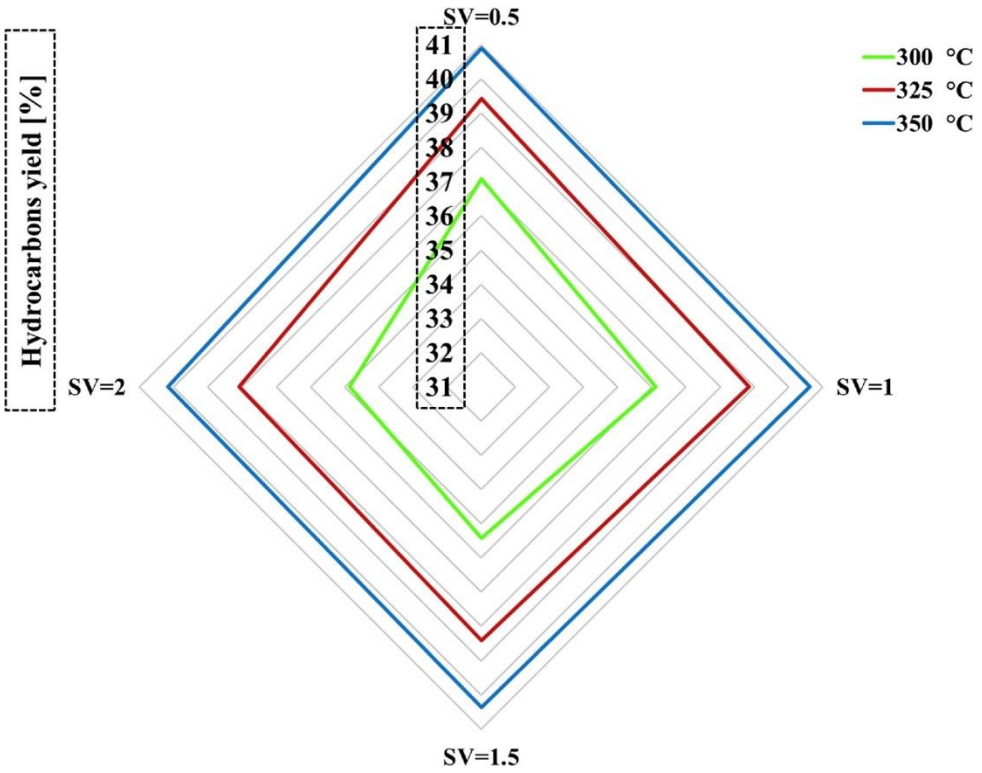

Figure 19. Effect of SV on hydrocarbons yield at different temperatures after 24 h at 1 MPa.

As explained in "Effect of Pressure" section, pressure plays an important role in hydrocarbons yield. Therefore, the influence of SV at different pressures are examined and results are illustrated in **Figure. 20**.

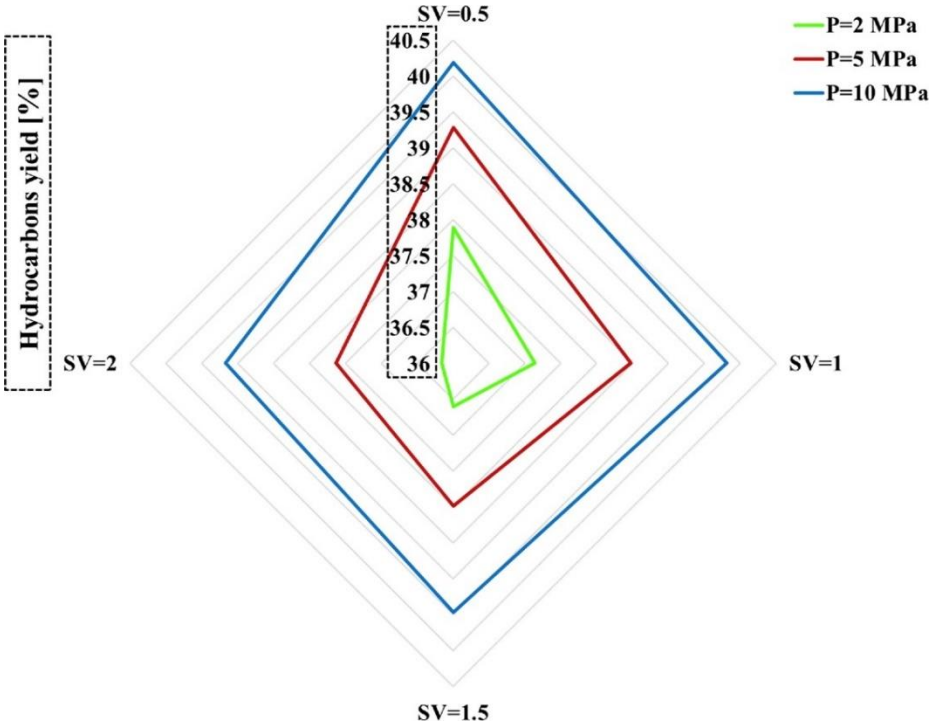

Figure 20. Effect of SV on hydrocarbons yield at different pressures after 24 h at 300 °C.

It can be observed in **Figure 20** that, in a distinct SV, pressure increase leads to enhanced hydrocarbon yield, and this increase is more considerable at higher SVs. Conversely, at a constant pressure, the yield of hydrocarbons decreases, particularly at higher SVs. Moreover, it can be inferred that the dependence on pressure decreases at higher SVs as the yield of hydrocarbons remains relatively constant compared to that at low pressure (P = 2 MPa).

4.3 Distribution of products in annular and membrane reactors

In this section, the results of modeling and literature reviews on the distribution of products in both an annular and membrane reactor have been compared. **Figures 21 (a)** and **21 (b)** display the patterns of CO and hydrocarbon yields in annular and membrane reactors, respectively. The production of hydrocarbons is more significant in membrane reactors, which have steeper slopes at the beginning than annular reactors. This is due to the in-situ removal of water, which results in higher CO_2 and CO consumption, as elaborated in the section that compares the performances of membrane and annular reactors. However, the order of the three primary products

(CH_4, C_2H_4, and C_3H_6) changes and differs from that in the annular reactor. This can be attributed to the kinetic parameters that correspond to the inhibiting effect of water, which was estimated for a fixed-bed reactor. In the presence of water in the annular reactor, the production of C_2H_4 and CH_4 is more restricted than that of C_3H_6. In other words, water plays a more dominant role in inhibiting the production of C_2H_4 and CH_4, and selective removal of water can alleviate this inhibition, leading to an increase in their yield. Our recently published articles discuss the impact of operating parameters such as temperature, pressure, and feed ratio on the performance of both membrane and annular reactors.

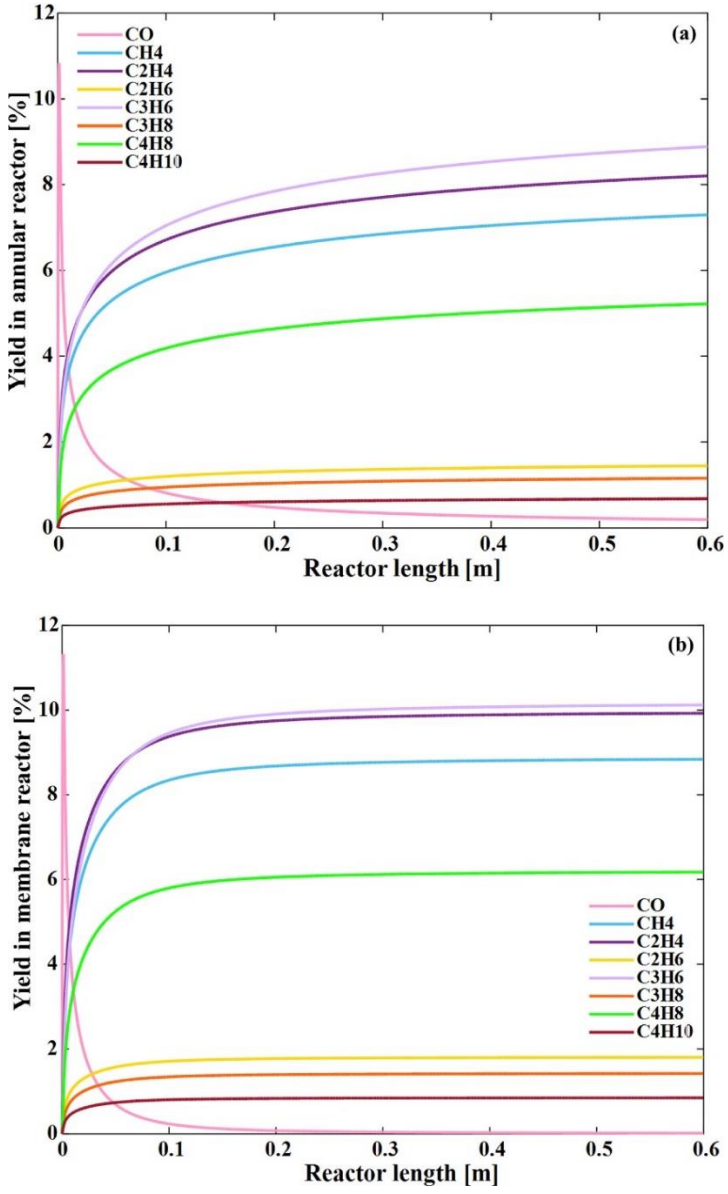

Figure 21. Distribution of products in (a) the annular reactor and (b) the membrane reactor in terms of yield.

Figures 22 (a) and **(b)** show a comparison of the yields of olefins and paraffins obtained from both reactors. It is evident that, like the annular reactor, the primary products are olefins rather than paraffins, although the increase in the yield of paraffins is more significant. Removing water to shift the equilibrium towards the right side of the RWGS reaction seems to have a more beneficial impact on the yields of paraffins than on the yields of olefins.

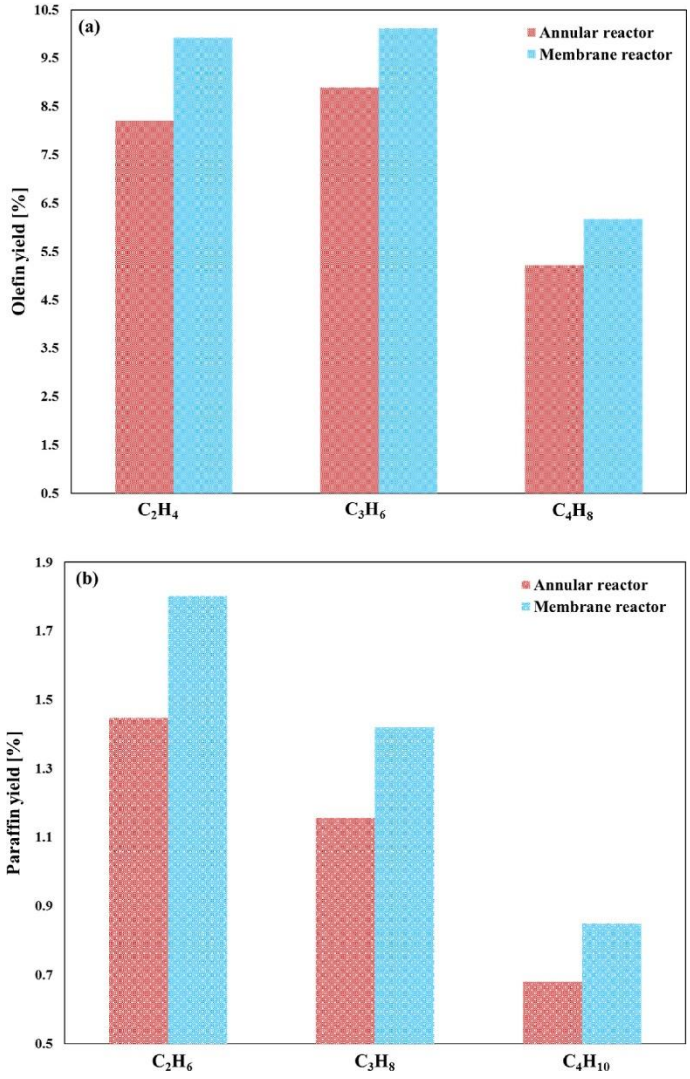

Figure 22. Comparison between the yields of annular and membrane reactors for (a) olefins and (b) paraffins.

4.4. Performance of cylindrical and spherical reactors

The cost-effectiveness and flexible operating conditions of spherical reactors have made them a popular choice for pilot or industrial reactors. According to a study, in order to evaluate the performance of different reactor types in CO_2 hydrogenation to

hydrocarbons, it is assumed that spherical reactors have the same volume and surface area as CR reactors, AFSR reactors, and RFSRs [13].

4.4.1 Axial flow spherical reactor (AFSR) performance

Figure 23 compares the CO_2 hydrogenation to hydrocarbon conversion capabilities of AFSR-1 and AFSR-2. It should be highlighted that the volume and surface area of both reactors AFSR-1 and 2 is the same as the conventional one.

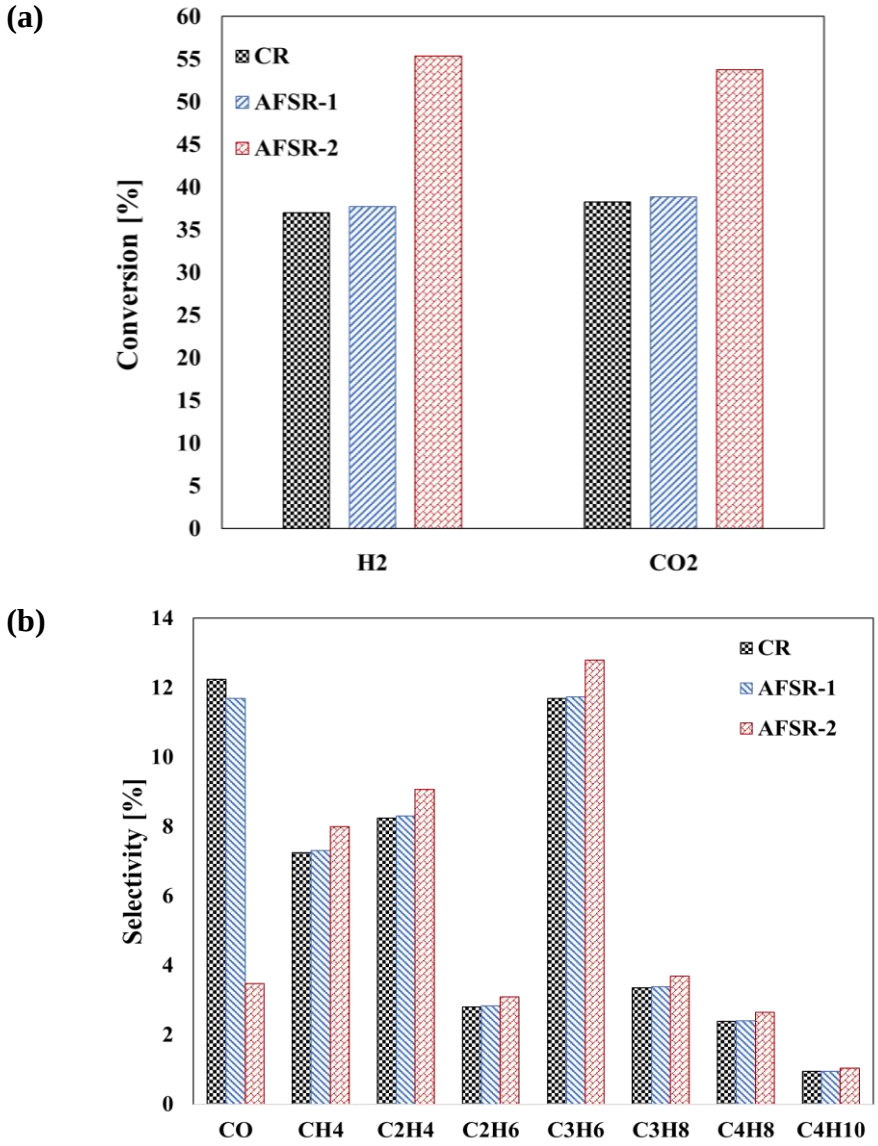

Figure 23 (a) conversions of reactants and b) distribution of products in AFSR-1, AFSR-2, and CR.

The AFSR-2 demonstrates better performance in terms of products distribution and conversion when compared to both CR and AFSR-1, however, there is little difference between AFSR-1 and CR. This highlights the importance of heat transfer surface area in this system by showing that the AFSR can only function properly if the spherical reactor's surface area (and not its volume) matches that of the CR. The exterior surface of the reactor (i.e., the reactor wall) that comes into contact with the jacket is referred to as the heat transfer surface area. A faster rate of heat transfer may be produced via a bigger surface area. More CO_2 conversion and, thus, greater CO production—which serves as the feed for the FT reaction—are produced by AFSR-2 because it has a bigger surface area than AFSR-1 and is therefore more easily able to supply the heat needed for the RWGS reaction. As seen in **Figure 24**, the increased conversions in AFSR-2 result in higher hydrocarbon yields.

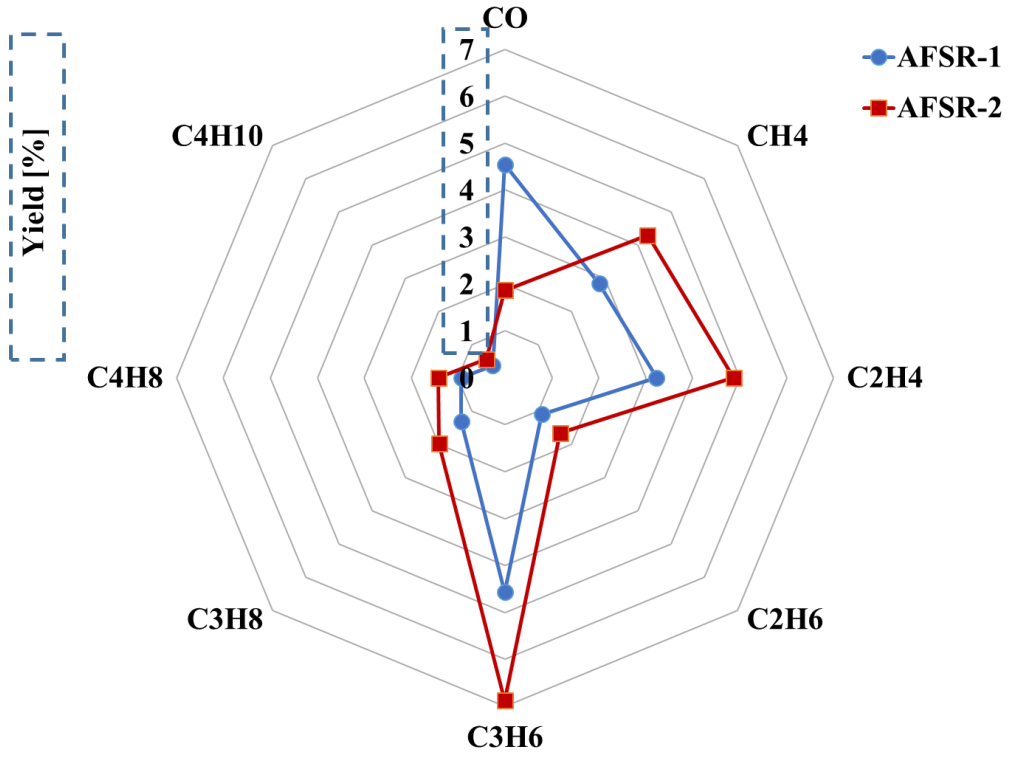

Figure 24 Evaluating the product yields in both reactor configurations, the AFSR-1 and AFSR-2.

Figure 24 shows that the CO yield in AFSR-2 is lower, indicating that AFSR-2's reaction rates for both CO generation and consumption are greater. This may be because AFSR-2 has a bigger volume. As a result, additional hydrocarbons are

produced, especially CH_4 and light olefins like C_2H_4 and C_3H_6. Compared to CR, the total hydrocarbon production was significantly increased by AFSR-2 by around 54.5%, whilst AFSR-1 only exhibited a small increase of 2.3%.

4.4.2 Performance of radial flow spherical reactor (RFSR)

Figure 25 displays the results of the comparison between the performances of RFSR-1 and RFSR-2 with CR in terms of reactant conversion and product selectivity. For comparison, the performance of the top-performing reactor from the previous section, AFSR-2, is also displayed. For each reactor, there are two options for the location of the jacket, which are indicated by "i" and "o".

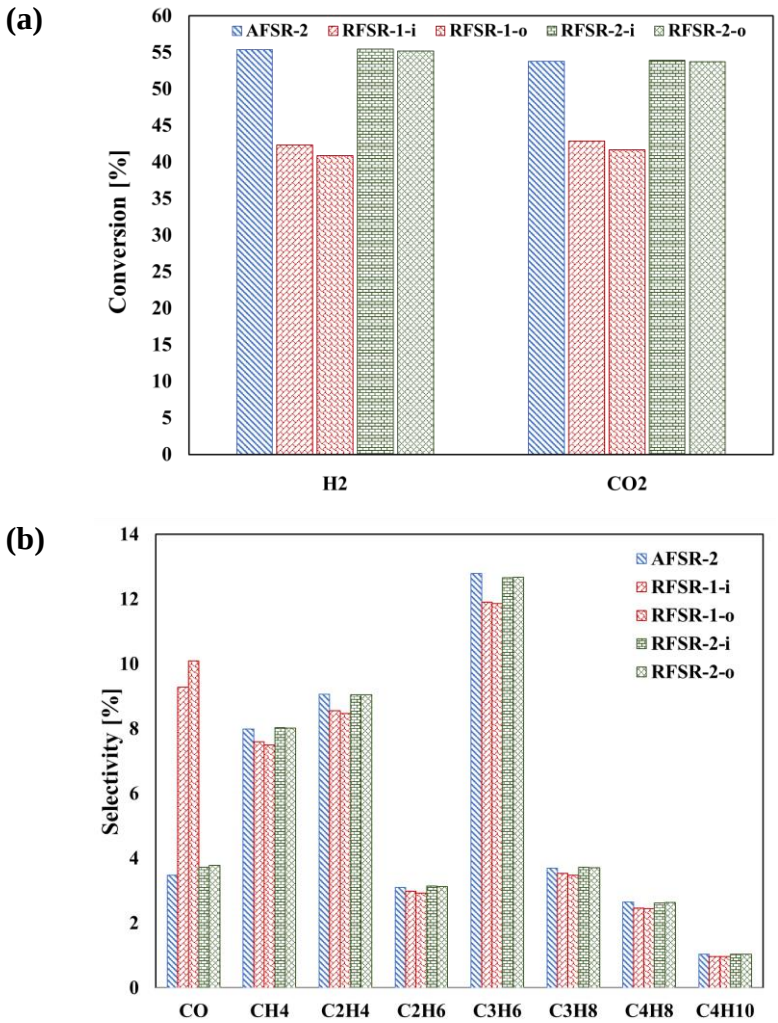

Figure 25 a) Reactant conversions and b) product distribution in AFSR-2, RFSR-1-i, RFSR-1-o, RFSR-2-i, and RFSR-2-o.s

The outcomes show that RFSR-2 (both i and o) outperforms RFSR-1. Additionally, the performance of RFSR-2-i is nearly identical to that of AFSR-2. This leads to the conclusion that, rather than having the same volume, spherical reactors perform better when their surface area is equal to their lateral area. Moreover, the performance seems to be better when the jacket is within the spherical reactor. The temperature profiles, however, are different and are shown separately in **Figure 26**. The jacket is situated outside RFSR-1-o and RFSR-2-o and within RFSR-1-i and RFSR-2-i, it should be noted.

The temperature profiles of RFSRs show that those with inner jackets experience greater temperature changes, while those with outer jackets have lower temperatures (**Figure 26 (a-d)**). This suggests that the position of the jacket is more significant than the diameter of the reactor in a radial setup. A more comprehensive analysis and discussion of the comparison between cylindrical and spherical reactor configurations can be found in our recent publication [47].

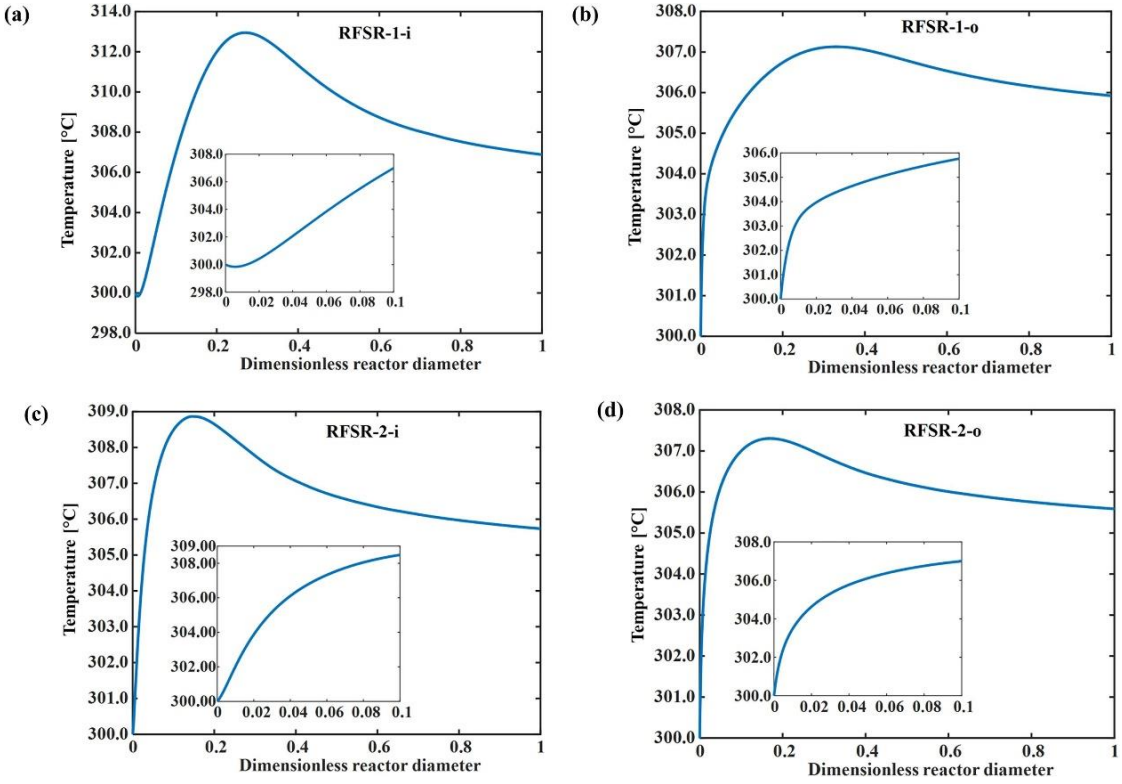

Figure 26 Temperature profiles for a) RFSR-1-i, b) RFSR-1-o, c) RFSR-2-i and d) RFSR-2-o.

4.5 Analysis of variance

Table 2 displays the statistical significance and impact of the primary variables and their interactions on the yields of various products. All of the primary variables, except for E (φ) in the yield of C_4H_8, have p-values below 0.05 and are considered highly significant in determining the product distribution. The variable D (θ) has the largest impact and is the most significant factor for the yields of C_3H_6, C_3H_8, C_4H_8, and C_4H_{10} due to its highest value. For the yields of C_2H_4 and C_2H_6, variables C (Tt) and E (φ) are the most significant factors, respectively. The significant effects of each product are highlighted in blue in **Table 2**. To avoid repetition and unnecessary data, the results for minimizing CO yield and maximizing CO_2 conversion have been excluded, as they align with the objective of maximizing the desired product yields.

The Pareto charts in **Figure 27** show how reactor temperature (Tr:A), shell temperature (Ts:B), and tube temperature (Tt:C) affect yields of C_2H_4, C_2H_6, and C_3H_6, but not C_3H_8, C_4H_8, and C_4H_{10}, respectively. **Table 2** displays the statistical significance and impact of the primary variables and their interactions on the yields of various products. All of the primary variables, except for the tube pressure ratio (E:φ) in the yield of C_4H_8, have p-values below 0.05 and are considered highly significant in determining the product distribution. The variable of sweep ratio (θ:D) has the largest impact and is the most significant factor for the yields of C_3H_6, C_3H_8, C_4H_8, and C_4H_{10} due to its highest value. For the yields of C_2H_4 and C_2H_6, variables C and E are the most significant factors, respectively. The significant effects of each product are highlighted in blue in **Table 2**. To avoid repetition and unnecessary data, the results for minimizing CO yield and maximizing CO_2 conversion have been excluded, as they align with the objective of maximizing the desired product yields.

Table 2. Values of probability and variable contributions

Input	y_{CH_4}		$y_{C_2H_4}$		$y_{C_2H_6}$		$y_{C_3H_6}$		$y_{C_3H_8}$		$y_{C_4H_8}$		$y_{C_4H_{10}}$	
	P-value	**% Cnt.**	**P-value**	**% Cnt**	**P-value**	**% Cnt**	**P-value**	**% Cnt**	**P-value**	**% Cnt**	**P-value**	**% Cnt**	**P-value**	**% Cnt**
A-Tr	**0.0007**	**0.38**	**< 0.0001**	**8.57**	**< 0.0001**	**2.60**	**< 0.0001**	**5.03**	**< 0.0001**	**1.49**	**< 0.0001**	**7.89**	**< 0.0001**	**3.06**
B-Ts	0.6765	0.00	**< 0.0001**	**8.24**	**< 0.0001**	**1.86**	**< 0.0001**	**4.84**	**< 0.0001**	**2.42**	**< 0.0001**	**6.74**	**< 0.0001**	**5.80**
C-Tt	**< 0.0001**	**0.63**	**< 0.0001**	**16.86**	**< 0.0001**	**4.82**	**< 0.0001**	**8.74**	**< 0.0001**	**3.53**	**< 0.0001**	**12.50**	**< 0.0001**	**13.28**
D-θ	**< 0.0001**	**49.39**	**< 0.0001**	**8.26**	**< 0.0001**	**14.20**	**< 0.0001**	**42.36**	**< 0.0001**	**52.21**	**< 0.0001**	**31.92**	**< 0.0001**	**30.00**
E-φ	**< 0.0001**	**39.56**	**< 0.0001**	**8.70**	**< 0.0001**	**51.70**	**< 0.0001**	**11.28**	**< 0.0001**	**20.46**	0.9849	0.00	**< 0.0001**	**18.06**
AB	0.9187	0.00	**< 0.0001**	**5.57**	**< 0.0001**	**1.24**	**< 0.0001**	**3.20**	**< 0.0001**	**1.69**	**< 0.0001**	**4.69**	**< 0.0001**	**3.42**
AC	0.4179	0.02	**< 0.0001**	**3.66**	**< 0.0001**	**0.84**	**< 0.0001**	**2.12**	**< 0.0001**	**1.04**	**< 0.0001**	**2.93**	**< 0.0001**	**2.94**
AD	**< 0.0001**	**1.59**	0.0888	0.41	0.6571	0.01	0.0066	0.52	**< 0.0001**	**0.72**	0.0485	0.38	0.9624	0.00
AE	0.0439	0.12	**< 0.0001**	**3.51**	0.0006	0.59	**< 0.0001**	**2.57**	**< 0.0001**	**1.21**	**< 0.0001**	**3.38**	0.006	0.97
BC	0.2464	0.04	**< 0.0001**	**6.22**	**< 0.0001**	**1.21**	**< 0.0001**	**3.83**	**< 0.0001**	**2.20**	**< 0.0001**	**5.50**	**< 0.0001**	**3.88**
BD	0.0032	0.27	0.0445	0.58	0.4156	0.03	0.0105	0.46	**< 0.0001**	**0.54**	0.0099	0.68	0.1141	0.30
BE	0.0028	0.28	0.0162	0.85	0.1632	0.08	0.0065	0.52	**< 0.0001**	**0.56**	0.0098	0.68	0.0279	0.60
CD	0.2782	0.03	0.0002	2.43	0.0004	0.65	**< 0.0001**	**1.26**	**< 0.0001**	**0.63**	0.0002	1.65	0.0002	1.96
CE	**< 0.0001**	**0.59**	**< 0.0001**	**2.71**	0.0083	0.33	**< 0.0001**	**1.79**	**< 0.0001**	**1.58**	**< 0.0001**	**2.44**	0.0009	1.50
DE	**< 0.0001**	**2.57**	**< 0.0001**	**4.89**	**< 0.0001**	**16.23**	0.0688	0.22	**< 0.0001**	**1.18**	**< 0.0001**	**3.44**	0.001	1.46
ABC	0.8913	0.00	**< 0.0001**	**5.76**	**< 0.0001**	**1.28**	**< 0.0001**	**3.30**	**< 0.0001**	**1.76**	**< 0.0001**	**4.81**	**< 0.0001**	**3.59**

ABD	0.1524	0.06	0.0280	0.70	0.1339	0.10	0.0133	0.42	0.0008	0.36	0.0130	0.63	0.0503	0.46
ABE	0.0003	0.44	0.1163	0.34	0.7488	0.00	0.0369	0.29	0.0003	0.42	0.0626	0.34	0.1315	0.27
ACD	0.0923	0.08	0.0363	0.63	0.2271	0.06	0.0095	0.47	0.0006	0.38	0.0141	0.61	0.0673	0.40
ACE	0.1323	0.06	0.0189	0.81	0.0965	0.12	0.0086	0.48	0.0007	0.37	0.0131	0.63	0.0383	0.52
ADE	0.0834	0.09	0.4763	0.07	0.3023	0.05	0.4496	0.04	0.7058	0.00	0.9179	0.00	0.8637	0.00
BCD	0.6686	0.01	0.0021	1.48	0.0146	0.28	0.0006	0.91	< **0.0001**	**0.55**	0.0011	1.17	0.0014	1.37
BCE	0.0011	0.35	0.0250	0.73	0.2244	0.06	0.0105	0.46	< **0.0001**	**0.53**	0.0136	0.62	0.0558	0.44
BDE	0.0003	0.44	0.0334	0.65	0.3568	0.04	0.0090	0.48	< **0.0001**	**0.55**	0.0105	0.67	0.193	0.20
CDE	0.0053	0.24	0.0439	0.58	0.2806	0.05	0.0158	0.40	0.0003	0.44	0.0333	0.45	0.0478	0.48
ABCD	0.1328	0.06	0.0376	0.62	0.1691	0.08	0.0183	0.38	0.0011	0.34	0.0171	0.57	0.0734	0.39
ABCE	0.0003	0.44	0.1088	0.36	0.7217	0.01	0.0355	0.30	0.0003	0.43	0.0575	0.35	0.1383	0.26
ABDE	0.0003	0.45	0.1270	0.32	0.8007	0.00	0.0314	0.31	0.0004	0.41	0.0511	0.37	0.3097	0.12
ACDE	0.0109	0.20	0.2171	0.21	0.6763	0.01	0.1306	0.15	0.0081	0.21	0.1491	0.20	0.3434	0.10
BCDE	0.0043	0.25	0.0139	0.89	0.1347	0.10	0.0040	0.59	< **0.0001**	**0.54**	0.0063	0.77	0.0542	0.45
ABCDE	0.0002	0.48					0.0372	0.29	0.0005	0.40				
R^2	**0.9914**		**0.9563**		**0.9862**		**0.9802**		**0.9916**		**0.9699**		**0.9628**	
$R^2_{adj.}$	**0.9831**		**0.9165**		**0.9737**		**0.9611**		**0.9835**		**0.9427**		**0.9290**	
$R^2_{pred.}$	**0.9656**		**0.8356**		**0.9482**		**0.9209**		**0.9665**		**0.8871**		**0.8602**	
Adeq. prec.	**34.2415**		**24.6056**		**34.4353**		**24.7732**		**36.692**		**24.0391**		**19.1839**	

Pareto charts of hydrocarbons are used in **Figure 27** to depict the important variables and their t-value magnitudes. The primary variables with p-values less than 0.0001 and over the Bonferroni limit that affect the yield of C_3H_6 are D, E, C, A, B, BC, ABC, AB, AE, AC, CE, and CD, according to the information in **Table 2** and **Figure 27**. D has the most significant main effect among them, contributing 42.36%, while BC has the most significant two-factor interaction, contributing 3.83%. In contrast to variables with p-values higher than 0.05 and t-values below the t-limit, which are of minor importance, variables with t-values below the Bonferroni limit but above the t-limit are moderately significant. The significant variables for C_2H_4 and C_4H_8 with p-values under 0.0001 are found. When the data in **Table 2** are compared, it is seen that the major factors AB, AC, AE, BC, CD, CE, and DE are shared by all olefins and paraffins. The important variables for CH4 yield are A, C, D, and E, with D accounting for 49.39% of the total. According to the Pareto graphic, the most important variables for CH_4 yield with t-values over the Bonferroni limit are D, E, DE, AD, C, CE, ABCDE, ABDE, ABE, BDE, and ABCE (**Figure 27**).

Also, as shown in **Table 2**, the determination coefficients R^2 and R^2_{adj} are almost equal to one, and R^2_{pred} agrees rather well with R^2_{adj}, demonstrating the capacity of empirical models to predict actual data. For the answers, the following model expression (**Eq. 33**) is suggested:

$$y = a_0 + \sum_{i=1}^{n} a_i x_i + \sum_{i=1}^{n-1} \sum_{j=2}^{n} a_{ij} x_i x_j + \sum_{i=1}^{n-2} \sum_{j=2}^{n-1} \sum_{k=3}^{n} a_{ijk} x_i x_j x_k + \sum_{i=1}^{n-3} \sum_{j=2}^{n-2} \sum_{k=3}^{n-1} \sum_{l=4}^{n} a_{ijkl} x_i x_j x_k x_l \quad (33)$$

(a)

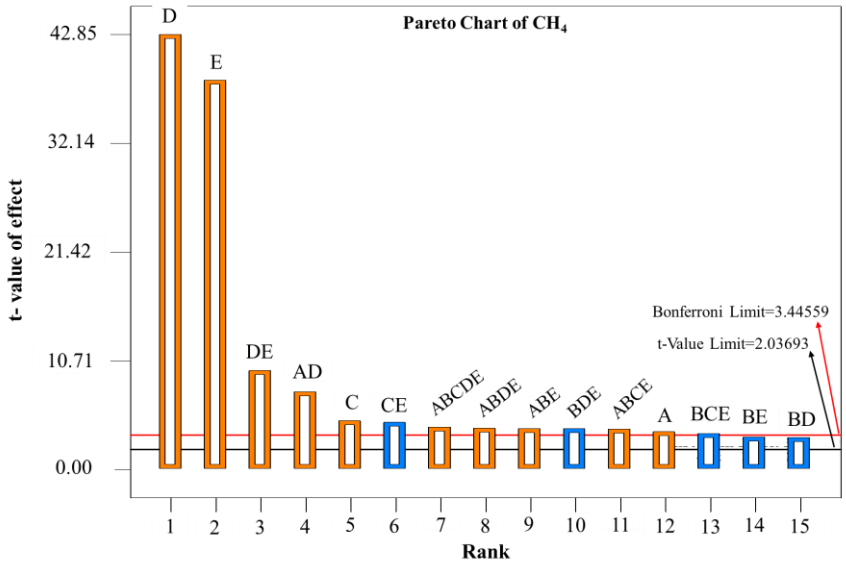
Pareto Chart of CH_4
t- value of effect
42.85
32.14
21.42
10.71
0.00
D
E
DE
AD
C
CE
ABCDE
ABDE
ABE
BDE
ABCE
A
BCE
BE
BD
Bonferroni Limit=3.44559
t-Value Limit=2.03693
1 2 3 4 5 6 7 8 9 10 11 12 13 14 15
Rank

(b)

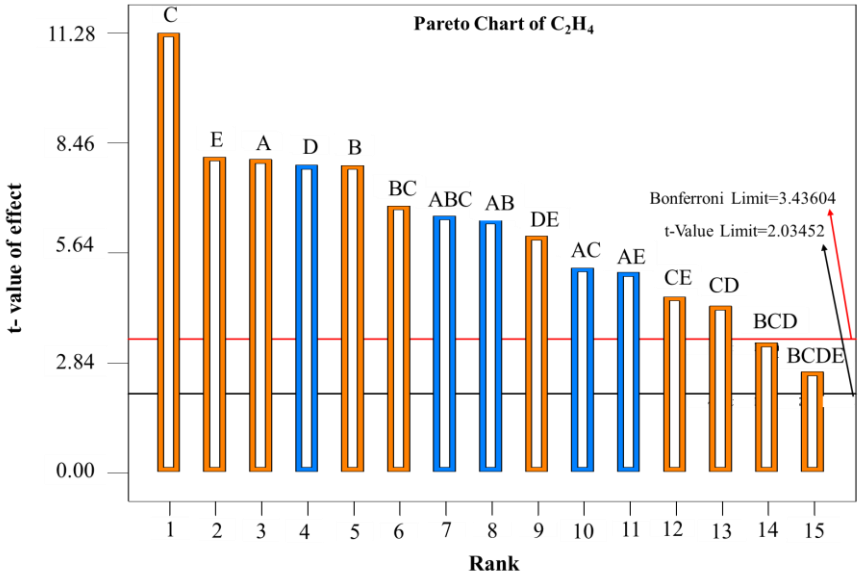
Pareto Chart of C_2H_4
t- value of effect
11.28
8.46
5.64
2.84
0.00
C
E
A
D
B
BC
ABC
AB
DE
AC
AE
CE
CD
BCD
BCDE
Bonferroni Limit=3.43604
t-Value Limit=2.03452
1 2 3 4 5 6 7 8 9 10 11 12 13 14 15
Rank

(c)

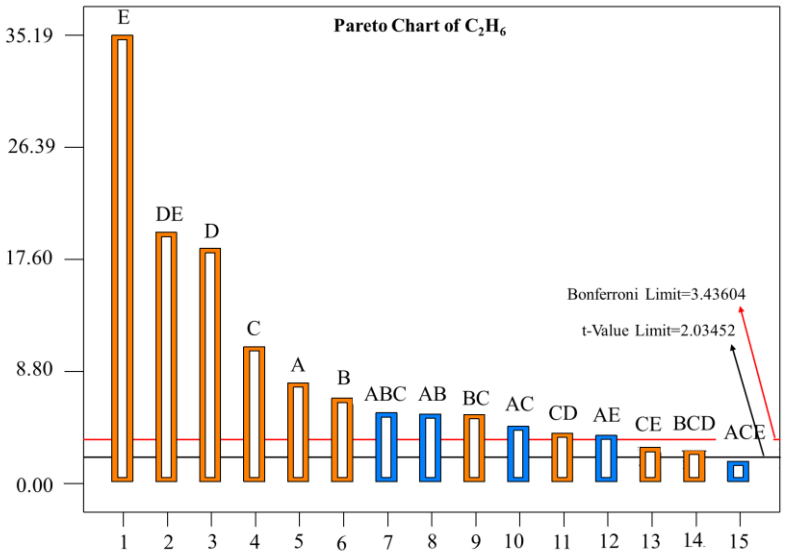
Pareto Chart of C_2H_6
35.19
26.39
17.60
8.80
0.00
E
DE
D
C
A
B
ABC
AB
BC
AC
CD
AE
CE
BCD
ACE
Bonferroni Limit=3.43604
t-Value Limit=2.03452
1 2 3 4 5 6 7 8 9 10 11 12 13 14 15

(d)

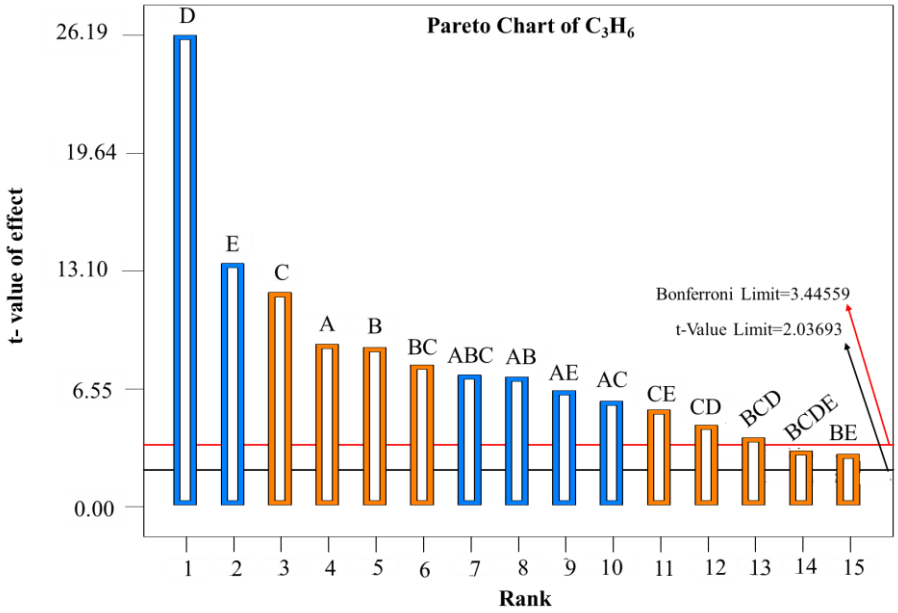
Pareto Chart of C_3H_6
t- value of effect
26.19
19.64
13.10
6.55
0.00
D
E
C
A
B
BC
ABC
AB
AE
AC
CE
CD
BCD
BCDE
BE
Bonferroni Limit=3.44559
t-Value Limit=2.03693
1 2 3 4 5 6 7 8 9 10 11 12 13 14 15
Rank

(e)

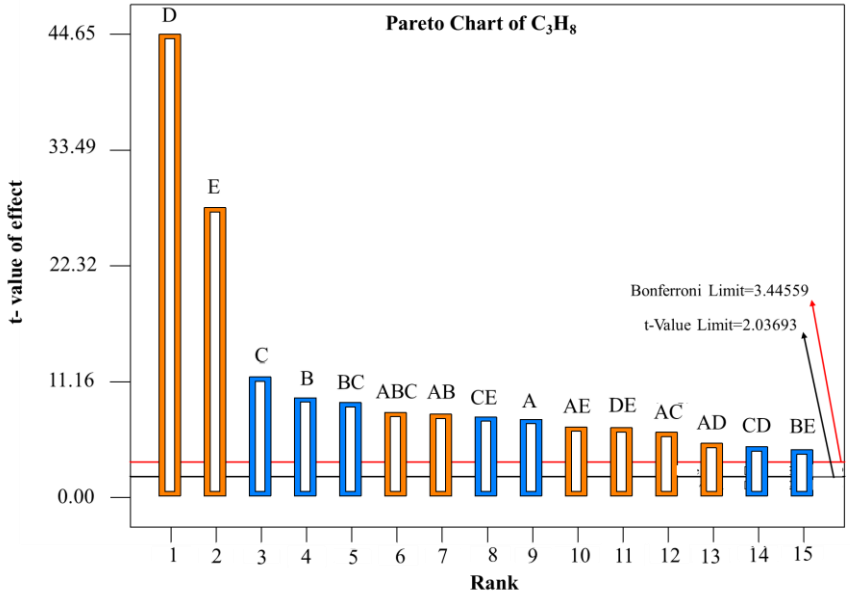
Pareto Chart of C_3H_8
t- value of effect
44.65
33.49
22.32
11.16
0.00
D
E
C
B
BC
ABC
AB
CE
A
AE
DE
AC
AD
CD
BE
Bonferroni Limit=3.44559
t-Value Limit=2.03693
1 2 3 4 5 6 7 8 9 10 11 12 13 14 15
Rank

(f)

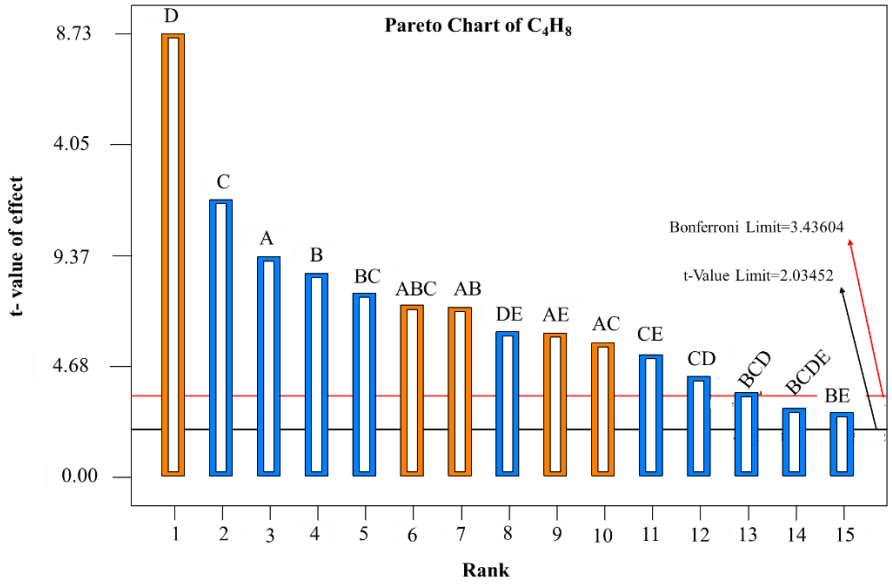

(g)

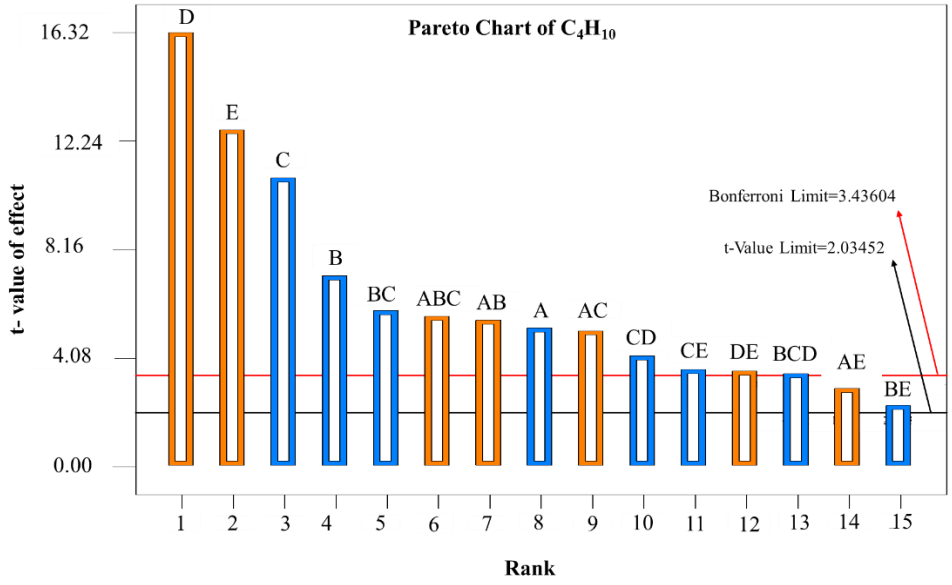

Figure 27. Pareto charts of a) CH_4 b) C_2H_4 c) C_2H_6 d) C_3H_6 e) C_3H_8 f) C_4H_8 g) C_4H_{10}.

4.6 Effect of single parameter changes

The Pareto charts in **Figure 27** show how reactor temperature (A), shell temperature (B), and tube temperature (C) affect yields of C_2H_4, C_2H_6, and C_3H_6, but not C_3H_8, C_4H_8, and C_4H_{10}, respectively. As a result, in the CO_2 hydrogenation process, the temperature immensely impacts how the products are distributed. According to the data given by Owen et al. [56] and Ronda-Lloret et al. [57], when the temperature rises, lighter hydrocarbons are created in greater amounts whereas heavier hydrocarbons are produced in smaller amounts. Iglesia et al. [58] have showed that the output of CH_4 is mostly unaffected by temperature.

The Pareto charts in **Figure 27** show how reactor temperature (A), shell temperature (B), and tube temperature (C) affect yields of C_2H_4, C_2H_6, and C_3H_6, but not C_3H_8, C_4H_8, and C_4H_{10}, respectively. As a result, in the CO_2 hydrogenation process, the temperature immensely impacts how the products are distributed. According to the data given by Owen et al. [56] and Ronda-Lloret et al. [57], when the temperature rises, lighter hydrocarbons are created in greater amounts whereas heavier hydrocarbons are produced in smaller amounts. Iglesia et al. [58] have showed that the output of CH_4 is mostly unaffected by temperature.

As a result, in the CO_2 hydrogenation process, the temperature immensely impacts how the products are distributed. According to the data given by Owen et al. [56] and Ronda-Lloret et al. [57], when the temperature rises, lighter hydrocarbons are produced in greater amounts whereas heavier hydrocarbons are produced in smaller amounts. Iglesia et al. [58] have showed that the output of CH_4 is mostly unaffected by temperature.

The yields of heavier hydrocarbons are positively impacted by the sweep ratio (D), but the yields of light olefins like C_2H_4 and C_3H_6 are negatively impacted. More water is removed from the reactor as a result of raising the sweep ratio, which changes the RWGS balance to favor the generation of more CO and, therefore, more hydrocarbons. To synthesize olefins, however, the water concentration in the reactor must reach a crucial point known as "saturate." The yield of olefins is only marginally impacted above this concentration. The yield of C_3H_6 is negatively impacted by the pressure ratio (E), demonstrating how important water concentration is to the yield of the primary product. More driving force is provided for water evacuation from the membrane reactor to the tube side by raising the pressure ratio.

4.7 Effect of simultaneous changes

The effects of simultaneous variable changes on the hydrocarbon yields are shown in **Figures 28** to **31**. Each of them depicts the impact of one variable on a hydrocarbon's yield at low and high concentrations of the other variable. The first parameter is shown on the x-axis, yield is shown on the y-axis, and two lines in black and red depict the second parameter's low and high values. An interaction occurs when the connection between hydrocarbon yield and one input variable varies depending on the value of another variable. According to **Table 2** and **Figure 27**, the most critical

interaction parameters for determining the best olefin and paraffin yields are AB, AC, AE, BC, CD, CE, and DE.

The interaction between A and B and its influence on product yields is shown in **Figure 28(a-f).** For both low and high levels of B, the yields of light hydrocarbons (C_2H_4, C_2H_6, and C_3H_6) rise as A rises, although the rise is more pronounced at low levels of B. Nevertheless, for both values of B, the yields of the heavier hydrocarbons (C_3H_8, C_4H_8, and C_4H_{10}) decline as A rises. When B is at a low level, A's impact on the yield is more pronounced. For light hydrocarbons, the interaction between A and B is negative, but for heavy hydrocarbons, it is positive. Lower shell temperatures have a substantial impact on the yields of heavy hydrocarbons, and as A falls, the yields of heavy hydrocarbons rise at low levels of B.

Figure 28(a-f) illustrates the interacting effect of A and B on product yields. The yields of light hydrocarbons (C_2H_4, C_2H_6, and C_3H_6) increase as A increases at both low and high levels of B, but the increase is more significant at low levels of B. However, the yields of heavier hydrocarbons (C_3H_8, C_4H_8, and C_4H_{10}) decrease as A increases at both levels of B. The effect of A on the yield is more prominent when B is at a low level. The interaction between A and B is negative for light hydrocarbons and positive for heavy hydrocarbons. The yields of heavy hydrocarbons are significantly affected when shell temperatures are lower, and as A decreases, the yields of heavy hydrocarbons increase at low levels of B.

The effects of A and E on hydrocarbon yields are shown in **Figures 29(a-f)**. The two-factor interaction is not significant when the lines depicting low and high levels are parallel, as is the case with C_2H_6 in **Figure 29(b)**. **Figures 29(a** and **c)** demonstrate that, for both low and high levels of E, increasing A leads to increased yields of C_2H_4 and C_3H_6. Whereas C_3H_6 yields are at their highest at low E, C_2H_4 yields are greater at high E. Whereas E has a favorable impact on C_2H_4 yields but a negative one on C3H6 yields, A has a positive impact on both. As a result, the yield of C_3H_6 increases while the yield of C_2H_4 drops when the pressure ratio is low. The crossing lines in **Figure 29(d-f)** show that C_4H_8 (**Figure 29(e)**) has the most significant two-factor interaction. **Figure 29(d** and **f**) show that yields of both C_3H_8 and C_4H_{10} fall with increasing A, particularly at low E, whereas yields increase at high E. The yields of heavy hydrocarbons rise when pressure ratios rise and vice versa at high reactor temperatures.

Figure 30(a-f) illustrates how the interaction of C and E affects product yields. According to the findings, CE has minimal impact on C_2H_6 yield (parallel lines) but significantly more on C_4H_8 yield (crossing lines), which is consistent with the information shown in Pareto charts. In both levels of E, the yields of light hydrocarbons rise as C rises, but the slopes of the changes are higher in the high E level. Moreover, when E grows, the yield of C_2H_4 rises, but C_3H_6's yield falls since E has a negative impact on it.

Figure 31(a-f) illustrates how D and E have an impact on product yields. According to the findings, DE has no impact on the yield of C_3H_6, despite the fact that both D and E have considerable detrimental impacts. This shows that neither the value of E nor the effect of D is affected by one another. Nonetheless, **Figure 31(e)** crossing's lines show that DE is a significant factor in determining the yield of C_4H_8. The yield of C_2H_4 declines as D rises, independent of the value of E, whereas the yield of C_2H_6 rises at high levels of E. Moreover, at both levels of E, D has a favorable impact on yields that grows as the molecular weight of the hydrocarbon increases.

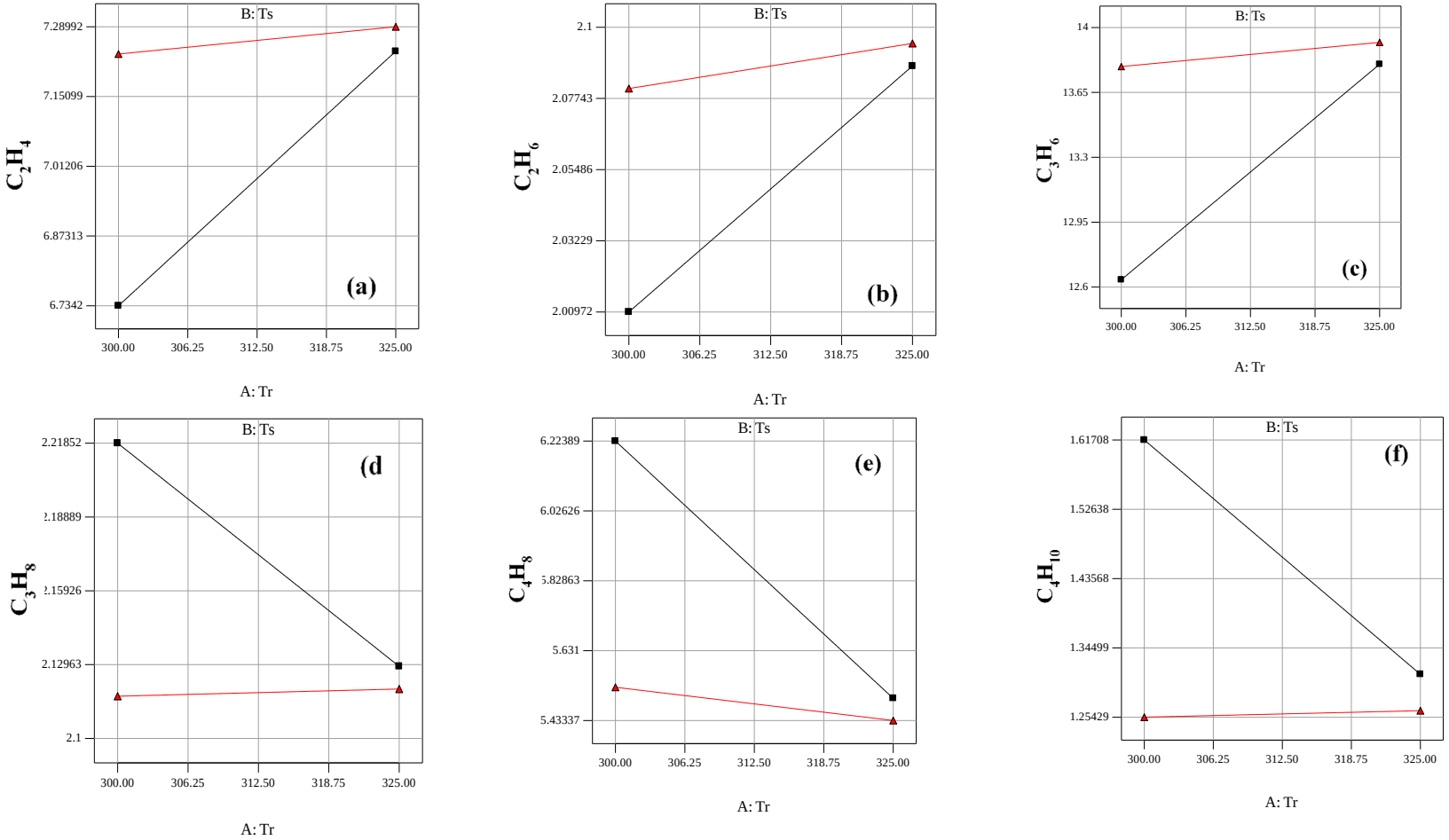

Figure 28. Effect of simultaneous changes in A and B on yield of various hydrocarbon products.

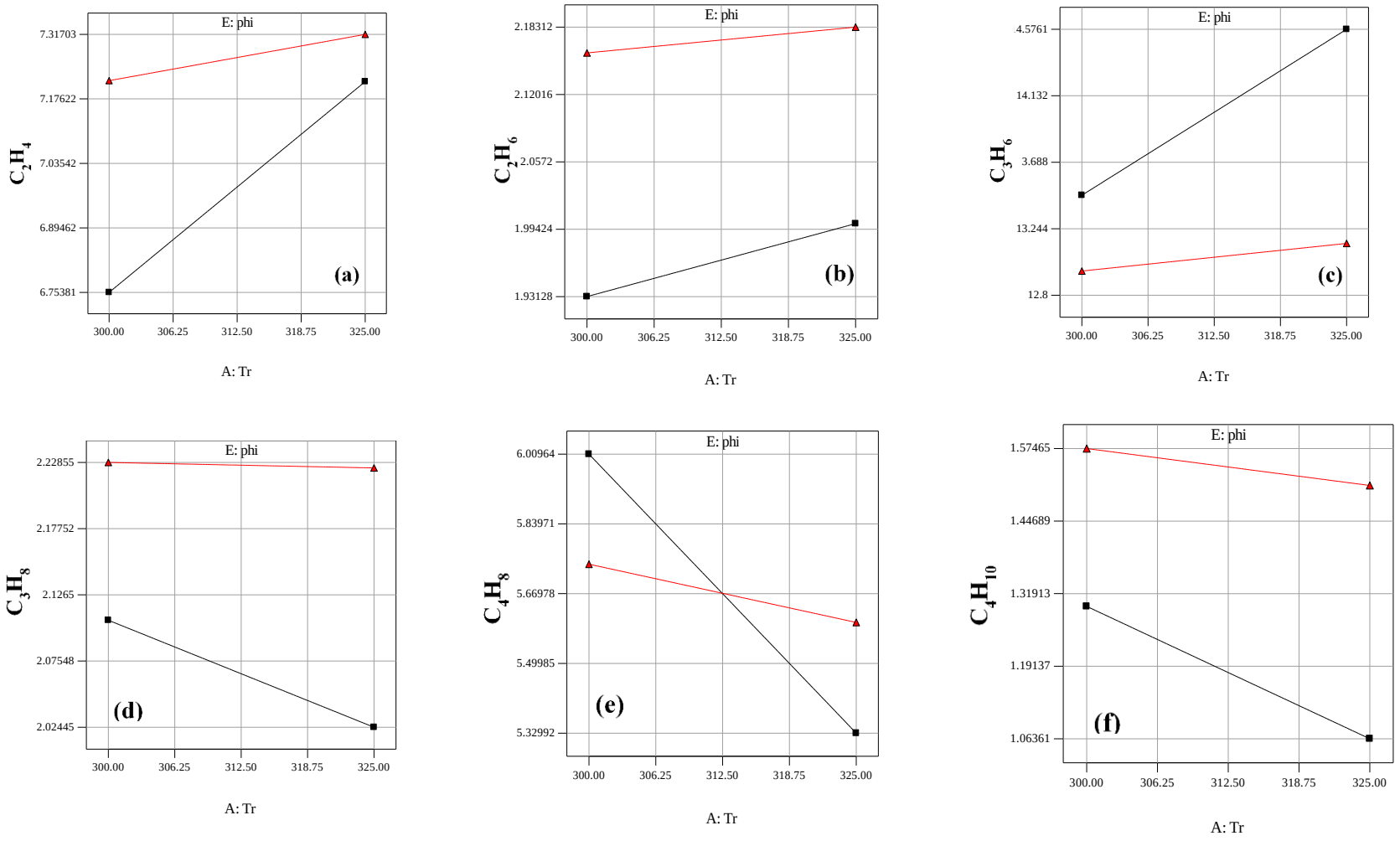

Figure 29. Effect of simultaneous changes in A and E on yield of various hydrocarbon products.

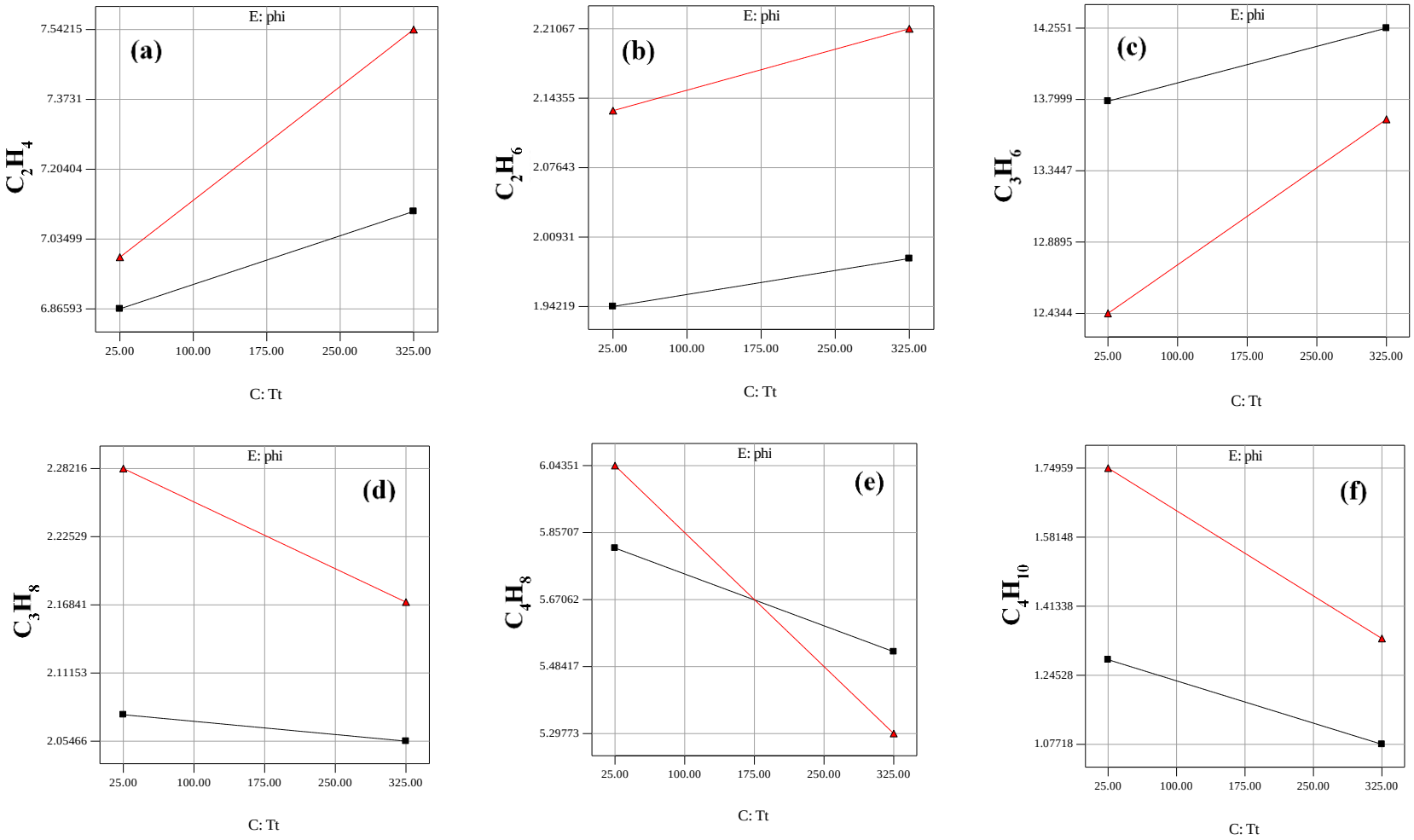

Figure 30. Effect of simultaneous changes in C and E on yield of various hydrocarbon products.

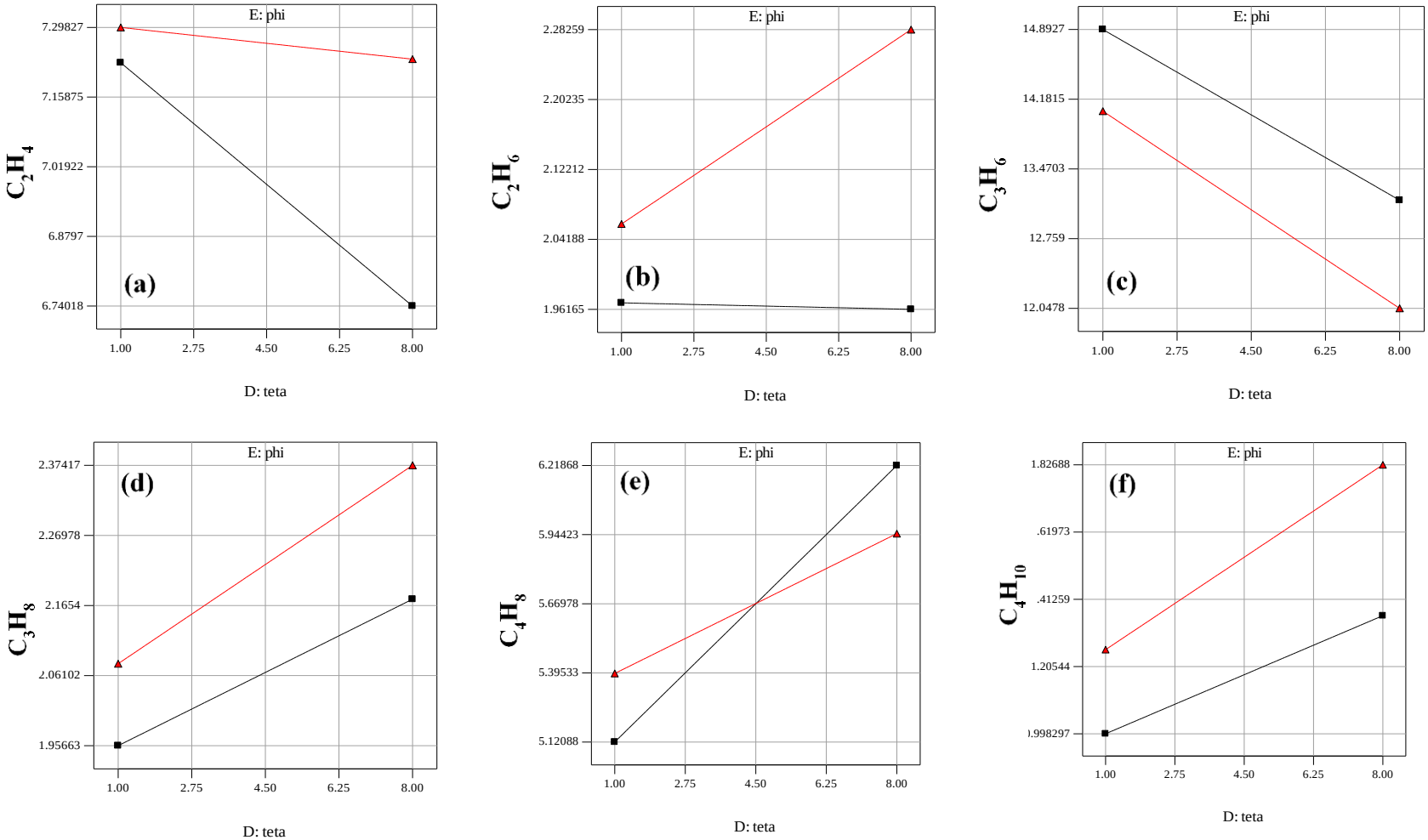

Figure 31. Effect of simultaneous changes in D and E on yield of various hydrocarbon products.

In **Figure 32(a-f)**, it is observed that increasing A leads to an increase in yields of C_2H_4, C_2H_6, and C_3H_6 at both low and high C. However, this increase is more significant at low C levels. As the molecular weight increases, the yields decrease with increasing A, regardless of the level of E, with steeper decreases at low C levels. **Figure 33(a-f)** demonstrates that yields of light hydrocarbons increase as B increases, particularly at high C levels, whereas yields of heavy hydrocarbons drop. High temperatures are necessary for the shell and tube for high yields of light hydrocarbons, while only one of them is permitted for large yields of heavy hydrocarbons. The production of low-molecular-weight hydrocarbons can be increased by injecting hydrogen from the shell into the reactor compartment at high temperatures, but the yield of heavy hydrocarbons can be severely impacted. According to **Figure 30(a-f)**, the pressure ratio significantly affects the yield of C_4H_8 while having little to no impact on the yield of C_2H_6. Increasing C leads to higher yields of light hydrocarbons, with steeper slopes at high E levels, while the yield of C_2H_4 increases with E while that of C_3H_6 decreases.

The interaction impact of C and D on the product yields is shown in **Figure 34(a-f)**. The findings demonstrate that raising C increases light hydrocarbon yields, especially at high levels of D. Nevertheless, when C rises, the yields of heavy hydrocarbons fall, which is especially apparent at the high level of E. D has a detrimental effect on olefins (C_2H_4 and C_3H_6), and yields are greater at low levels of D. Last but not least, the yields for heavy hydrocarbons dramatically decline when C rises to a higher level of D where larger yields may be produced.

The Pareto chart (**Figure 27 (a)**) demonstrates that the most important variables influencing CH_4 yield are DE, AD, and CE. While raising C has a beneficial impact on output at high levels of E, raising the reactor temperature increases CH_4 production at high levels of D. With a steeper slope at high values of E, the yield rises with D at both levels of E.

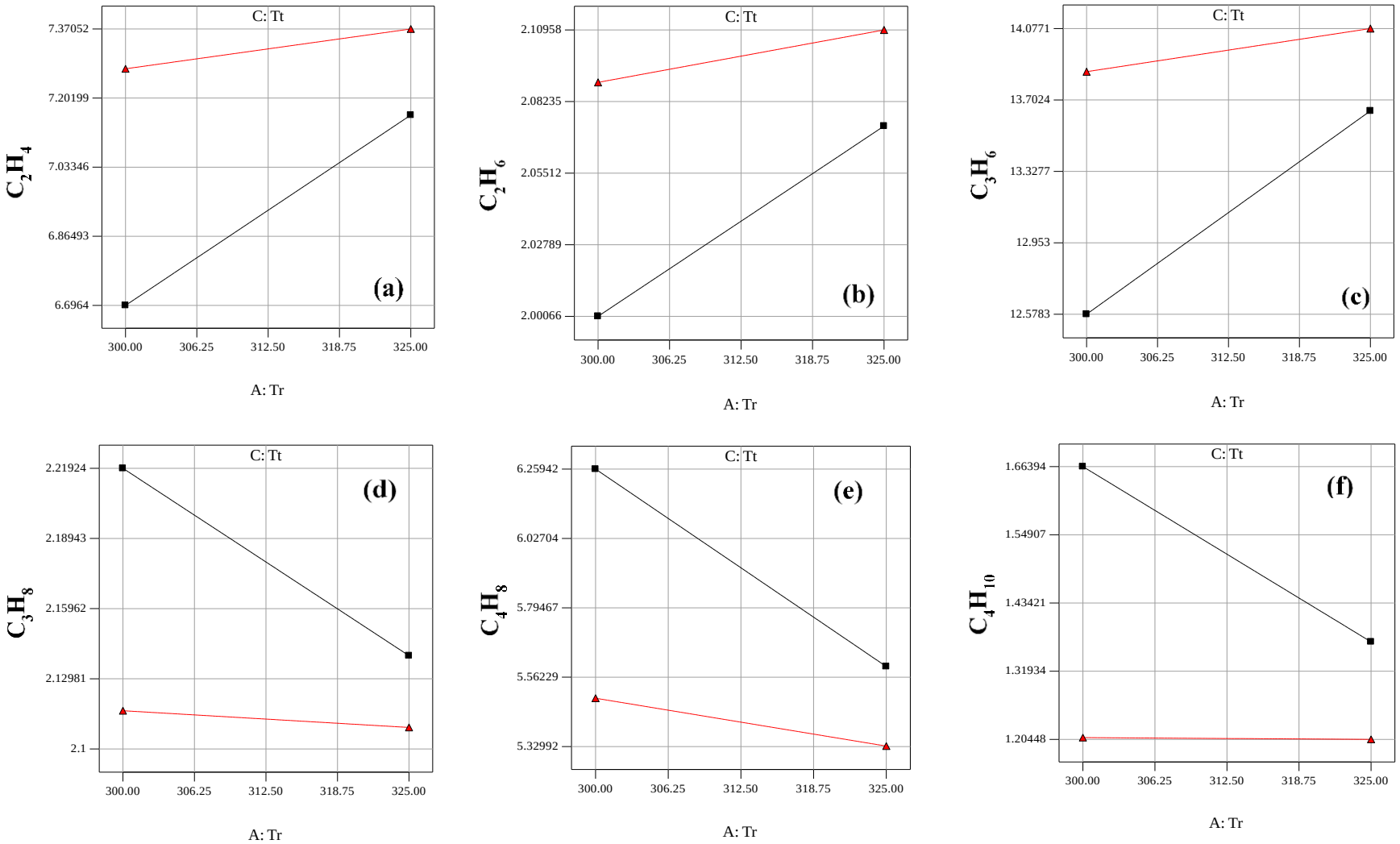

Figure 32. Effect of simultaneous changes in A and C on yield of various hydrocarbon products.

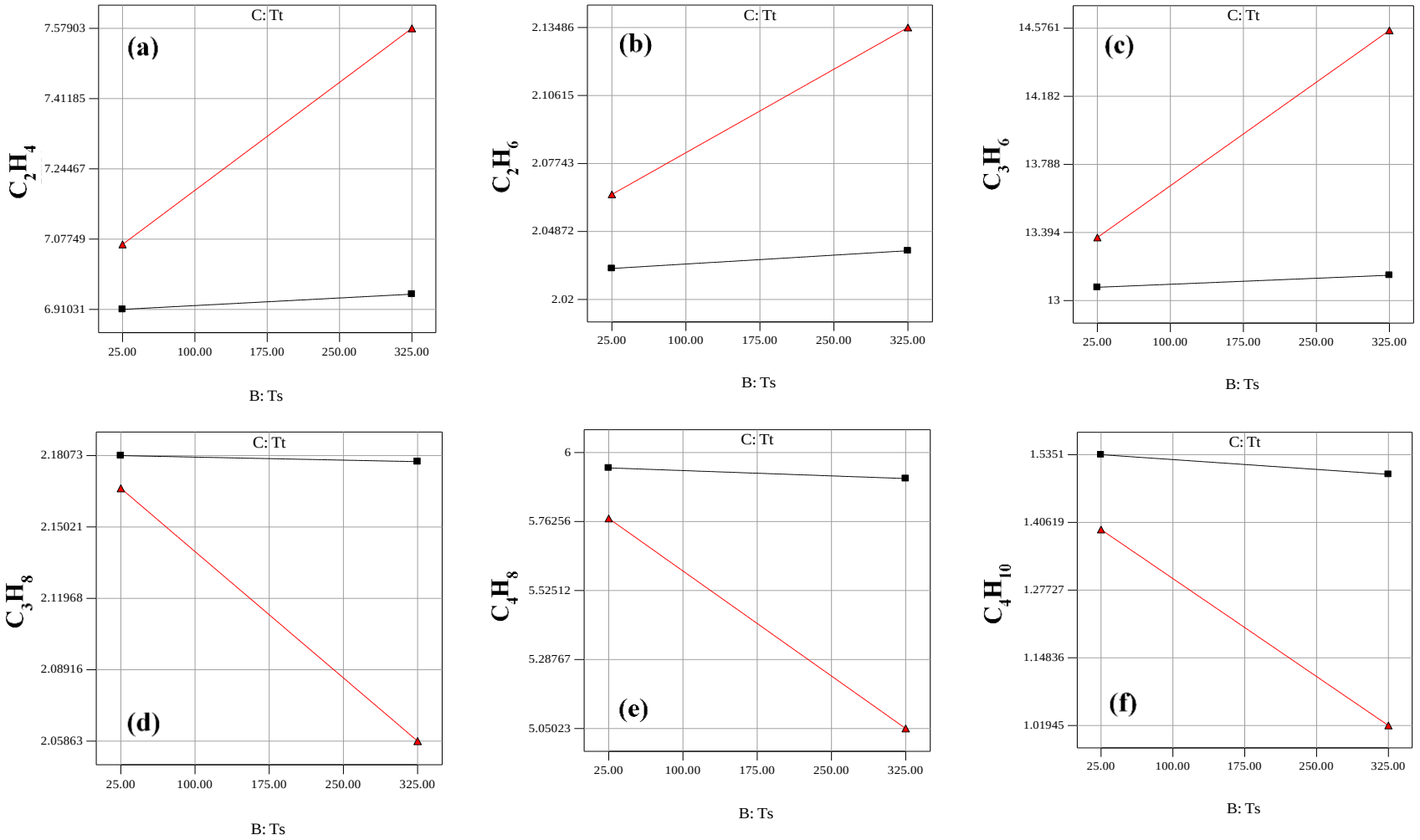

Figure 33. Effect of simultaneous changes in B and C on the yields of various hydrocarbon products.

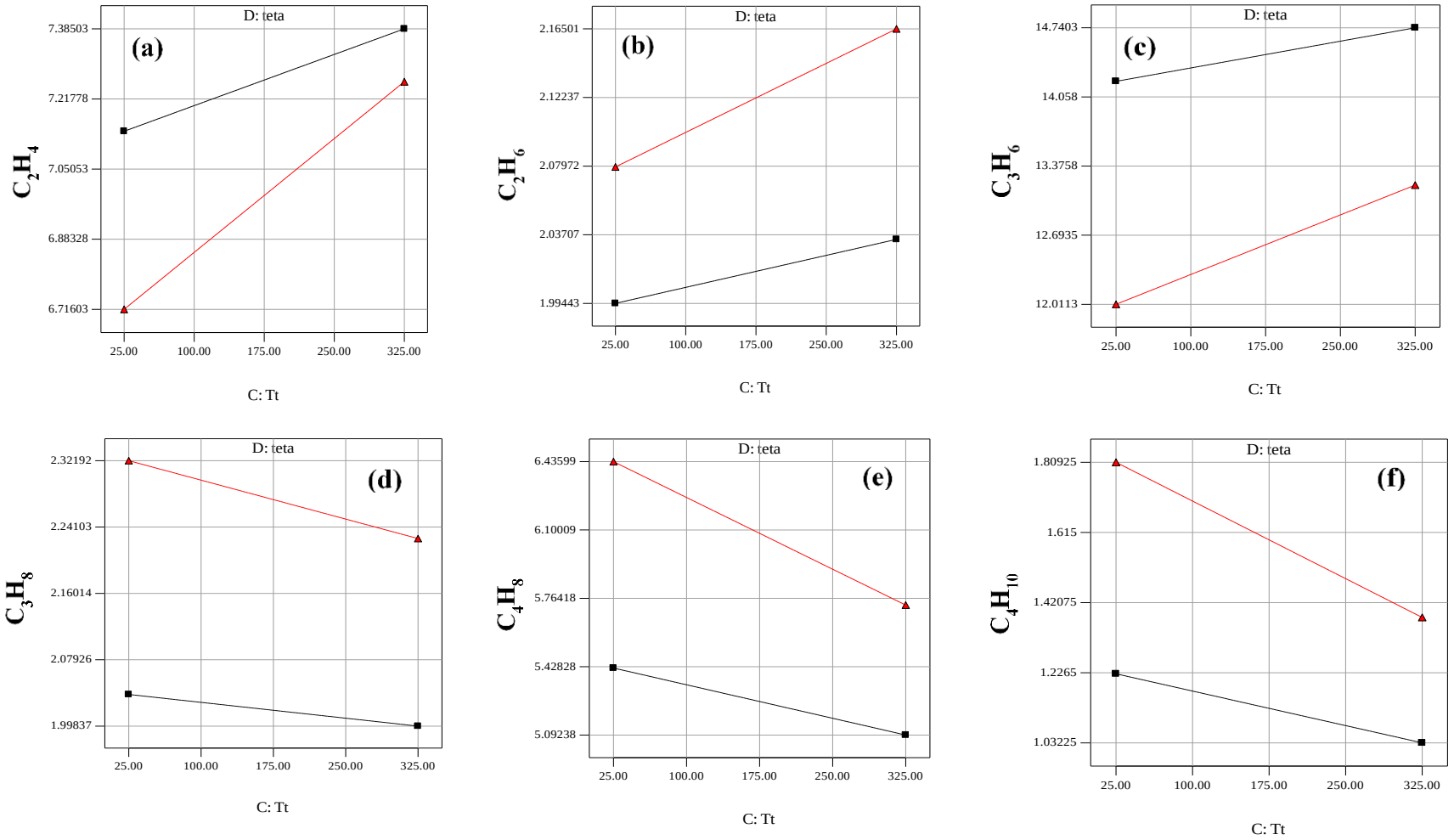

Figure 34. Effect of simultaneous changes in C and D on yield of various hydrocarbon products.

4.8 Optimization

As stated in **Table 3**, optimization aims to maximize the yield of olefins while minimizing the output of paraffin and CH4. **Table 3** clearly displays the relevance of each response. The last column of **Table 3** lists the ideal circumstances for attaining this objective. Two-factor interactions and 3-D surface and contour plots of the effects can be used to examine the best spot. C_2H_4 and C_3H_6 are two examples of light hydrocarbons, whereas C_4H_8 is an example of a heavy hydrocarbon. Similar to how C_2H_6 was added as a light paraffin, C_3H_8, and C_4H_{10} were included as heavy paraffin. According to the Pareto charts in **Figure 27,** AB affects the yields of heavy hydrocarbons more favorably than the yields of light hydrocarbons. Moreover, **Figure 35** shows that to maximize the output of olefins while reducing the synthesis of paraffins, a high reactor temperature is required.

Table 3. Limitations, importance, goals and solution of the responses in the optimization.

Name	Lower limit	Importance	Goals	Upper limit	Solution
Tt (°C)	25	3	is in range	325	325
Ts (°C)	25	3	is in range	325	306.96
Tr (°C)	300	3	is in range	325	325
φ	1	3	is in range	8	1
θ	1	3	is in range	8	1
$y_{C_2H_4}$	6.317	5	maximize	8.7345	7.58367
y_{CH_4}	6.051	3	minimize	6.719	6.08815
$y_{C_3H_6}$	10.668	5	maximize	15.718	15.7048
$y_{C_2H_6}$	1.880	3	minimize	2.4533	2.01626
$y_{C_4H_8}$	3.825	5	maximize	6.8141	4.62081
$y_{C_3H_8}$	1.894	3	minimize	2.4946	1.89474
$y_{C_4H_{10}}$	0.751	3	minimize	2.3107	0.819256

(a)

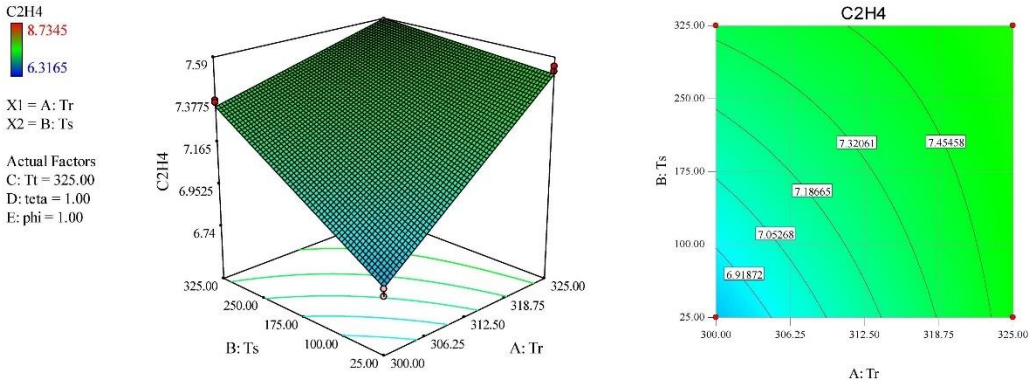
C2H4
8.7345
6.3165
X1 = A: Tr
X2 = B: Ts
Actual Factors
C: Tt = 325.00
D: teta = 1.00
E: phi = 1.00
C2H4
7.59
7.3775
7.165
6.9525
6.74
325.00
250.00
175.00
100.00
25.00
B: Ts
300.00
306.25
312.50
318.75
325.00
A: Tr
C2H4
325.00
250.00
175.00
100.00
25.00
B: Ts
7.32061
7.45458
7.18665
7.05268
6.91872
300.00
306.25
312.50
318.75
325.00
A: Tr

(b)

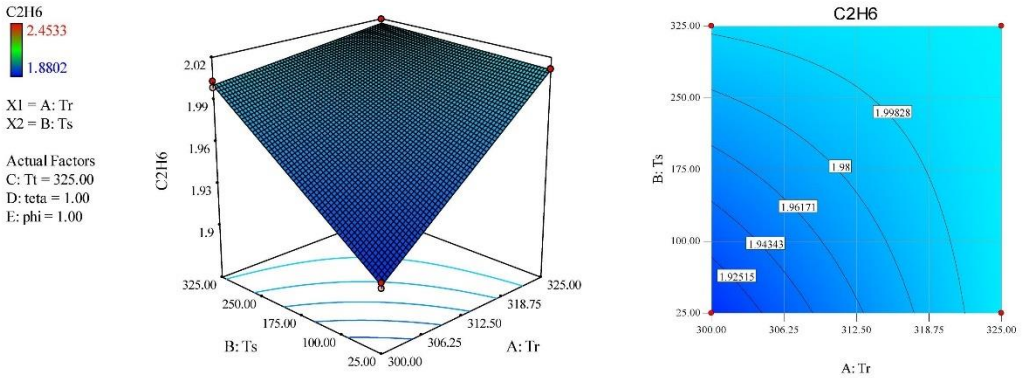
C2H6
2.4533
1.8802
X1 = A: Tr
X2 = B: Ts
Actual Factors
C: Tt = 325.00
D: teta = 1.00
E: phi = 1.00
C2H6
2.02
1.99
1.96
1.93
1.9
325.00
250.00
175.00
100.00
25.00
B: Ts
300.00
306.25
312.50
318.75
325.00
A: Tr
C2H6
325.00
250.00
175.00
100.00
25.00
B: Ts
1.99828
1.98
1.96171
1.94343
1.92515
300.00
306.25
312.50
318.75
325.00
A: Tr

(c)

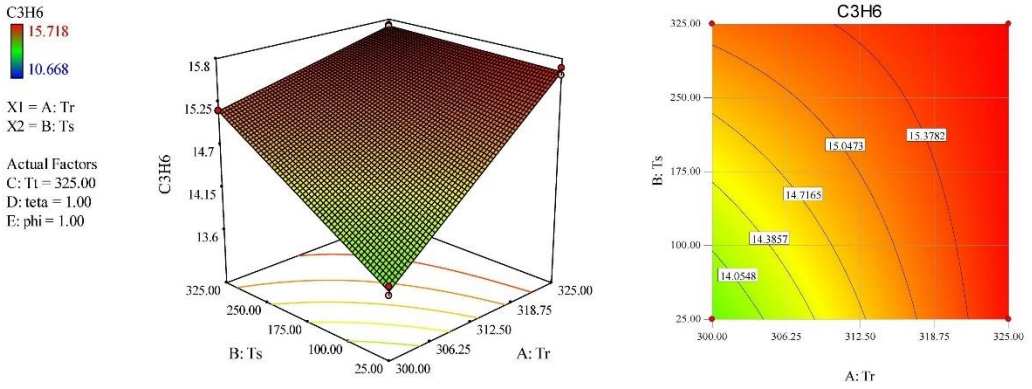
C3H6
15.718
10.668
X1 = A: Tr
X2 = B: Ts
Actual Factors
C: Tt = 325.00
D: teta = 1.00
E: phi = 1.00
C3H6
15.8
15.25
14.7
14.15
13.6
325.00
250.00
175.00
100.00
25.00
B: Ts
300.00
306.25
312.50
318.75
325.00
A: Tr
C3H6
325.00
250.00
175.00
100.00
25.00
B: Ts
15.3782
15.0473
14.7165
14.3857
14.0548
300.00
306.25
312.50
318.75
325.00
A: Tr

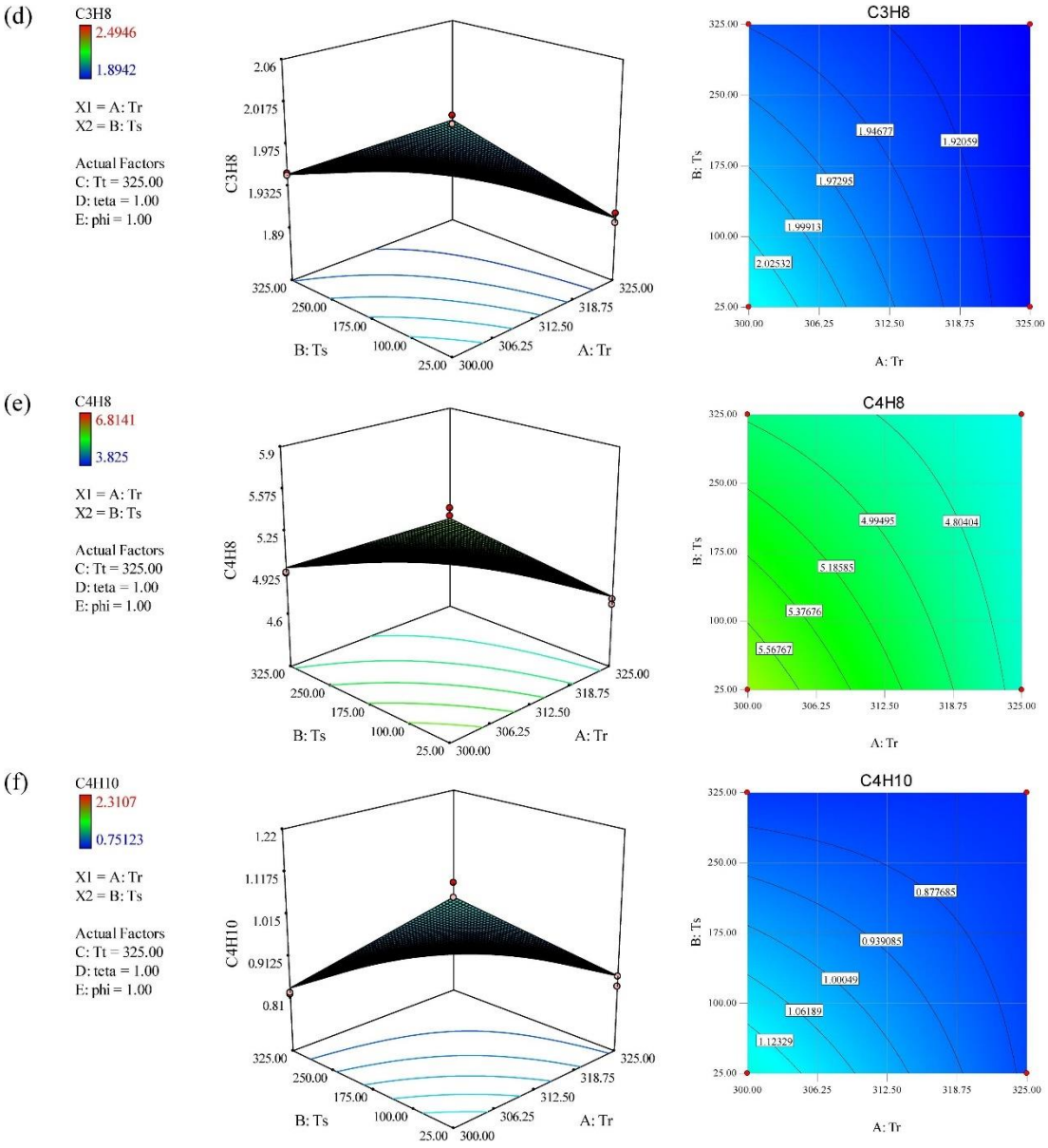

Figure 35. 3-D and contour plots of simultaneous changes in A and B on the yield of various hydrocarbon products.

Furthermore, as depicted in **Figure 36**, optimizing the C_3H_6 yield requires a low-pressure ratio, which also helps reduce the paraffin yields, but maximizing the C_2H_4 and C_4H_8 yields need an increase in pressure ratio. Maximizing olefin yields involves a trade-off since C_2H_4 and C_3H_6 demand high temperatures for the reactor and shell whereas C_4H_8 yield may be maximized at lower temperatures. Moreover, whereas C_3H_8 and C_4H_{10} yields can be decreased at high levels of A and C, C_2H_6 yields require low levels of both A and C to do so. The similar problem develops when modifying tube and shell temperatures to achieve optimum, making the influence of temperature complicated and difficult to understand. In particular, high tube and shell temperatures

are needed to maximize C_2H_4 and C_3H_6 yields, whereas high shell and low tube temperatures are ideal for boosting C_4H_8 yield. Therefore, in order to minimize C_3H_8 and C_4H_{10} yields and produce paraffins, the exact opposite circumstances must exist. Moreover, when both temperatures are at their lowest points, the C_2H_6 output can be lowered [46].

a)

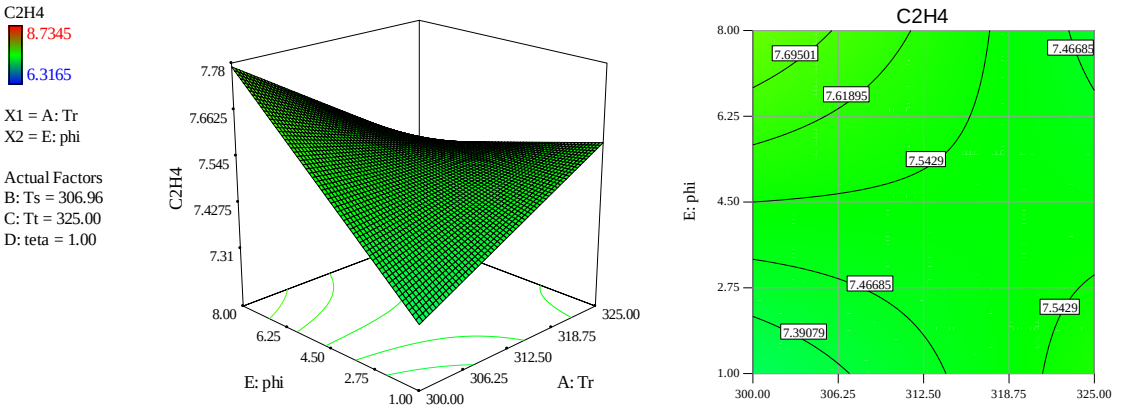

b)

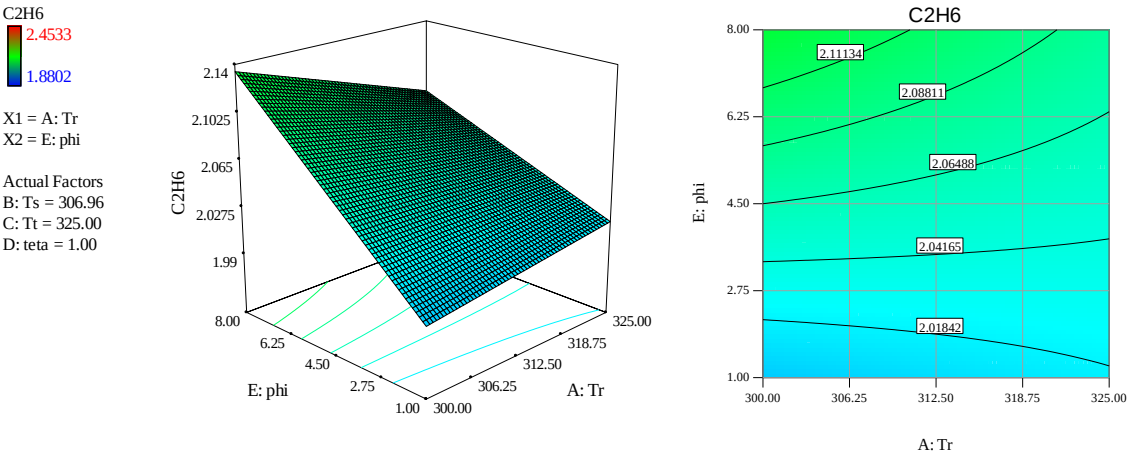

c)

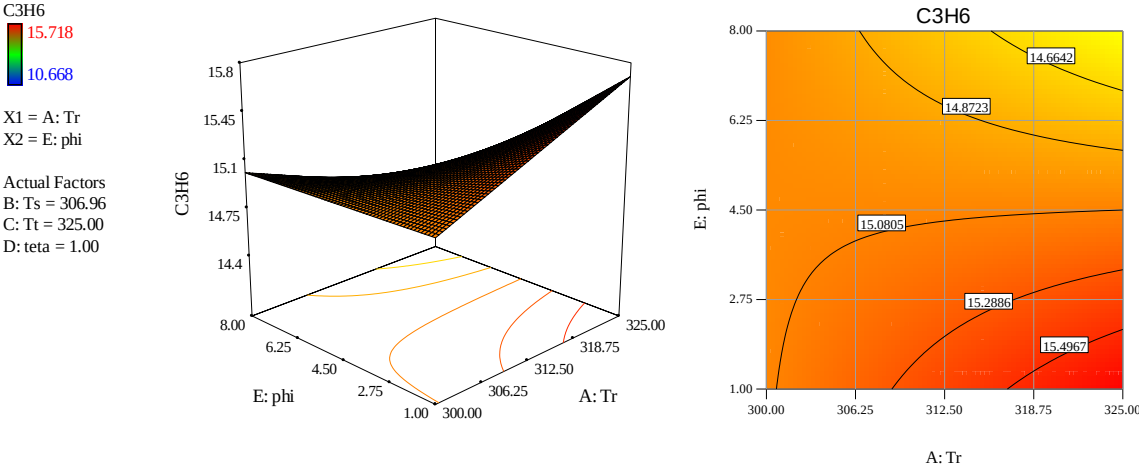

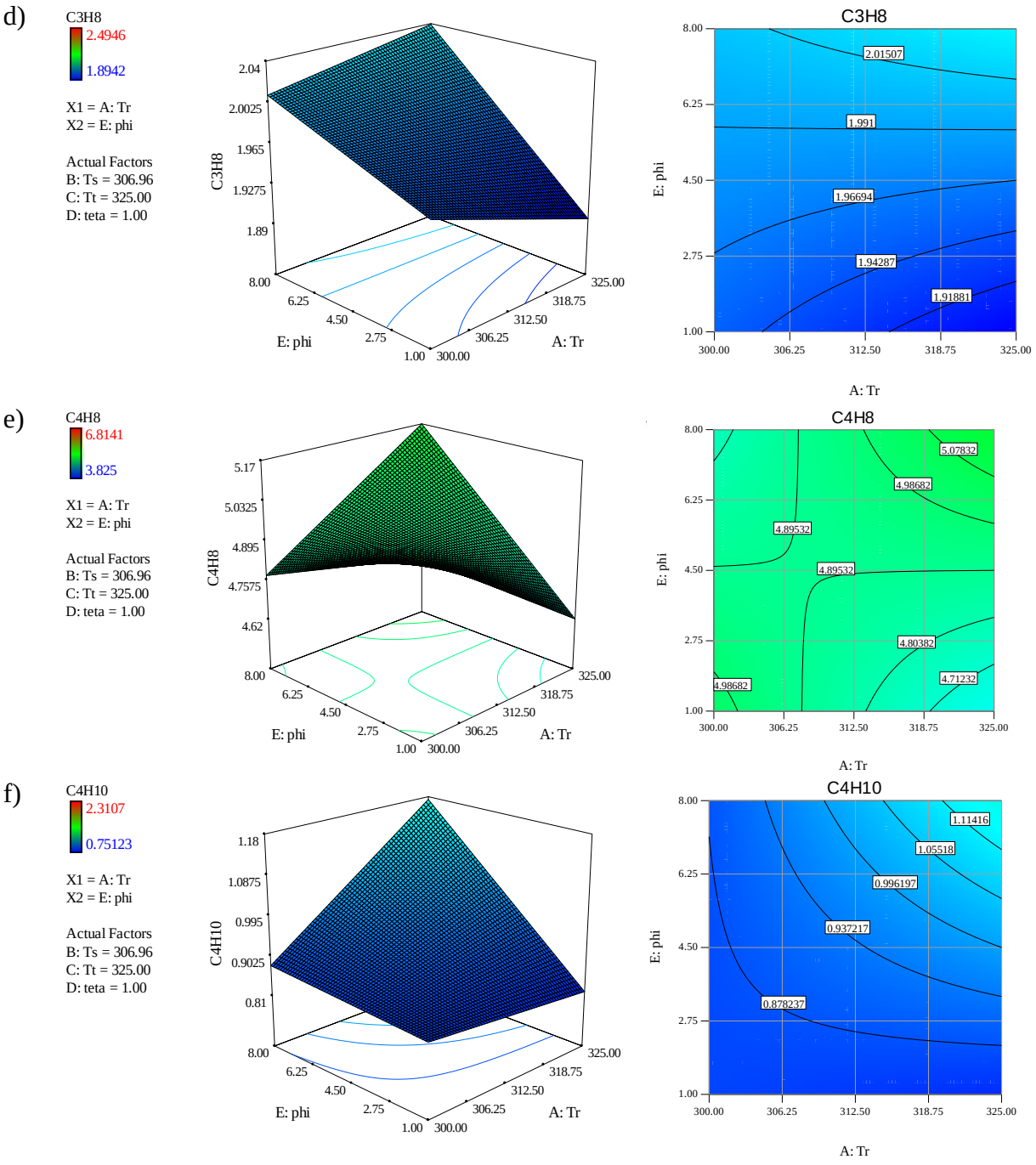

Figure 36. 3-D and contour plots of simultaneous changes in A and E on the yield of various hydrocarbon products.

Moreover, the impacts of sweep and pressure ratios are taken into account while determining the ideal conditions for CO_2 hydrogenation to hydrocarbon. **Figure 37** shows that high tube temperatures and low pressure ratios are required to produce the best yields of C_2H_4 and C_3H_6. On the other hand, the opposite trend is shown for the maximal C_4H_8 yield. It is advised to have a high level of C and a low level of E in order to reduce the yields of C_3H_6 and C_4H_{10}. Both C and E should be at low levels in

order to minimize C_2H_6 and CH_4. Low sweep ratios and high tube temperatures work together to successfully improve light olefin yields while reducing paraffin yields. none of the factors can be independently evaluated to ascertain the optimal conditions since the interactions between the factors are crucial. **Figure 38** demonstrates that a lower value of E is appropriate for producing more C3H6, demonstrating that high E values negatively affect the production of the desired olefin (C_3H_6). **Figure 31** shows a similar pattern for the interaction impact of DE, which is in line with findings from prior research [59] and those mentioned by Iglesia [60] regarding the saturation concentration of water in the mixture. As a result, both D and E should be reduced to optimize C_3H_6 production. Additionally, a high amount of A and a low level of D are required to reduce the undesirable product CH_4. To reduce CH_4 output, high reactor temperatures and low sweep and pressure ratios are also necessary.

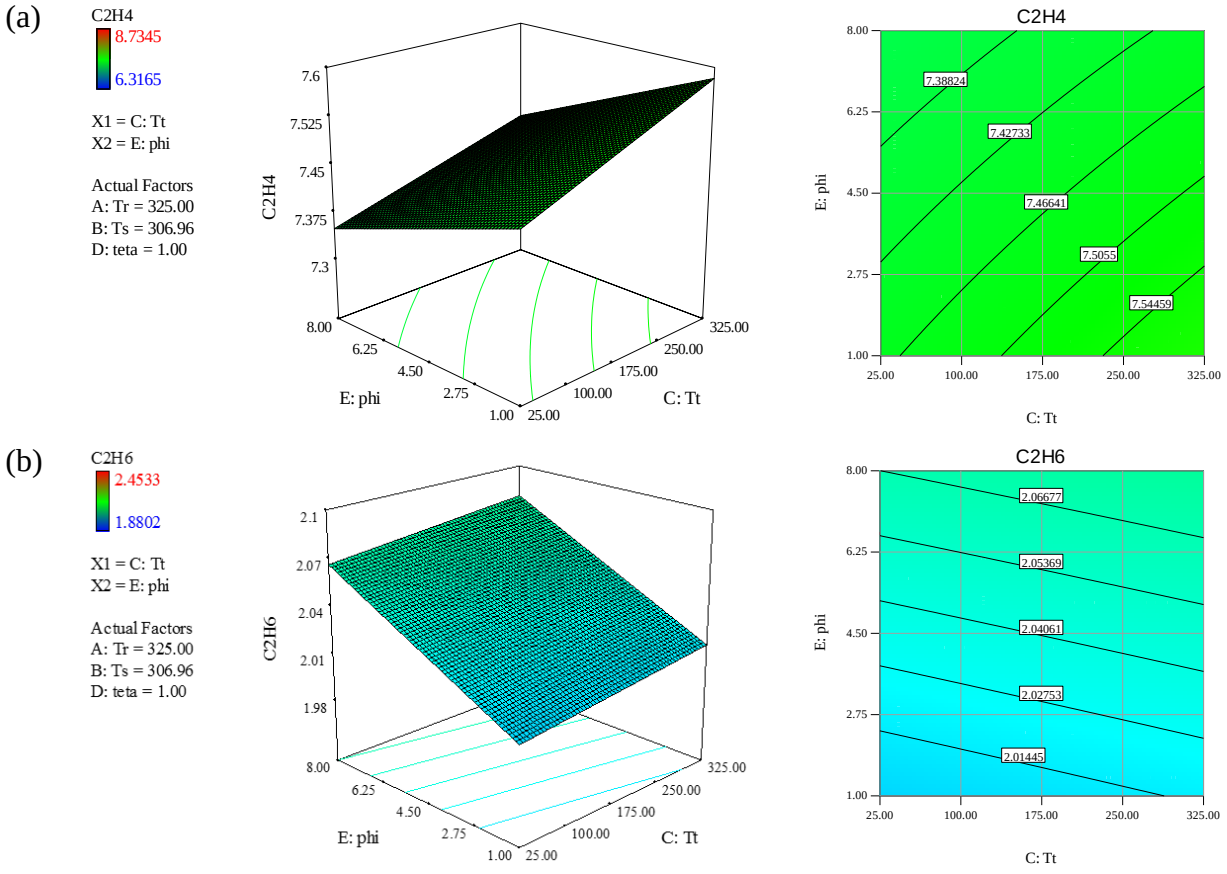

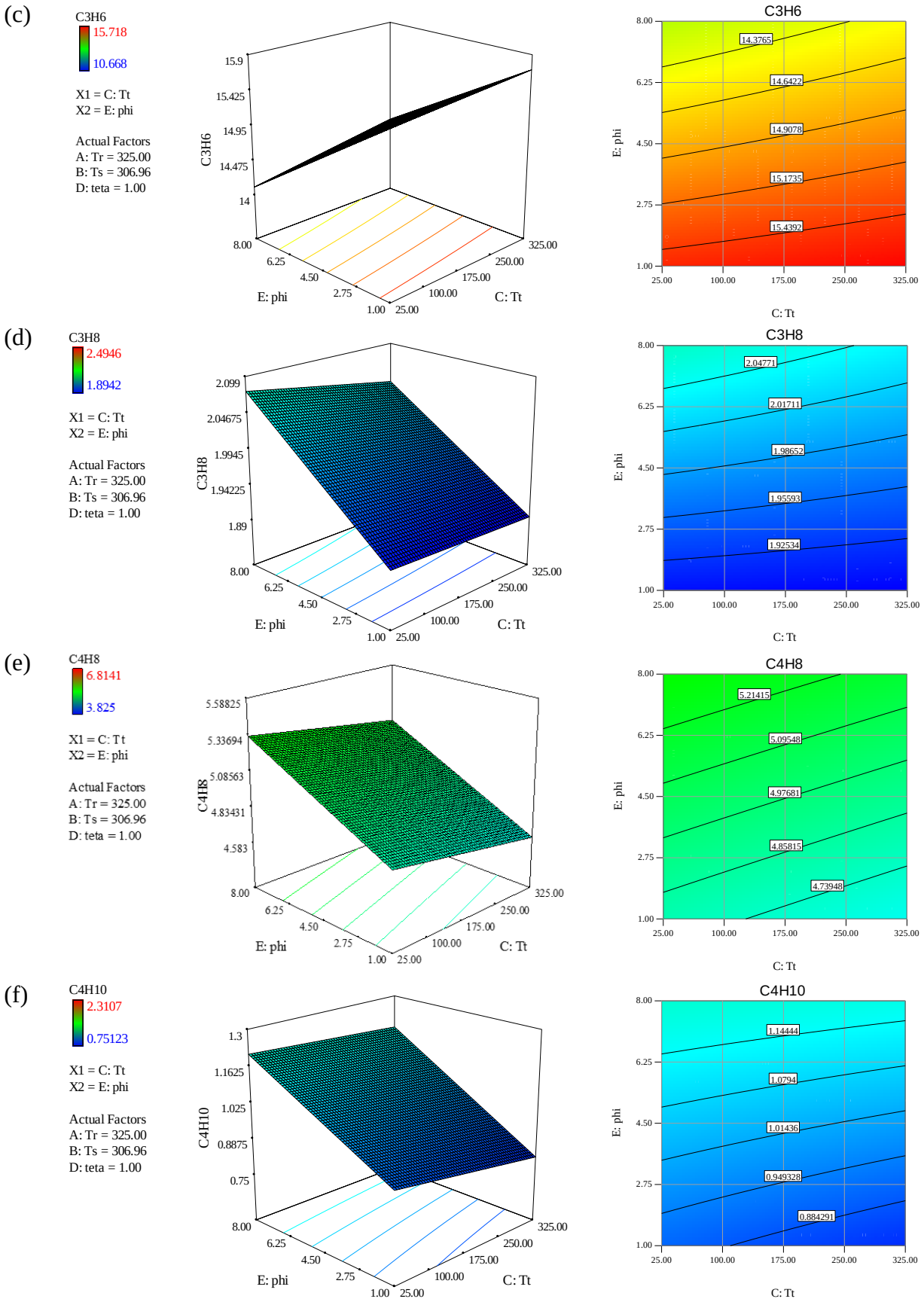

Figure 37. 3-D and contour plots of simultaneous changes in C and E on the yield of various hydrocarbon products.

(a)

C2H4
8.7345
6.3165

X1 = D: teta
X2 = E: phi

Actual Factors
A: Tr = 325.00
B: Ts = 306.96
C: Tt = 325.00

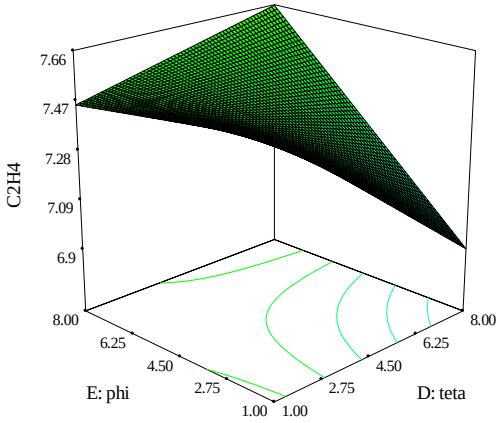

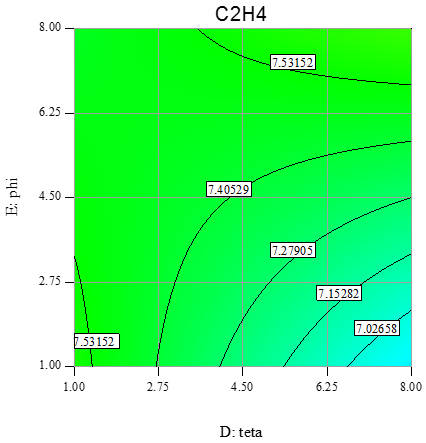

(b)

C2H6
2.4533
1.8802

X1 = D: teta
X2 = E: phi

Actual Factors
A: Tr = 325.00
B: Ts = 306.96
C: Tt = 325.00

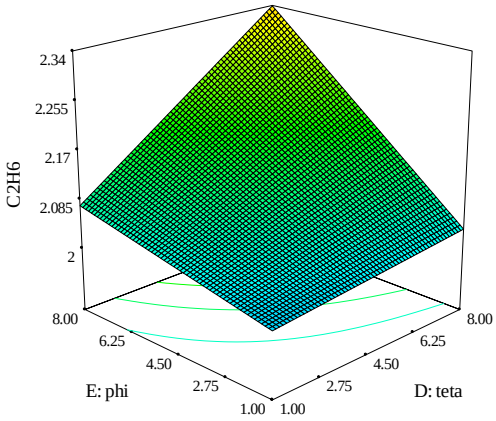

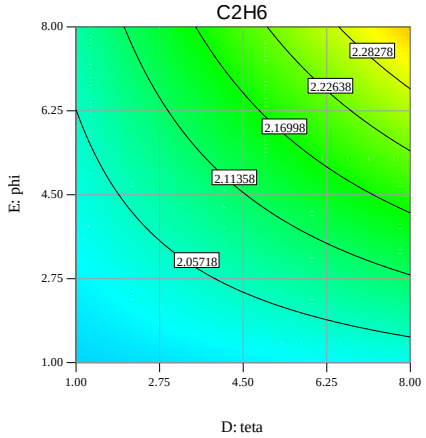

(c)

C3H6
15.718
10.668

X1 = D: teta
X2 = E: phi

Actual Factors
A: Tr = 325.00
B: Ts = 306.96
C: Tt = 325.00

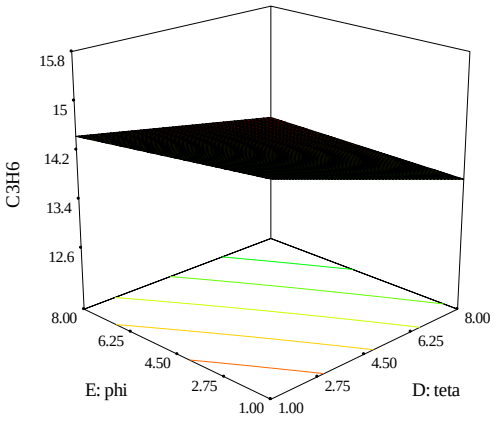

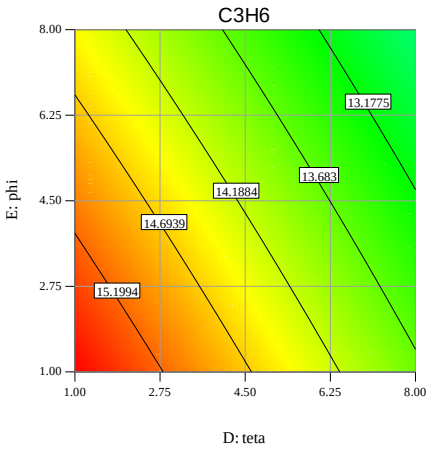

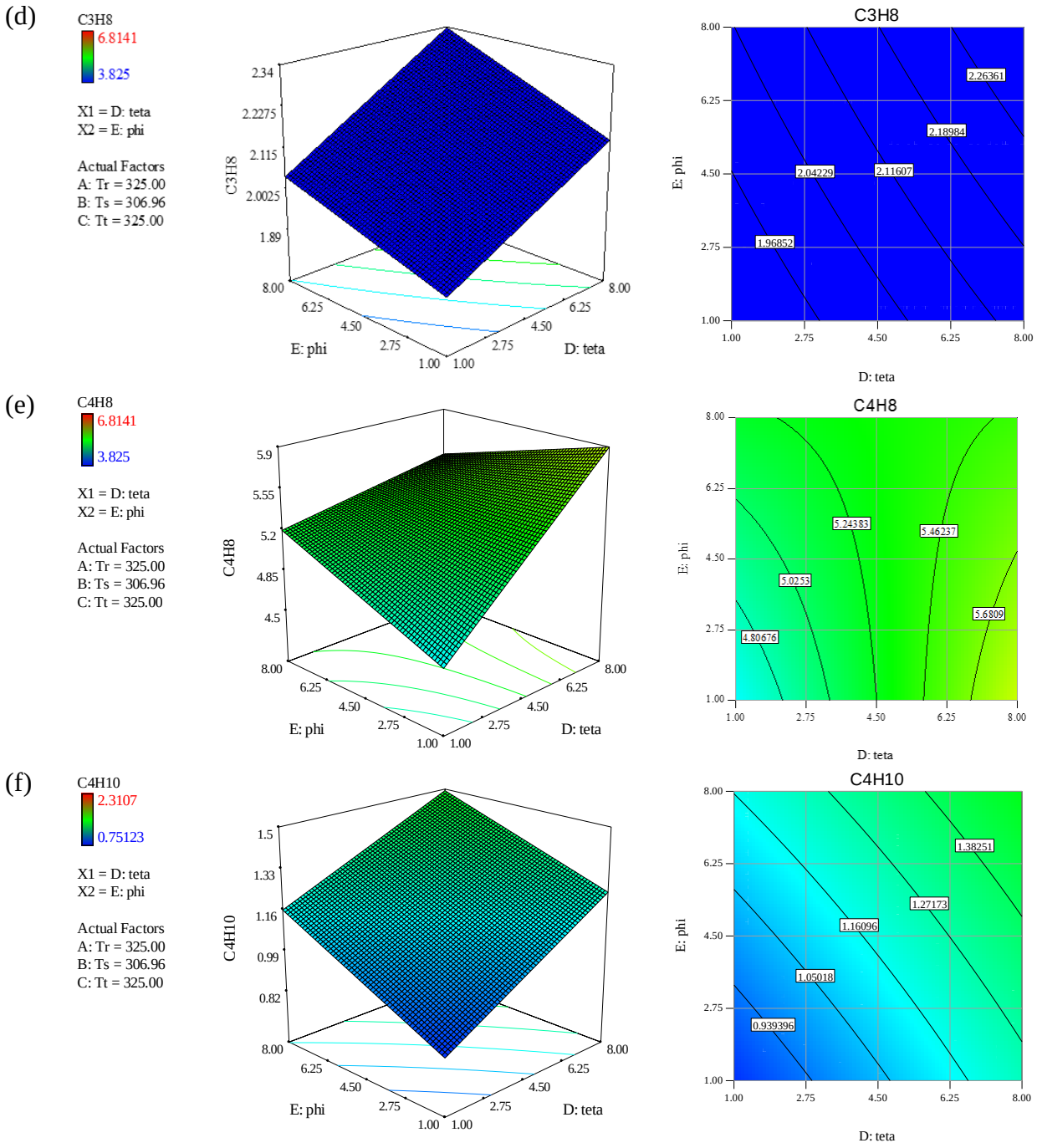

Figure 38. 3-D and contour plots of simultaneous changes in D and E on the yield of various hydrocarbon products.

There is no obvious direct association between the hydrocarbon yields and the variables, as shown in **Table 4** summary of the impacts of single and two-factor factors on the yields. Despite this, by taking into account the most important effects and the optimization goals, the optimum condition can be determined. It's crucial to remember that in our prior investigation on the fixed-bed system, it was found that the reaction cannot occur below 300°C, while hot spot formation limits the reactor's performance

above 325°C. Therefore, the reactor temperature was chosen to be within this range. Also, the significance of each yield was determined separately, placing restrictions on the optimization. The priority was set to maximize olefins yield (importance = 5), while paraffins and methane's yields were given a lower priority (importance = 3). The optimization was prioritized with the goal of maximizing the yield among the approximately 30 potential alternatives. It is important to note that in order to get the desired answer, the range had to be constrained because the optimization result was not unique.

Table 4. Effects of a single factor and a pair of factors on the yields

	A	**B**	**C**	**D**	**E**	**AB**	**AC**	**AD**	**AE**	**BC**	**CE**	**CD**	**DE**	**ABC**
y_{CH_4}	+		+	+	+			+			-		+	
$y_{C_2H_4}$	+	+	+	-	+	-	-		-	+	+	+	+	-
$y_{C_2H_6}$	+	+	+	+	+	-	-		-	+	+	+	+	-
$y_{C_3H_6}$	+	+	+	-	-	-	-		-	+	+	+		-
$y_{C_3H_8}$	-	-	-	+	+	+	+	+	+	-	-	-	+	+
$y_{C_4H_8}$	-	-	-	+		+	+		+	-	-	-	-	+
$y_{C_4H_{10}}$	-	-	-	+		+	+		+	-	-	-	-	+

- Each row's most significant single and two-factor impacts are highlighted in green.
- Red fills the rows with the maximizing target.
- There is no data in the rows with the minimization aim.

5 Conclusions

To estimate kinetic parameters via optimization, a one-dimensional heterogeneous model for CO_2 hydrogenation in a fixed-bed reactor was compared with experimental results. The results indicated that the ABC algorithm was more accurate and reliable than the DE algorithm in predicting hydrocarbon distribution, with an average error of 6.3% and 32.9%, respectively. Although there were variances in catalyst properties and reaction conditions, the kinetic parameters derived from the ABC algorithm were mostly in line with those reported in earlier research. The catalyst demonstrated greater selectivity towards olefins than paraffin, with propylene being the most efficient product. Additionally, the olefin/paraffin ratio was higher in high-carbon hydrocarbons. The production and consumption of CO were found to be dependent on the rates of RWGS and FT reactions, respectively, which were affected by equilibrium limitations at various temperatures.

Furthermore, it was proven that inlet temperature played the key role in determining equilibrium shift and, subsequently, reaction rates. Results revealed that, light olefins (i.e., C_3H_6 and C_2H_4) were the most important products of this process, while hydrocarbons exhibiting 4 carbons were produced less. It was confirmed that CO and hydrocarbons yield were highly temperature dependent, whereas the influence of other parameters such as pressure and SV was less noticeable. In other words, at high temperatures, hydrocarbons yield became less sensitive to variations in pressure and SV; therefore, the process was almost solely temperature dependent. However, at mild temperatures (i.e., around 300 °C), pressure rise and SV reduction had positive effects on hydrocarbon yield. Moreover, it was indicated that pressure had an improving effect only to some extent and that a further increase in pressure beyond 10 MPa had no remarkable positive influence on hydrocarbon yield.

Spherical reactors were found to offer better CO_2 hydrogenation performance than CR, with AFSR-2 and RFSR-2-i providing the highest CO_2 conversion and hydrocarbon selectivity. The temperature increase in these reactors was also less than in RFSRs. Temperature fluctuations in RFSRs were better controlled via a constant-temperature jacket in RFSR-1-o and RFSR-2-o, highlighting the significance of jacket location

regardless of reactor volume. Additionally, spherical reactors had considerably lower pressure drops than CR.

The statistical analysis indicated that the relationship between input variables and hydrocarbon yields was complex and not straightforward. Nevertheless, by adjusting the levels of input variables, the desired hydrocarbon distribution could be achieved. It was determined that increasing temperatures led to the production of lighter hydrocarbons, while lower sweep and pressure ratios favored the production of light olefins. Optimal operating conditions (Tr = 325 °C, Ts = 306.96 °C, Tt = 325 °C, θ = 1 and φ =1) were identified for achieving maximum olefin yields and minimum yields of paraffins and CH_4. In general, optimization could be achieved by maintaining Tr, Ts, and Tt at high levels and θ and φ at low levels. Thus, mathematical modeling is an efficient and reliable approach to investigating and forecasting reactor performance, providing valuable insights into key parameters for designing advanced reactor configurations in the CO_2 hydrogenation process. Nonetheless, additional research is required to evaluate the impact of significant factors on reaction rates and product distribution.

References

1. Hwang, S.-M., et al., *Mechanistic insights into Cu and K promoted Fe-catalyzed production of liquid hydrocarbons via CO2 hydrogenation.* Journal of CO2 Utilization, 2019. **34**: p. 522-532.
2. Eliasson, B., C.-j. Liu, and U. Kogelschatz, *Direct Conversion of Methane and Carbon Dioxide to Higher Hydrocarbons Using Catalytic Dielectric-Barrier Discharges with Zeolites.* Industrial & Engineering Chemistry Research, 2000. **39**(5): p. 1221-1227.
3. Riedel, T., et al., *Kinetics of CO2 Hydrogenation on a K-Promoted Fe Catalyst.* Industrial & Engineering Chemistry Research, 2001. **40**(5): p. 1355-1363.
4. Iglesias G, M., et al., *Chemical energy storage in gaseous hydrocarbons via iron Fischer–Tropsch synthesis from H2/CO2—Kinetics, selectivity and process considerations.* Catalysis Today, (0).
5. Kim, J.-S., et al., *Performance of catalytic reactors for the hydrogenation of CO2 to hydrocarbons.* Catalysis Today, 2006. **115**(1–4): p. 228-234.
6. Ding, F., et al., *Effect of SiO2-coating of FeK/Al2O3 catalysts on their activity and selectivity for CO2 hydrogenation to hydrocarbons.* RSC Advances, 2014. **4**(17): p. 8930-8938.
7. Drab, D.M., et al., *Hydrocarbon Synthesis from Carbon Dioxide and Hydrogen: A Two-Step Process.* Energy & Fuels, 2013. **27**(11): p. 6348-6354.
8. Kim, K., et al., *Moving bed adsorption process with internal heat integration for carbon dioxide capture.* International Journal of Greenhouse Gas Control, 2013. **17**(0): p. 13-24.

9. Ruiz, E., et al., *Bench-scale study of electrochemically assisted catalytic CO2 hydrogenation to hydrocarbon fuels on Pt, Ni and Pd films deposited on YSZ.* Journal of CO2 Utilization, 2014. **8**(0): p. 1-20.

10. Saeidi, S., et al., *Effect of operating conditions and effectiveness factor on hydrogenation of CO2 to hydrocarbons.* International Journal of Hydrogen Energy, 2019. **44**(54): p. 28586-28602.

11. Iranshahi, D., et al., *Progress in spherical packed-bed reactors: Opportunities for refineries and chemical industries.* Chemical Engineering and Processing-Process Intensification, 2018. **132**: p. 16-24.

12. Shahhosseini, H.R., et al., *Comparison of conventional and spherical reactor for the industrial auto-thermal reforming of methane to maximize synthesis gas and minimize CO2.* International Journal of Hydrogen Energy, 2017. **42**(31): p. 19798-19809.

13. Iranshahi, D., et al., *Utilising a radial flow, spherical packed-bed reactor for auto thermal steam reforming of methane to achieve a high capacity of H2 production.* Chemical Engineering and Processing-Process Intensification, 2017. **120**: p. 258-267.

14. Hashimoto, K., et al., *Global CO2 recycling—novel materials and prospect for prevention of global warming and abundant energy supply.* Materials Science and Engineering: A, 1999. **267**(2): p. 200-206.

15. Saeidi, S., N.A.S. Amin, and M.R. Rahimpour, *Hydrogenation of CO_2 to value-added products—A review and potential future developments.* Journal of CO_2 utilization, 2014. **5**: p. 66-81.

16. Saeidi, S., et al., *Recent advances in CO_2 hydrogenation to value-added products — Current challenges and future directions.* Progress in Energy and Combustion Science, 2021. **85**: p. 100905.

17. Guo, L., et al., *Enhanced Liquid Fuel Production from CO_2 Hydrogenation: Catalytic Performance of Bimetallic Catalysts over a Two-Stage Reactor System.* ChemistrySelect, 2018. **3**(48): p. 13705-13711.

18. Lee, J.-F., et al., *Hydrogenation of carbon dioxide on iron catalysts doubly promoted with manganese and potassium.* The Canadian Journal of Chemical Engineering, 1992. **70**(3): p. 511-515.

19. Riedel, T., et al., *Comparative study of Fischer–Tropsch synthesis with H_2/CO and H_2/CO_2 syngas using Fe-and Co-based catalysts.* Applied Catalysis A: General, 1999. **186**(1-2): p. 201-213.

20. Liu, J., et al., *Fe-MOF-derived highly active catalysts for carbon dioxide hydrogenation to valuable hydrocarbons.* Journal of CO_2 Utilization, 2017. **21**: p. 100-107.

21. Abelló, S. and D. Montané, *Exploring Iron-based Multifunctional Catalysts for Fischer–Tropsch Synthesis: A Review.* ChemSusChem, 2011. **4**(11): p. 1538-1556.

22. Saeidi, S., et al., *Mechanisms and kinetics of CO_2 hydrogenation to value-added products: A detailed review on current status and future trends.* Renewable and Sustainable Energy Reviews, 2017. **80**: p. 1292-1311.

23. Suksumrit, K., S. Kleiber, and S. Lux, *The Role of Carbonate Formation during CO2 Hydrogenation over MgO-Supported Catalysts: A Review on Methane and Methanol Synthesis.* Energies, 2023. **16**(7): p. 2973.

24. Saeidi, S., et al., *Recent advances in reactors for low-temperature Fischer-Tropsch synthesis: process intensification perspective.* Reviews in Chemical Engineering, 2015. **31**(3): p. 209-238.

25. Saeidi, S., et al., *Progress in reactors for high-temperature Fischer–Tropsch process: determination place of intensifier reactor perspective.* International Journal of Chemical Reactor Engineering, 2014. **12**(1): p. 639-664.

26. Lee, S.-C., et al., *The effect of binders on structure and chemical properties of Fe-K/ γ -Al2O3 catalysts for CO2 hydrogenation.* Applied Catalysis A: General, 2003. **253**(1): p. 293-304.

27. Shams, K. and S. Najari, *Dynamics of intraparticle desorption and chemical reaction in fixed-beds using inert core spherical particles.* Chemical Engineering Journal, 2011. **172**(1): p. 500-506.

28. Hartig, F. and F.J. Keil, *Large-scale spherical fixed bed reactors: modeling and optimization.* Industrial & Engineering Chemistry Research, 1993. **32**(3): p. 424-437.

29. Hartig, F., F. Keil, and V. Kafarov, *Optimization of Complex Reactions by Mixed-Integer Iterative Dynamic Programming.* Theoretical Foundations of Chemical Engineering, 1995. **30**: p. 50-60.

30. Keil, F.J. and C. Rieckmann, *Optimization of three-dimensional catalyst pore structures.* Chemical Engineering Science, 1994. **49**(24, Part A): p. 4811-4822.

31. Iranshahi, D., et al., *Thermal integration of sulfuric acid and continuous catalyst regeneration of naphtha reforming plants.* Chemical Engineering & Technology, 2018. **41**(3): p. 637-655.

32. Zhang, L., et al., *Entropy generation rate minimization for hydrocarbon synthesis reactor from carbon dioxide and hydrogen.* International Journal of Heat and Mass Transfer, 2019. **137**: p. 1112-1123.

33. Zhang, L., et al., *Entropy generation minimization for reverse water gas shift (R WGS) reactors.* Entropy, 2018. **20**(6): p. 415.

34. Li, P., et al., *Entropy generation rate minimization for methanol synthesis via a CO_2 hydrogenation reactor.* Entropy, 2019. **21**(2): p. 174.

35. Zhang, L., et al., *Multi-objective optimization for helium-heated reverse water gas shift reactor by using NSGA-II.* International Journal of Heat and Mass Transfer, 2020. **148**: p. 119025.

36. Waldron, C., et al., *Model-based design of transient flow experiments for the identification of kinetic parameters.* Reaction Chemistry & Engineering, 2020. **5**(1): p. 112-123.

37. Waldron, C., et al., *An autonomous microreactor platform for the rapid identification of kinetic models.* Reaction Chemistry & Engineering, 2019. **4**(9): p. 1623-1636.

38. Matera, S., et al., *Progress in accurate chemical kinetic modeling, simulations, and parameter estimation for heterogeneous catalysis.* ACS Catalysis, 2019. **9**(8): p. 6624-6647.

39. Berger, R.J., et al., *Dynamic methods for catalytic kinetics.* Applied Catalysis A: General, 2008. **342**(1-2): p. 3-28.

40. Slotboom, Y., et al., *Critical assessment of steady-state kinetic models for the synthesis of methanol over an industrial Cu/ZnO/Al2O3 catalyst.* Chemical Engineering Journal, 2020. **389**: p. 124181.

41. Seidel, C., et al., *Kinetic modeling of methanol synthesis from renewable resources.* Chemical Engineering Science, 2018. **175**: p. 130-138.

42. Willauer, H.D., et al., *Modeling and kinetic analysis of CO_2 hydrogenation using a Mn and K-promoted Fe catalyst in a fixed-bed reactor.* Journal of CO_2 Utilization, 2013. **3–4**: p. 56-64.

43. Rohde, M., et al., *Fischer–Tropsch synthesis with CO2-containing syngas from biomass–Kinetic analysis of fixed bed reactor model experiments*, in *Studies in surface science and catalysis*. 2004, Elsevier. p. 97-102.

44. De Falco, M., L. Di Paola, and L. Marrelli, *Heat transfer and hydrogen permeability in modelling industrial membrane reactors for methane steam reforming*. International Journal of Hydrogen Energy, 2007. **32**(14): p. 2902-2913.

45. Rohde, M.P., et al., *Fischer–Tropsch synthesis with in situ H2O removal – Directions of membrane development.* Microporous and Mesoporous Materials, 2008. **115**(1–2): p. 123-136.

46. Najari, S., et al., *Modeling and statistical analysis of the three-side membrane reactor for the optimization of hydrocarbon production from CO2 hydrogenation.* Energy conversion and management, 2020. **207**: p. 112481.

47. Najari, S., et al., *Kinetic parameters estimation via dragonfly algorithm (DA) and comparison of cylindrical and spherical reactors performance for CO2 hydrogenation to hydrocarbons.* Energy conversion and management, 2020. **226**: p. 113550.

48. Najari, S., et al., *Modeling and optimization of hydrogenation of CO_2: Estimation of kinetic parameters via Artificial Bee Colony (ABC) and Differential Evolution (DE) algorithms.* International Journal of Hydrogen Energy, 2019. **44**(10): p. 4630-4649.

49. Karaboga, D. and B. Akay, *A comparative study of artificial bee colony algorithm.* Applied mathematics and computation, 2009. **214**(1): p. 108-132.

50. Bonabeau, E., et al., *Swarm intelligence: from natural to artificial systems*. 1999: Oxford university press.

51. Mirjalili, S., *Dragonfly algorithm: a new meta-heuristic optimization technique for solving single-objective, discrete, and multi-objective problems.* Neural Computing and Applications, 2016. **27**(4): p. 1053-1073.

52. Saeidi, S., et al., *A comparative study between Modified Data Envelopment Analysis and Response Surface Methodology for optimisation of heterogeneous biodiesel production from waste cooking palm oil.* Journal of Cleaner Production, 2016. **136**.

53. Mohammadian, N., et al., *Optimization of Synthesis Conditions of Carbon Nanotubes via Ultrasonic-Assisted Floating Catalyst Deposition Using Response Surface Methodology.* Nanomaterials, 2018. **8**: p. 316.

54. Umer, M., et al., *Synergistic effects of single/multi-walls carbon nanotubes in TiO2 and process optimization using response surface methodology for photo-catalytic H2 evolution.* Journal of Environmental Chemical Engineering, 2019. **7**(5): p. 103361.

55. Miladinović, M.R., et al., *Modeling and optimization of sunflower oil methanolysis over quicklime bits in a packed bed tubular reactor using the response surface methodology.* Energy conversion and management, 2016. **130**: p. 25-33.

56. Owen, R.E., et al., *Kinetics of CO_2 Hydrogenation to Hydrocarbons over Iron–Silica Catalysts.* 2017. **18**(22): p. 3211-3218.

57. Ronda-Lloret, M., G. Rothenberg, and N.R. Shiju, *A Critical Look at Direct Catalytic Hydrogenation of Carbon Dioxide to Olefins.* ChemSusChem, 2019. **12**(17): p. 3896-3914.

58. Iglesias G, M., et al., *Chemical energy storage in gaseous hydrocarbons via iron Fischer–Tropsch synthesis from H_2/CO_2—Kinetics, selectivity and process considerations.* Catalysis Today, 2015. **242**: p. 184-192.

59. Najari, S., G. Gróf, and S. Saeidi, *Enhancement of hydrogenation of CO_2 to hydrocarbons via In-Situ water removal.* International Journal of Hydrogen Energy, 2019. **44**(45): p. 24759-24781.

60. Iglesia, E., *Design, synthesis, and use of cobalt-based Fischer-Tropsch synthesis catalysts.* Applied Catalysis A: General, 1997. **161**(1): p. 59-78.

Declaration

I declare that this dissertation, entitled "**Modeling and Simulation of Novel Catalytic Reactors for CO_2 Hydrogenation to Hydrocarbon at Different Modes and Operating Conditions,**" is entirely my own work, except for the references cited. This dissertation has not been previously accepted for any degree and has not been simultaneously submitted for any other degree.

Acknowledgement

I would like to begin by expressing my gratitude to my creator for bestowing upon me the ability to think critically and the determination to overcome difficult obstacles. This support allowed me to gain a deeper understanding of myself and my life philosophy. Throughout my research project, I received support and encouragement from many people who played an instrumental role in my success. During my years of research, I have shared numerous conversations with my friends and colleagues at various levels, and I am grateful for their contributions, although it is not possible to mention all of them here. If I had to name a few people, I would like to begin with my trusted friend and mentor, Prof. Gyula Gróf, and Dr. András Sápi.

List of publications

Web of Science ResearcherID: N-2359-2018 ; Google Scholar; ResearchGate

1. ***S. Saeidi***, NAS. Amin, MR. Rahimpour "**Hydrogenation of CO_2 to Value-added Products–A Review and Potential Future Developments**", *CO_2 utilization journal*, 5 (2014), 66–81 (**Most cited**).
   DOI: https://doi.org/10.1016/j.jcou.2013.12.005

2. ***S. Saeidi*,*** Sara Najari, Farhad Fazlollahi, Maryam Khoshtinat Nikoo, Fatemeh Sefidkon, Jiří Jaromír Klemeš, Larry L. Baxter **"Mechanisms and kinetics of CO_2 hydrogenation to value-added products: A detailed review on current status and future trends"** *Renewable and Sustainable Energy Reviews,* 80 (2017), 1292–1311.
   DOI: https://doi.org/10.1016/j.rser.2017.05.204

3. ***S. Saeidi****, S. Najari, V. Hessel, K. Wilson, Frerich J. Keil, P Concepcion, S.L. Suib, Alírio E. Rodrigues "**Recent advances in CO_2 hydrogenation to value-added products — Current challenges and future directions"** *Progress in Energy and Combustion Science*. 85 (2021), 100905. (**Most cited**). DOI: https://doi.org/10.1016/j.pecs.2021.100905

4. *Sara Najari, Gyula Gróf,* ***S. Saeidi****, *Fausto Gallucci* **"Modeling and optimization of hydrogenation of CO_2: Estimation of kinetic parameters via Artificial Bee Colony (ABC) and Differential Evolution (DE) algorithms"** *International Journal of Hydrogen Energy* 44 (2019), 4630-4649.
   DOI: https://doi.org/10.1016/j.ijhydene.2019.01.020

5. *Sara Najari, Gyula Gróf,* ***S. Saeidi**** **"Enhancement of hydrogenation of CO_2 to hydrocarbons via In-Situ water removal"** *International Journal of Hydrogen Energy*, 44 (2019), 24759-24781.
   DOI: https://doi.org/10.1016/j.ijhydene.2019.07.159

6. ***S. Saeidi*,*** *Sara Najari, Gyula Gróf, Fausto Gallucci* **"Effect of operating conditions and effectiveness factor on hydrogenation of CO_2 to hydrocarbons"** *International Journal of Hydrogen Energy*, 44 (2019), 28586-28602. DOI: https://doi.org/10.1016/j.ijhydene.2019.08.255

7. S. Najari, G. Gróf, ***S. Saeidi****, P. Bihari, W-H. Chen, **"Modeling and statistical analysis of the three-side membrane reactor for the optimization of hydrocarbon production from CO_2 hydrogenation"**, *Energy Conversion and Management*, 207 (2020) 112481.
   DOI: https://doi.org/10.1016/j.enconman.2020.112481
8. Sara Najari, ***S. Saeidi****, Gyula Gróf, Frerich J. Keil, Alírio E. Rodrigues **"Kinetic parameters estimation via dragonfly algorithm (DA) and comparison of cylindrical and spherical reactors performance for CO_2 hydrogenation to hydrocarbons"** *Energy Conversion and Management*, 226, (2020), 113550. DOI: https://doi.org/10.1016/j.enconman.2020.113550